Construction and validation of a detailed kinetic model of glycolysis in asexual *Plasmodium falciparum*: A feasibility study.

by

Gerald Patrick Penkler

Thesis presented in partial fulfilment of the requirements for the degree of Master of Science at the Department of Biochemistry, University of Stellenbosch

Department of Biochemistry
University of Stellenbosch
Private Bag X1, 7602 Matieland, South Africa

Study leaders: Prof J.L. Snoep
Prof. M. Rautenbach

December 2009

Declaration

By submitting this thesis electronically, I declare that the entirety of the work contained therein is my own, original work, that I am the owner of the copyright thereof (unless to the extent explicitly otherwise stated) and that I have not previously in its entirety or in part submitted it for obtaining any qualification.

Signature: .....
G.P. Penkler

Date: .....

Abstract

Construction and validation of a detailed kinetic model of glycolysis in asexual *Plasmodium falciparum*: A feasibility study.

G.P. Penkler

Department of Biochemistry
University of Stellenbosch
Private Bag X1, 7602 Matieland, South Africa

Thesis:

December 2009

In Africa alone, *Plasmodium*, the causative agent of malaria is estimated to kill a child, under the age of five every thirty seconds [140]. The ability of the parasite to rapidly attain resistance, has resulted in immunity of the parasite to all, except one group of frontline drugs. The need to develop novel drugs, vaccines and prevention strategies that are accessible and affordable for third world countries is of the utmost importance to prevent needless human suffering and death.

The glycolytic pathway is an attractive drug target since it is the principal source of ATP for the parasite. Many of the glycolytic enzymes have been studied and proposed as drug targets, but the importance of these enzymes for the function of the pathway as a whole has not been considered. It is known, from the frameworks of metabolic control analysis, that control of the flux and metabolite concentration can be divided among the individual steps.

Differential control analysis of *Plasmodium* and erythrocyte glycolysis may reveal potential drug targets. These analyses require a detailed kinetic model of *Plasmodium* glycolysis, and the feasibility of constructing and validating such a model was the aim of this study.

In this work we determined the feasibility of constructing and validating a detailed kinetic model for the *Plasmodium falciparum* glycolytic pathway.

Whether the construction and validation of this kinetic model was feasible or not was decided on the basis of the ability to: i) culture and isolate sufficient asexual parasites for enzymatic and steady state assays , ii) obtain kinetic parameters such as K_m and V_{max} for each glycolytic enzyme, either from literature or experimentally, iii) measure glycolytic fluxes, iv) determine glycolytic intermediate concentrations, v) construct a kinetic model from the kinetic parameters and vi) validate it with steady state glycolytic fluxes and metabolite concentrations

Each of the above criteria were successfully addressed. In summary, the kinetic parameters and glycolytic fluxes that were measured experimentally, were used to construct and partially validate a detailed kinetic model, respectively. Further validation of the model by means of steady state metabolite concentrations was shown to be possible with the development of a suitable protocol to measure the glycolytic intermediate concentrations.

The model presented in this work may play an important role in drug target identification and improving the current understanding of host-parasite interactions and glycolytic regulation.

Uittreksel

Construction and validation of a detailed kinetic model of glycolysis in asexual *Plasmodium falciparum*: A feasibility study.

G.P. Penkler

Departement Biochemie
Universiteit van Stellenbosch
Privaatsak X1, 7602 Matieland, Suid-Afrika

Tesis:

Desember 2009

Plasmodium, die parasiet wat malaria veroorsaak, is in Afrika alleen elke dertig sekondes verantwoordelik vir die afsterwe van 'n kind jonger as vyf jaar. Die parasiet se vermoë om vinnig weerstand op te bou het daartoe gelei dat Plasmodium weerstandbiedend is teen byna alle nuwe teen-malaria middels, behalwe vir 'n enkele toonaangewende groep. Die ontwikkeling van nuwe malaria teen-middels is van uiterste belang om lyding te voorkom.

'n Goeie teiken vir teen-malaria middels is die glikolitiese padweg omdat dié metaboliese padweg essensieël is vir die produksie van ATP, die energiebron van die parasiet. Desondanks die feit dat meeste van die glikolitiese ensieme al goed bestudeer en as teiken voorgestel is, is dit steeds onduidelik hoe hierdie ensieme saam funksioneer om die metaboliese weg, as geheel, tot stand te bring.

Metaboliese kontrole analise het aangetoon dat die glikolitiese beheer verdeel

is tussen die onderskeie glikolitiese ensieme, m.a.w. geen enkele ensiematiese stap het volledige beheer oor die fluksie van die glikolitiese padweg nie. Die afsonderlike analise en vergelyking van Plasmodium - en rooibloedselglikolise met behulp van differensiële metaboliese kontrole analise sal moontlik gebruik kan word om gasheervriendelike teikens vir nuwe middels aan te toon. So 'n analise benodig 'n omvattende kinetiese model van Plasmodium glikolise. Derhalwe was die doel van hierdie studie om vas te stel hoe uitvoerbaar dit is om 'n kinetiese model van Plasmodium glikolise te konstrueer en te valideer.

Die uitvoerbaarheid van die konstruksie en validering van die kinetiese model was geasseseer op grond van die vermoë om: i) parasietkulture te kweek en genoegsame parasiete, wat in die aseksuele fase is, te isoleer sodat ensiembepalings en bestendige toestand-bepalings gedoen kan word, ii) kinetiese parameters soos Km - en Vmax-waardes vir elke glikolitiese ensiem, hetsy vanuit literatuur of eksperimentele werk, te verkry, iii) glikolitiese fluksie te meet, iv) glikolitiese intermediaatkonsentrasies te bepaal, v) 'n kinetiese model van die bepaalde kinetiese parameters op te stel en vi) die model te valideer met glikolitiese flukswaardes en metaboliet- konsentrasies wat in die bestendige toestand verkry is.

Elk van die bogenoemde kriteria was met sukses in hierdie studie aangespreek. Ter opsomming, die eksperimenteel bepaalde kinetiese parameters en glikolietiese flukswaardes was gebruik om onderskeidelik 'n gedetaileerde kinetiese model te konstrueer en gedeeltelik te valideer. Daar was getoon dat verdere validering van die model deur middel van bestendige toestand metabolietkonsentrasies moontlik is met die ontwikkeling van 'n geskikte protokol om glikolitiese intermediaatkonsentrasies te meet. Die model, soos opgestel in hierdie studie, kan moontlik 'n belangrike rol speel om teikens vir nuwe malaria teen-middels te identifiseer en om gasheer-parasiet interaksies en glikolitiese regulering beter te verstaan.

Acknowledgements

I would like to express my sincere gratitude to the following people and organisations whose contributions have made this work possible:

- Prof Snoep for patiently guiding this work in the right direction.
- Prof Rautenbach for enthusiastic discussion and input.
- Mr. Arends for assistance and managing the lab in a most efficient and cheerful manner.
- Prof Hoppe for *Plasmodium* cultures and the knowledge to culture them.
- Dr Wiehart for providing *Plasmodium* cultures after bouts of contamination.
- Riaan & Franco for the numerous discussions & debates covering a wide range of subject matter, mostly not work related, but providing much needed comic relief.
- National Bioinformatics Network for funding.
- My friends for past and continued good times.
- My family for their support & encouragement.

Dedications

To my loving parents,
Mom & Dad

Contents

List of Figures

List of Tables

Abbreviations

Acetyl-CoA	Acetyl-coenzyme A
ADP	Adenosine diphosphate
ALD	Fructose bisphosphate Aldolase (E.C. 4.1.2.13)
APADH	3-acetylpyridine adenine dinucleotide
ATP	Adenosine triphosphate
DDT	Dichlorodiphenyltrichloroethane
DHAP	Dihydroxyacetone Phosphate
2,3 DPG	2,3-Diphosphoglycerates
ENO	Enolase (E.C. 4.2.1.11)
ETC	Electron Transport Chain
F1,6BP	Fructose 1,6-Bisphosphate
F1P	Fructose -1-Phosphate
F6P	Fructose 6-Phosphate
$FADH_2$	Reduced flavin adenine dinucleotide
G3PDH	Glyceraldehyde-3-phosphate dehydrogenase (E.C. 1.2.1.12)
G6P	Glucose 6-Phosphate
G6PD	Glucose-6-phosphate- 1-dehydrogenase (E.C. 1.1.1.49)
G6PDH	Glucose-6-phosphate isomerase (E.C. 5.3.1.9)
GAP	Glyceraldehyde Phosphate
GAPDH	Glyceraldehyde-3-Phosphate Dehydrogenase (E.C. 1.2.1.12)
GFATM	Global Fund to Þght AIDS, Tuberculosis and Malaria.
GlycerolPDH	α-Glycerol phosphate dehydrogenase (E.C. 1.1.1.8)
GLUT1	Glucose Transporter 1
GLUT5	Glucose Transporter 5
GTP	Guanosine Triphosphate
HEPES	4-(2-hydroxyethyl)piperazine-1-ethanesulfonic acid
HK	Hexokinase (E.C. 2.7.1.1)
kDa	Kilodalton
Lac	Lactate
LDH	L-Lactate Dehydrogenase (E.C. 1.1.1.27)
MMV	Medicines for Malaria Venture
mRNA	Messenger RNA
MCT	Monocarboxylate Transporter
MCA	Metabolic Control Analysis

NAD^+	Oxidised Nicotinamide adenine dinucleotide
NADH	Reduced Nicotinamide adenine dinucleotide
$NADP^+$	Oxidised Nicotinamide dinucleotide phosphate
NADPH	Reduced Nicotinamide dinucleotide phosphate
NPO	Non profit organisation
ODN	Oligodeoxynucleotides
PDH	Pyruvate Dehydrogenase Complex
PEP	Phosphoenolpyruvate
PFK	Phosphofructokinase (E.C. 2.7.1.11)
PGI	Phosphoglucoisomerase (E.C. 5.3.1.9)
PfHT1	*Plasmodium falciparum* hexose transporter 1
3PGA	3-Phosphoglycerate
2PGA	2-Phosphoglycerate
PGK	Phosphoglycerate Kinase (E.C. 2.7.2.3)
6PGL	6-Phosphogluconolactononase (E.C. 3.1.1.31)
PGM	Phosphoglycerate Mutase (E.C. 5.4.2.1)
PK	Pyruvate Kinase (E.C. 2.7.1.40)
PNP	Nucleoside phosphorylase
PPP	Pentose Phosphate Pathway
PRPP	Phosphoriboyl-1-pyrophosphate
PRTases	Phosphoribosyl transferases
PvHT1	*Plasmodium vivax* hexose transporter 1
Pyr	Pyruvate
R5P	Ribulose 5-phosphate
ROS	Reactive Oxygen Species
TCA	Tricarboxylic Acid Cycle
TPI	Triosphosphate Isomerase (E.C. 5.3.1.1)
U	Units
WHO	World Health Organisation

Chapter 1

General Introduction

Malaria, caused by the *Plasmodium* species, is transmitted by the bite of a female *Anopheles* mosquito and has plagued the human race for millenia. It is estimated that in Africa alone, *Plasmodium* (especially *P. falciparum*) kills a child under the age of 5, every 30 seconds[140]. Intensive insecticide spraying and the discovery of chloroquine completely eradicated malaria from Europe and North America. The hopes of global eradication, however, were dashed as the parasite adapted remarkably rapidly, becoming resistant to insecticides and overcoming drug therapy. The latter has been overcome so effectively, that some strains are resistant to all but one (artemisinin) frontline antimalarial drugs[140]. Globally, researchers are attempting to discover novel methods of overcoming *Plasmodium* infections by targeting the parasite in both mosquito and human hosts. The advent of genomics, proteomics, and metabolomics; relatively new disciplines whose results can be integrated in systems biology approaches, has allowed researchers to search for targets on a much broader scale, making it possible to analyse complete pathways or even systems at cellular and organ level.

Carbohydrate metabolism, particularly the glycolytic pathway is potentially an excellent drug target, since the parasite derives most, if not all of its ATP from the pathway[52]. As such, several targets in this pathway have been proposed. The hexose transporter[109], aldolase[157], triosephosphate isomerase[112], lactate dehydrogrenase[14] have all been well studied and suggested as potential drug targets. Although researchers have looked at these enzymes in isolation, to

date the glycolytic pathway of none of the *Plasmodium* species has been studies as a whole. Through the theoretical framework of metabolic control analysis we now know that instead of a single rate limiting step, control of the flux and intermediate metabolite concentrations can be divided among the individual steps. Obviously, enzymes which exert a large control on the flux and intermediates would present preferential targets to those exerting a low control. Since the parasite is a eukaryotic organism, its glycolytic enzymes would be expected in many cases, to have high homology to the human enzymes. As such, compounds targeting the parasite glycolytic enzymes could potentially be toxic to the human. If, however, an enzyme in the host pathway has low control and the corresponding parasite enzyme has a high control, the drug would have to be less selective, as inhibition of the host enzyme would have little effect on the host compared to the parasite. This differential control can play an important role in drug target identification.

1.1 Project Outline

The aim of this study was to establish the feasibility of constructing and validating a detailed kinetic model of glycolysis in the asexual *Plasmodium falciparum*.

The project consisted of both experimental and theoretical aspects, each with distinctive criteria to be met in order to establish the feasibility of creating and validating the kinetic model.
The criteria for the experimental aspects included the ability to i) establish cultures of asexual *P. falciparum D10* and isolate sufficient trophozoites for kinetic and steady state assays, ii) obtain kinetic parameters for the glycolytic enzymes experimentally or from literature and iii) measure steady state fluxes and metabolite concentrations.
The criteria for the theoretical aspects of the project included the ability to i) construct and ii) validate the kinetic model using the determined kinetic parameters and steady state fluxes and metabolite concentrations, respectively.

The study is presented in experimental and theoretical categories and the aims can be summarised as follows:

The experimental work consisted of:

- The maintenance of asexual *Plasmodium falciparum D10* cultures for the isolation of trophozoites.
- An extensive literature search for kinetic parameters for each glycolytic enzyme in *Plasmodium*.
- The kinetic characterisation of as many of the glycolytic enzymes as possible under *in vivo* conditions.
- The development of a method for the measurement of steady state fluxes and internal metabolite concentrations in *P. falciparum* trophozoites.

The theoretical work was comprised of:

- The construction of a kinetic model using the determined kinetic parameters.
- The partial validation of the model using steady state flux data obtained in this study.
- Brief model analysis.

Overall the construction of a detailed kinetic model of *P. falciparum* glycolysis would provide a better fundamental understanding of *Plasmodium* glycolysis, but more importantly it could be used as a tool for more applied studies. Such studies would include 1) comparing the distribution of metabolic control found in *P. falciparum* to that of the erythrocyte and 2) investigating the effect of parasite infection on the energy metabolism of the erythrocyte host in terms of metabolic flux and control. These studies may be important for drug target indentification and improving the current understanding of patient pathophysiology, respectively.

Chapter 2

Review of *Plasmodium* Life Cycle, History and Carbon Metabolism

The human malarial parasite has been extremely successful in evading the immune systems of its human and mosquito hosts. The emergence of resistance, to all but one group of frontline drugs, has necessitated the search for novel anti-malarials, vaccines and preventative measures. The following review covers the *Plasmodium* life cycle, gives a historical overview of its discovery and treatment and is followed by a comprehensive literature study of the asexual *Plasmodium* energy metabolism. The energy metabolism, being the subject of this thesis, consists of glycolysis, the pentose phosphate pathway, tricarboxylic acid cycle and some ancillary pathways. Each is examined with specific focus on the enzymes and their kinetic characterisation. The aim of this review is to familiarise the reader with *Plasmodium*, its history, treatment and energy metabolism.

2.1 Plasmodium Life Cycle

Traditionally four species of malaria, *Plasmodium vivax, malariae, falciparum* and *ovale*, are capable of infecting humans. Recently a fifth, the simian *P. knowlessi* has also been identified in humans[34]. The malarial parasite

is transmitted by the bite of an infected female *Anopheles* mosquito, which contains the sporozoite form of the parasite within its salivary glands[97]. An estimated 15-200 sporozoites are injected by the mosquito[154], which remain at the bite site for 5-15 min[134]. Sporozoites migrate through the dermis to a blood vessel and circulate until they reach the liver. They infect hepatocytes by crossing the sinusoidal cellular layer separating the blood and liver parenchyma[97]. This entire migration from skin to liver may be as short as 20 minutes[97]. The speed and selectivity of this process have indicated that sporozoite invasion of hepatocytes involves parasite-encoded surface proteins and host molecules[51]. The sporozoites form liver schizonts, which undergo schizogony - a series of nuclear divisions followed by cytokinesis[152]. Each mature schizont may, thus, release thousands of invasive merozoites into the blood stream[102]. *Plasmodium vivax* has a dormant, hypnozoite, stage where sporozoites can persist for long periods without undergoing schizogony[97]. The released merozoites invade erythrocytes, thereby initiating the asexual cycle of the parasite.

Within the erythrocyte, merozoites develop into trophozoites. The early trophozoite form is known as the ring stage. Trophozoites ingest the abundant haemoglobin of their host by an endocytic process[152]. After almost complete consumption of the erythrocyte, trophozoites undergo further schizogony and form multinucleated blood-stage schizonts. The latter undergo cell division to form up to 32 merozoites[152]. Rupturing of erythrocytes releases numerous merozoites, which consequently invade new erythrocytes.

During the asexual blood cycle not all parasites form merozoites, as some develop into male and female gametocytes[78]. These precursors of the gametocytes are dormant and are only activated if they are ingested by an *Anopheles* mosquito during a blood meal[78]. The formation of gametes within the mosquito midgut is followed by fertilization, resulting in a diploid zygote. The zygote undergoes a single round of meiotic division and develops into a motile ookinete, which penetrates the midgut and forms an oocyst on the basolateral lamina[78]. After growth and development, the oocyst may contain more than 10 000 sporozoites, which invade the salivary glands[78] and thus complete a full cycle.

2.2 Historical Overview: *Plasmodium* discovery and treatment history

Malaria, ague and "marsh fever" are just a few names for the disease which has plagued civilisations for millennia. Throughout the world, moist areas below 2000m in altitude and between the tropics of Capricorn and Cancer have been subject to malaria invasion[11].

Before the cause of malaria was known, the trademark and often fatal tertiary and quaternary chills and fevers of malaria were greatly feared. Romans and Greeks ascribed the fevers to different quantities of heat producing bile[58], or the presence of black bile which was supposedly released by the spleen[65]. Remedies thus predominantly consisted of phlebotomies and rest. Others believed that the fevers had divine origin[58] or that 'noxious air', which was typically found around insect plagued marshes, was responsible[65]. These beliefs and the fact that mosquito transmission was unsuspected hampered the discovery of a cure, as well as prevented the recruitment of mosquito preventative measures.

The extent to which malaria has impacted human history is debatable, but it certainly played a large role in European history, where it is held responsible for depopulation of important regions of early Rome as well as altering land utilisation methods in Italy[58]. Additionally, across Europe large tracts of land near marshes, swamp and coastal deltas had been rendered uninhabitable[65]. This highlights the significance of the discovery of the miraculous 'fever bark' during the early 1600's.
The bark of the cinchona tree (*Cinchona spp*) contains, amongst others, the alkaloid quinine, which cured malaria. The discovery of the foul-tasting and bitter bark is itself incredible since the tree was first discovered in the high foothills of the Andes where malaria never existed[115]. Twenty three *Cinchona spp* are known, although some scholars argue that eight of these are variants and thus only fifteen species occur[65]. It is known, however, that the quinine content differs substantially between species[65,115]. How or by whom the therapeutic effects of cinchona bark were discovered is not known exactly. Numerous legends exist, but discrepancies and irregularities go a long way in discrediting them[65]. Whether it was discovered by native South Americans,

the Jesuits or Spanish invaders is perhaps of little consequence compared to the magnitude of the discovery itself. Unfortunately, even though a bark infusion was successfully used to treat and cure infected patients in the early 1600's, the 'Peruvian bark', or 'Jesuits bark' was treated with skepticism in Europe and only gained widespread recognition as a cure for the ague during the late 1600's[65].

Once the bark was finally recognised as the malarial cure, the British, Dutch and Indian governments imported huge quantities of bark from South America to counter the widespread prevalence of malaria amongst their numerous colonies. The limited and unreliable cinchona bark supply from South America all but forced Britain, Netherlands, India and later the United States to go to great lengths to acquire plants and establish vast cinchona plantations. For an in depth coverage of the history of the cinchona discovery, procuration and cultivation, I refer the reader to *The fever trail: In search of the cure for malaria*[65].

In 1876 Dr Patrick Manson, a medical officer discovered the filarial parasite inside mosquitoes that had fed on soldiers infected with elephantiasis (a parasitic infection of the filarial worm). Even though he never discovered the transmission of the filarial worm from the mosquito to the human, he conveyed his findings of human to mosquito transmission to Sir Ronald Ross[65,115]. In 1880, Alphonse Laveran discovered 'certain parasitic elements' in his malarial patients. Ten years later, Ross, similar to the observations of Manson and Laveran, identified oocytes in the stomach wall of an *Anopheles* mosquito that had fed on a malaria infected patient. Ross also observed the avian malaria oocytes burst and sporozoites migrate to the salivary glands via the thoracic cavity[65,115] . These findings together with those of the malaria parasite being found in both the insect and human proved the dual host malarial life cycle. Ross is also responsible for fully recording the avian malaria parasite life cycle within the mosquito. Professor Giovanni Grassi, at Rome University was the first to note that *Plasmodium* was mosquito specific and the human infecting strains were restricted to the *Anopheles* mosquito[65,115] . In 1902, Ross received the Nobel Prize for his malaria work.

2.2.1 Antimalarial History

Soon after the discovery of quinine as the active compound in cinchona bark, chemists tried to synthesise it. During the first and second world wars, malaria ravaged troops due to the limited cinchona bark supply and the disruption of supply lines by hostile forces. The Germans, especially were desperate to find a synthetic compound and subsequently invested heavily in developing and finding suitable compounds[65]. In 1926 a German research team discovered the synthetic plasmochin and later in 1932, atabrine. These compounds, although effective were toxic with unpleasant side-effects. A breakthrough came in 1934 with the discovery of the 4-amino quinolines (resochin and sontochin), which similar to quinine, targeted the blood stage parasites, but much more rapidly[65]. Strangely, the formulas for these compounds where given to the Farben's American sister company, Winthrop Stearns, where they were shelved. During the second world war the shortage of quinine and the unpleasant side effects of new synthetics such as atabrine caused French doctors to suggest to the Americans that they look at sontochin again, since the French were using it successfully. Through sontochin, chloroquine was discovered and found to be identical to the resochin which had been shelved for 10 years. Chloroquine and its derivatives are arguably, to date, the most successful antimalarials being cheap to synthesise and highly effective against all forms of *Plasmodium*. In fact the development of the effective plasmodicals as well as the development of potent insecticides were thought to be the end of malaria plague, which is exemplified by the statement made by W.K Blackie in his book (1947) *Malaria: With Special Reference to the African Forms*[11], "The outlook for the future is thus full of promise...".

2.3 Current Malaria Drug Status

2.3.1 Drug Resistance

For approximately 20 years, chloroquine drove malaria back. Effective patient treatments and strict insecticide spraying regimes (notoriously with DDT) cleared Malaria from Europe, parts of Africa and most of North America. The

success of chloroquine was short-lived and in 1962 scientists noted resistance occuring in Vietnam, Thailand, Cambodia and Malaya[65]. During the Vietnam war, US medics started prescribing a a cocktail of chloroquine and primaquine to US soldiers in an attempt to overcome resistance. The rapidly mutating parasite soon rendered the cocktail ineffective.
A new line of drug was discovered and published by the Chinese in 1979. Artemisinin obtained from *Artemisia annua*, also known as *qing-hoa* or sweet wormwood, cured malaria, including chloroquine-resistant strains more rapidly and with less toxicity than chloroquine[65]. Artemisinin and its derivatives are currently the only drugs for which no real resistance is known, although the emergence of slight resistance may already be occuring in Cambodia[99].
To extend the therapeutic time of antimalarials the WHO suggests various combinations of the remaining effective drugs. The original idea by WHO to globally eradicate malaria has been replaced by the idea of 'rolling back malaria', which was initiated in 1998[140]. The Roll Back Malaria initiative aims to slowly, using preventative measures (e.g. mosquito netting and repellents), insecticides, education and treatment, push the boundaries of malaria back. The ability of *Plasmodium* and *Anopheles* to develop resistance to antimalarials and insecticides respectively, necessitates the development of novel drugs and insecticides. The need for substantial funding for this research is being realised with the initiation of NPOs such as, amongst others, the Medicines for Malaria Venture (MMV) and Global Fund to fight AIDS, Tuberculosis and Malaria (GFATM), Gates Foundation and the Wellcome Trust.

2.3.2 Current and Future Treatment and Prevention Regimes

2.3.2.1 Current Treatment Measures

There are three major antimalarial drug groups, namely the quinolines, pyrimethamines and artemisinins.
Drugs predominantly target the asexual blood stage of the parasite, although the 8-amino quinolines also target the liver stages via an unknown mechanism of action[57]. *P. vivax* and *P. ovale* produce dormant hypnozoites in the liver, which result in recurring malaria. The development of resistance to the only

known drugs that target the liver stage of the parasite is concerning and it is thus essential that new drugs target this stage. Development of antimalarials that target the liver stage is challenging due to the technical difficulty of establishing insectariums in order to produce sufficient numbers of sporozoite infected hepatocytes[57]. Why drugs that are effective against the asexual phase of the parasite are not against the sexual phase is unknown. It may be a question of target accessibility or differing metabolism.

Several drug targets in the asexual *Plasmodium* stages are known. Some have been localised to the cytosol (e.g. folate inhibitors, pyrimethane-sulfadoxine) or specific organelles such as the mitochondrian (atovaquone, tafenoquine), apicoplast (azithromycin, doxycycline) and digestive vacuole (falcipain inhibitors). Quinine and its derivatives (chloroquin, quinine, mefloquine) are thought to prevent haem detoxification and biomineralisation by forming complexes with haem[57,125]. Even though such a diverse range of sites have been targeted, resistance to all the drugs mentioned above exists, which has lead to a dramatic increase in malaria infections. Currently the only effective treatment is with the costly artemisinin and its derivatives (artemether, artesumate, artemotil). WHO proposes various combinations such as artemether / lumefantrine, artesunate / amodiaquin, artesunate / sulphadoxine-pyremethaminm, artesunate / mefloquine and amodiaquine / sulphadoxine-pyremethamine. These combinations have not only decreased the treatment course time from 7 days of artemisinin monotheraphy compared to three days of combination therapy[100] *teste*[158], but also increase the therapeutic time of the individual drugs. In theory two distinct modes of action should allow the combination therapy to overcome resistance to one of the drugs. The combination therapies are effective and well tolerated[158]. The real problem with the combination therapies is that they are more expensive, with the result that often less effective monotherapies are used. Poorer countries thus require large amounts of donor funding if malaria is to be pushed back and eradicated.

2.3.2.2 Malaria Prevention

The slow battle against malaria is being fought on numerous fronts including the killing or modification of the insect vector; prevention of transmission from

human to mosquito and *vice versa* and targeting sexual and asexual phases.

Malaria infection rates are directly coupled to the presence of infected female *Anopheles* mosquitos. The vector population density is a function of season and climate conditions, whereas the percentage of infected mosquitos would be a function of the number of infected human hosts near the vector population. Removal of the vector would, in essence, eradicate malaria, as evidenced by the success of intensive DDT spraying in the US and Europe. The ecological hazard of DDT, resulted in the preferred use of pyrethroid based insecticides. Resistance to these insecticides has, however, limited their effectiveness[140]. Indoor residual spraying is an effective means of removing the vector. Physical prevention of malaria by using insecticide treated bed nets has been shown to decrease child mortality substantially in Africa[48].
Since pyrethroids are the only licenced insecticides for the use on "insecticide treated bednets", the development of novel effective insecticides is required. The rapid reproduction rate of *Anopheles* has the disadvantage that even slight resistance to insecticides results in a rapid rebound of the vector population[25]. The development of combinations of pesticides may help in overcoming resistance for longer periods of time.
Novel methods of vector control is a field of active study. Understanding the mechanisms by which a mosquito selects a host, may lead to a means of attracting mosquitoes by making use of odorant receptors[86]. Genetic modification of the mosquito to induce resistance to malarial infection or by preventing development of the parasite within the mosquito may provide an novel method of *Plasmodium* control[39,93].

2.4 Drug Discovery

2.4.1 Future Treatment: Vaccine Development

The difficulty of distributing antimalarials, pesticides and insecticide treated bed nets in countries with poor medical and transportation infrastructure makes the idea of a malaria vaccine highly attractive. A vaccine that conferred total immunity for life, after one or two immunisations, would save millions of lives and go a long way in eradicating malaria globally. As of present the

perfect vaccine has remained elusive, due to the parasite's uncanny ability to vary its surface antigens[128]. Progress has been made, however, in developing vaccines against pre-erythrocytic parasites and liver stage parasites. These stages are accompanied by low numbers of parasites compared to the asexual phase and they do not portray clinical symptoms, which makes an appealing vaccine target[140].

Several stages of the *Plasmodium* life cycle within the human host, such as transmission, pre-erythrocytic, blood stage and gametocyte stages have been the target of vaccine development.
Pre-erythrocytic vaccines target the invading sporozoites and prevent them from infecting the hepatocytes. This stage is a highly appealing target, since it is asymptomatic. A promising randomised trial in Mozambique, involving over 2000 children under the age of five, showed that the vaccine prevented primary infection by *P. falciparum* by 45% and severe malaria by 58%[140].
Erythrocyte stage vaccines aim to prevent the merozoite invasion of erythrocytes. Merozoites have a number of antigenic surface proteins, but antigen polymorphism and the further difficulty in discovering other target antigens has impeded successful vaccine development[140]. Gametocyte stage vaccines would not aid in curing a patient, but would prevent transmission of parasite gametocytes to a vector mosquito. Such a vaccine used in combination with anti-malarial treatments or alternative stage vaccines would greatly aid in reducing the *Plasmodium* population within the mosquito population and thus indirectly reduce malaria infection rates.
An in depth review of malaria vaccine development is outside the scope of this work, I therefore refer the reader to the following reviews[57,128].

2.4.2 New Approach: Bioinformatics and Systems Biology

Drug discovery has progressed from the trial and error methods such as "try this plant", through isolated active components to high throughput screening of millions of compounds against a specific, or nonspecific target. Even though throughput has been dramatically increased, the number of new chemical entities reaching the market has not increased accordingly[38].
The availability of large databases containing qualitative and quantitative genomic, proteomic, metabolomic, molecular interaction data has given rise

to the development of analytical tools to integrate the data and extract useful information. This may lead to enhanced fundamental understanding, hypothesis testing, biotechnological innovation and drug discovery.

Since small changes in enzyme concentration (proteome) only lead to a small change in metabolic fluxes but may drastically alter metabolite concentrations, it has been proposed that studying the metabolism instead of the higher macromolecular 'omes' provides a more sensitive measure of changes brought about by disease or drug intervention[77]. Models of systems at a metabolic level are thus useful for drug discovery. Many models of systems at a metabolic level have been constructed and are available online for download (e.g BioModels - http://www.ebi.ac.uk/biomodels-main/) and/or interrogation (JWS Online - http://jjj.biochem.sun.ac.za/).
Two model analysis methods are mentioned throughout this thesis, namely metabolic control analysis and differential control analysis. Metabolic control analysis, founded by Kascer and Burns[74] and Heinrich and Rapoport[60], is a theoretical framework which quantifies the relative control of an enzyme on the steady state fluxes and metabolite concentrations. The framework moves away from the simplified view of a single 'rate-limiting' step and allows one to quantify the control contribution of each reaction step.
Differential control analysis is the comparison of the distribution of metabolic control in different models (e.g glycolysis models for *Trypanosoma* and erythrocyte) in an attempt to identify enzymes with high control in the parasite (*Trypanosoma*), but low control in the host[67].

Although all current models only cover a small portion of cellular metabolism, gene regulation, signaling pathways etc, the creation of a detailed silicon cell or organism is the ultimate goal. This is currently not possible with available experimental data, but models with a varying degree of detail have been constructed for whole cells, organs, regulatory networks, cell cycles and metabolic pathways.
It is generally accepted that *Plasmodium* is entirely dependent on glycolysis for energy during the asexual stages and this pathway is thus an attractive drug target, but its enzymes have been studied only in isolation. The construction of detailed glycolytic kinetic model will not only improve fundamental understanding of the pathway in terms of its regulation, but by using differential

control analysis can be used to identify potential drug targets.

2.5 Carbohydrate Metabolism

The malaria parasite's life cycle is complex and divided between the vertebrate and mosquito hosts and its carbohydrate metabolism is perfectly adapted to supply energy and intermediates for biosynthetic purposes. This project concentrates on the asexual stage of *Plasmodium* and as such this review covers the metabolism specific to the erythrocyte stage. During the asexual stage the erythrocyte serves two purposes: (i) as barrier from the immune system and (ii) as a source of metabolites. The parasite multiplies asexually, whilst actively digesting the erythrocyte haemoglobin for resources, before being released into the blood stream and infecting more red blood cells. Although the parasite has these salvage pathways which utilise the host resources, it is capable of certain *de novo* biosynthetic pathways, such as pyrimidine biosynthesis as well as having the ability to fix carbon dioxide.

Recently, the *P. falciparum* genome has been sequenced[54] and partially annotated[6]. However, there remains a lack of detailed knowledge regarding parasite metabolic pathways, enzymes in these pathways and structural information of the enzymes, has slowed the progress of innovative drug design. Understanding metabolic pathways, their regulation and metabolic control structures is essential for identifying key pathways and enzymes as drug targets. Enzymatic structural information is also indispensable, as host and parasites enzymes are often similar. Together pathway and structural information would allow researchers to potentially design specific and selective antimalarials, although differential control analysis between parasite and host may reveal targets that could be targeted selectively (drug selectively targets an enzyme), without the need for specificity (drug can inhibit both host and pathogen enzyme).
This review explores the carbohydrate metabolism (Fig. 2.1.) of the asexual *Plasmodium* and covers what is currently known about glycolysis, the pentose phosphate pathway and how these pathways are linked, together with the tricarboxylic acid cycle (Fig. 2.2.), to the electron transport chain. Since these pathways are also integrally linked to carbon dioxide fixation and the

purine salvage pathway these auxiliary pathways will also be briefly examined. Enzymes found in these metabolic pathways will be discussed with specific focus on their enzymatic characterisation, regulation and potential as drug targets.

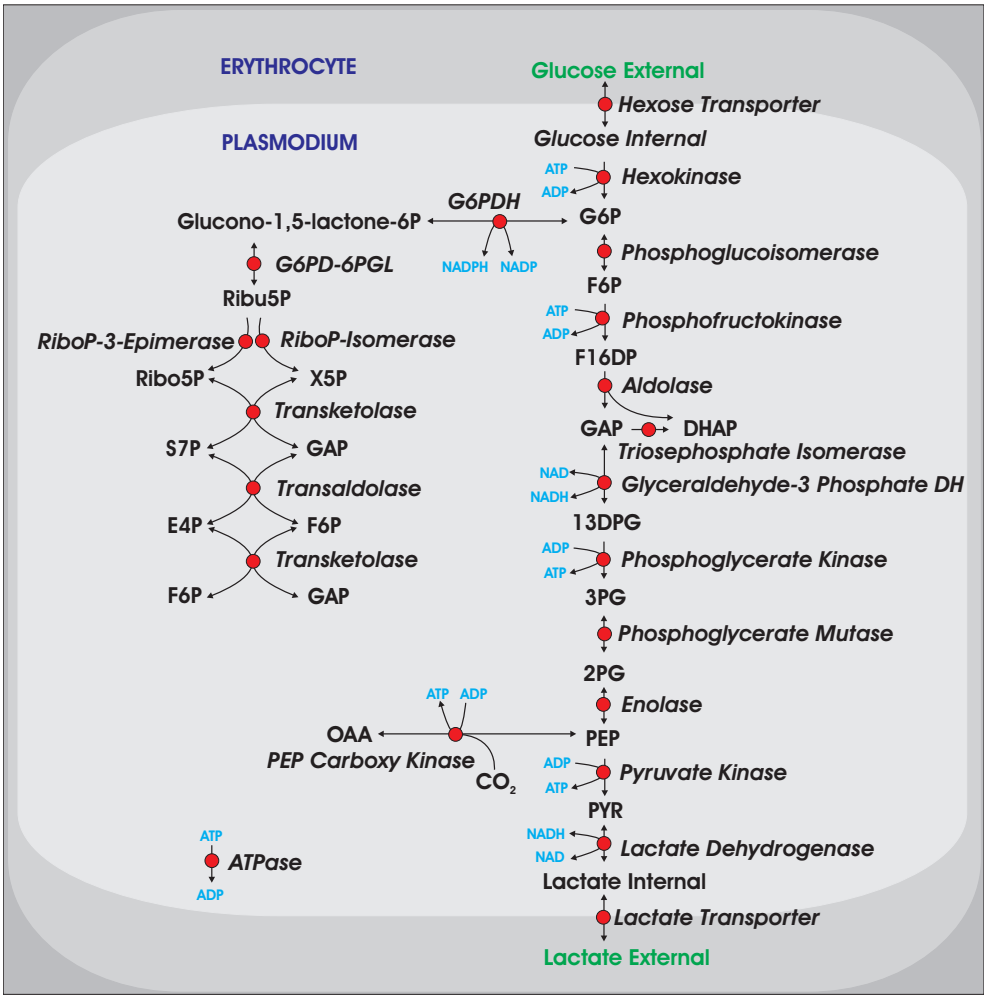

Figure 2.1: Schematic representation glycolysis, pentose phosphate pathway and carbon dioxide fixation in *Plasmodium*. The parasite and erythrocyte compartments are shown in different shades of grey. Enzymatic steps are portrayed as red circles and the enzyme names are shown in italics. See text for details.

2.5.1 Glycolysis

During the asexual phases all *Plasmodium* species are entirely dependent on glycolysis for ATP production[132]. It is for this reason that a great deal of research has been directed at characterising the enzymes of the glycolytic pathway (Fig. 2.1.) in an attempt to gain a better understanding of the pathway and to develop effective inhibitors. The asexual stages of malaria store no reduced carbon (energy) reserves and consequently the malarial parasite utilises glucose from the host serum[110,129]. Glucose is rapidly taken up by parasitised erythrocytes, where it is metabolised. In fact, upon infection glucose uptake has been shown to increase as much as 100 fold[87], inducing a significant increase in glycolytic flux[110]. It is, expected, however, that the rate of glucose uptake would be dependent on malarial species and experimental conditions. It has been shown that *P. falciparum* requires glucose or fructose[161,82] for growth, and cannot utilise ribose, mannose or galactose as a carbohydrate source[87].

Nearly all glucose, used by *Plasmodium*, passes through the anaerobic glycolytic pathway, with a net yield of two moles ATP and two moles lactate per mole glucose[129]. Indeed, the almost total conversion of glucose to lactate was initially presumed to indicate that the pentose phosphate pathway (PPP) did not exist, although it is now known that there is a low flux (relative to glycolysis) through the PPP.

The considerable increase in glucose uptake and rapid production of lactate necessitates an efficient transport system. Sufficient glucose needs to be taken from the blood to support the rapidly multiplying parasite. Additionally, excessive lactate buildup in the cell is toxic and the parasite thus has an efficient export system. Although, strictly speaking, hexose and lactate transport would not fall under glycolysis, these transport steps are an integral part of the pathway and thus warrant their inclusion.

2.5.1.1 Hexose transport

It has been reported that there is an approximate 100-fold increase in glucose uptake by erythrocytes infected with maturing asexual parasites[132]. Glucose

and fructose are transported into the erythrocyte via GLUT1 and GLUT5 respectively. The high density of the rapid transport protein in the erythrocyte membrane results in a glucose transport capacity that easily supplies the demand of the parasite[80]. Within the erythrocyte, the parasite has a hexose transporter, PHT1[161]. This transporter was expressed in *Xenopus oocytes* and shown to be a saturable, sodium-independent, and stereospecific transporter of both glucose and fructose[162]. The *P. vivax* and *P. falciparum* transporters, PvHT1 and PfHT1 respectively, have been kinetically characterised[69,70,161,162]. The hexose transporters' of *P. knowlesi* (simian) and *P. yoelii* (murine) have also been kinetically characterised[71]. Immunofluorescence microscopy has shown that PfHT1 resides in the parasite plasma membrane and not in the erythrocyte membrane[162]. Glucose and fructose are thus thought to cross the parasitophorous vacuolar membrane to the parasite plasma membrane via high-capacity non-selective channels[82].

It has been established that PfHt1 is a single copy gene with no close homologues[162]. Expression of the single PfHt1 transcript varies throughout the *P. falciparum* life cycle with mRNA levels peaking 8h post invasion of the erythrocytes.[162].

Inhibition of parasitic glucose uptake immediately leads to a decrease in ATP levels[161]. The potential of PfHT1 as a drug target has been examined with inhibitors in several studies[71,124,69,70] and reviewed by Patel *et al*[109].

2.5.1.2 Lactate Transport

In uninfected erythrocytes, lactate crosses the plasma membrane to the blood stream via three major pathways: (i) a specific H^+ monocarboxylate transporter, (ii) the band 3 anion exchanger, and (iii) by diffusion of the protonated form across the lipid bilayer[80]. The capacity of these transport systems, however, has been calculated to be inadequate for the removal of lactate produced by *Plasmodium* glycolysis in parasitised erythrocytes[75,80]. Studies have demonstrated that even when the aforementioned transporters are inhibited, there is still a rapid flux across the parasite erythrocyte membrane. This transport has been attributed to anion-selective diffusion pathways and a lactate-proton cotransporter[35,75,80]. The latter has been shown be a member of the monocarboxylate transporter (MCT) family[43]. Once the lactate is transported to the erythrocyte cytosol it is exported to the bloodstream via

the erythrocyte transporters and new anion-selective channels, induced by the parasite[35,43].

2.5.1.3 Glycolytic enzymes

"Many of the glycolytic enzymes occur as isozymes, each having different affinity (K_m) for the substrate and different V_{max} as well as different regulatory pathways"[129]. This is a significant factor in drug development, as inhibition of specific isozymes may not inhibit all the isozymes and drug potency may be reduced.
The next section will broadly review the current knowledge of the *Plasmodium* glycolytic enzymes - hexokinase, phosphoglucose isomerase (PGI), phosphofructokinase (PFK), aldolase, triose phosphate isomerase (TIM), glyceraldehyde-phosphate dehydrogenase (GAPDH), phosphoglycerate kinase (PGK), phosphoglycerate mutase (PGM), enolase, pyruvate kinase (PK) and lactate dehydrogenase (LDH). Selected kinetic parameters that have been published are tabulated at the end of the enzyme subsections in Table 2.1.

2.5.1.4 Hexokinase

The first reaction in glycolysis is catalysed by hexokinase, which phosphorylates glucose in an ATP dependent reaction, yielding glucose-6-phosphate (G6P) and ADP. The hexokinase gene, in *P. falciparum*, is located on chromosome 8, and is only 26% homologous to the human hexokinase[104,129] and codes for a 54 kDa protein[129].
Plasmodium hexokinase activity has been identified in extracts of infected erythrocytes[119,129,132]. Hexokinase activity in *P. berghei* isolates (thus including erythrocyte hexokinase) was 35 times higher than in uninfected erythrocytes[84]. Roth *et al.*[119] reported that *P. falciparum* infected erythrocytes had a 25-fold increase in hexokinase activity, compared to normal erythrocytes.
The enzyme has been partially kinetically characterised and it is reported that the parasitic enzyme has a lower K_m for glucose compared to human hexokinase[119]. For ATP, hexokinase had a K_m of 2 mM in *P. berghei*[84]. Regulation of this enzyme has not been studied, although glucose-6-phosphate is known to have feedback inhibition in some instances[144]. It has also been shown in the filarial roundworm, *Brugia malayi*, to be inhibited by ADP and

activated by glucose-6-phosphate[135].
Hexokinase has not been proposed as a drug target, although this enzyme has a high control on the glycolytic flux in some glycolytic models and thus, together with the poor homology to the human hexokinase, presents a potential drug target.

2.5.1.5 Phosphoglucose Isomerase

PGI catalyses the conversion of G6P to fructose-6-phosphate (F6P). *P. falciparum* isolates were shown to have three or four isozymes of PGI[138]. Upon erythrocyte infection by *P. falciparum*, PGI activity increases 4-9 fold[138].
Plasmodium PGI has a molecular mass of 66 kDA and is 34% homologous to the human enzyme[138], with the highest degree of similarity in the active sites[129]. The PGI gene of *P. falciparum* was cloned, characterised and expressed in *E. coli*. The gene was mapped to chromosome 18[76]. The high homology between the parasite and host enzyme at the active sites and the fact that PGI typically has a low metabolic control of the flux and intermediate concentrations is probably the reason that research has not been directed at inhibiting this enzyme. It is interesting to note, however, that antiserum raised against the enzyme, specifically inhibits parasite PGI activity, with no observed inhibition of the host enzyme[138].

2.5.1.6 Phosphofructokinase

PFK catalyses the phosphorylation of F6P to form fructose 1, 6-bisphosphate (F1,6BP). PFK from *P. berghei* has been isolated from infected erythrocytes and kinetically characterised in detail[17,18,19]. PFK is regulated by various ions and metabolites and is typically inhibited by ATP, phosphoenolpyruvate (PEP), 2,3-bisphosphoglycerate, citrate and activated by AMP, F6P, ADP, F1,6BP and fructose 2,6-bisphosphate[148] *teste*[17]. *Plasmodium*, however appears to have a unique mode of regulation and *P. berghei* PFK is inhibited strongly by ATP and Mg^{2+} ions and is activated by PEP, F6P and inorganic phosphate[17,18,19,20].
Various tissue specific isozymes are known for human tissues[41] but whether or not they exist within *Plasmodium* is unknown.

2.5.1.7 Aldolase

Aldolase catalyses the aldol cleavage of F1,6BP into dihydroxyacetone phosphate (DHAP) and glyceraldehyde-3-phosphate (GAP). Both *P. berghei* and *P. falciparum* aldolase proteins have been cloned, sequenced and expressed in *E. coli*[40,96]. The class I homotetrameric enzyme has a molecular mass of 160 kDa[79]. Only a single aldolase gene is present in *Plasmodium*[31]. The *P. falciparum* gene sequence, which codes for aldolase, is approximately 50% homologous to the three human isozymes[129].

Extremely high aldolase activity has been observed in *P. falciparum* infected erythrocytes, with peak activity between 32-36 hours[68,103,104]. This typically corresponds with the mature trophozoite stage, of the 48-hour blood-stage life cycle[157]. The peak aldolase activity corresponded to peak aldolase mRNA concentration, indicating transcriptional regulation[157]. This prompted Wanidworanun *et al.*[157] to test the antiplasmodial effect of several phosphorothioate antisense oligodeoxynucleotides (ODNs), which targeted several sites on the aldolase gene of *P. falciparum*. Nanomolar concentrations of ODN, targeting the gene splice donor site, resulted in 50% inhibition of parasitemia. It was suggested that a combination of ODNs, targeting different sites of the gene, might result in higher levels of inhibition[157].

The aldolase crystal structure of *P. falciparum*[79] revealed several potential drug targets. A specific area that differentiates the human and malarial aldolase, is a highly variable tail in the C-terminal region[110]. The tail has two consecutive Lys residues, which may be a target for drug design[110]. Interestingly, substituting the two lysine residues with the corresponding host amino acids, increased the catalytic rate[68]. The tail has been shown to be important for enzymatic catalysis[40], which increases its potential as a drug target.

Another difference is the presence of the, so-called, 290s loop. The loop forms part of a binding pocket, in conjunction with two nearby loops[110]. The binding pocket appears more hydrophobic and constricted than human isozyme A[110], which may be a property that can be utilised in inhibition design. There may be an interaction between the C-terminal tail and the binding pocket, as they are located close together[79]. Designing small hydrophobic inhibitors that bind to the binding pocket, and interact with the lysine residues, may selectively inhibit the parasite enzyme[79]. It is shown that, in mammalian cells, PFK,

aldolase and glyceraldehyde-3-phosphate (GAP) dehydrogenase are associated with cytoskeleton elements[110].

2.5.1.8 Triosephosphate isomerase

TIM catalyses the inter-conversion of DHAP and GAP. In *P. falciparum* the TIM gene is located on chromosome 14. It has been cloned, sequenced and expressed in *E. coli*[111]. The enzyme has been partially characterised in terms of its kinetics where the affinity of GAP was determined[91]. The gene has a single intron and is 42-45% homologous to TIM genes from other sources[129]. The enzyme is a dimer with a molecular mass of 28 kDa. The crystal structure of *P. falciparum* TIM was resolved at 2.2 Å[156]. A more recent crystal structure of TIM in complex with phosphoglycerate was resolved at 1.1 Å[108]. The structures revealed several differences between the human and parasite enzyme. Ser 96, which is conserved in most species, is replaced by Phe in the plasmodial enzyme[110]. Another highly conserved charged surface residue, Glu 183 is replaced by hydrophobic Leu in the parasite enzyme[110], which exposes a hydrophobic patch at a position adjacent to a positively charged region[156]. Met 13, which is found at the dimer interface of the human enzyme, is replaced by Cys 13[156]. The differences are being probed as potential drug targets as they may potentially, offer selectivity.

Although Met 13 at the dimer interface has not been directly targeted,[136] peptides, corresponding to residues 9-18 and 68-79, have been designed to bind at the dimer interface. The peptide that contained residues 68-79 had an IC_{50} range of 0.6 μM, which shows the potential of drugs designed to disrupt subunit interactions. A hydrophobic anionic molecule targeting the surface region of Leu 183 may specifically inhibit the parasite enzyme[156]. This led Joubert *et al.*[73] to look at anionic sulfonated dyes, some of which inhibited TIM at concentrations of less than 100 mM.

The TIM active site has an active site loop, called loop 6 (residues 166-176), which is capable of considerable movement and essential to catalysis[108]. Phe 96 appears to impede loop closure due to a steric clash with Ile 170 in loop 6[110], although both open and closed conformations were observed in a crystal structure of TIM-2-phosphoglycolate[108]. Since Phe 96 is unique to *Plasmodium* and interacts with the catalytic loop, it may show great potential as a drug target. Strategies for potentially inhibiting this enzyme are reviewed

by Ravindra *et al*[112].

2.5.1.9 Glyceraldehyde-3-phosphate dehydrogenase

This enzyme catalyses the conversion of GAP, P_i and NAD to 1,3-bisphosphoglycerate and NADH. It has been identified in the avian infecting species, *P. cathemerium* and *P. gallinaceum*[132] and in the case of *P. falciparum*, cloned and expressed in *E. coli*[37]. The estimated 36.6 kDa protein has 63.5% identity to the erythrocyte GAPDH[37]. The enzyme has not, as yet, been kinetically characterised.

2.5.1.10 Phosphoglycerate Kinase

PGK converts 1,3-phospoglycerate to 3-phosphoglycerate. Two isoenzymes of PGK have been isolated from *P. falciparum*[129]. This 45kDa protein is distinct from the host enzyme with differing isoelectric point, K_m, V_{max} and immunologic epitopes[129]. The gene is 60% homologous to other eukaryotic enzymes and found on chromosome 9[129]. Recently, the enzyme has been kinetically characterised and crystallised[106]. Some inhibitory studies have been performed and suramin was found to inhibit PGK expressed in *E. coli* with an IC_{50} of 7 μM[106].

2.5.1.11 Phosphoglycerate Mutase

The conversion of 3-phosphoglycerate to 2-phosphoglycerate is catalysed by PGM. The parasite enzyme has not been isolated or characterised, but a putative gene coding for PGM has been identified in *P. falciparum 3D7*[6].

2.5.1.12 Enolase

Enolase catalyses the inter-conversion of 2-phosphoglycerate and phospho-enolpyruvate. Enolase activity in *P. falciparum* infected red cells was found to be 15 times higher than uninfected erythrocytes[129]. The enolase gene has been

isolated, characterised and been mapped to chromosome 10[107,113]. The gene is 60-70% homologous to other eukaryotic enolase enzymes[113]. The enzyme is a homodimer, with a molecular size of 100 kDa[107]. For activity, enolase requires the binding of two bivalent cations (Mg^{2+} *in vivo*), per subunit[107]. The binding at site I leads to a conformational change within the enzyme, whereas binding at site II is essential for catalysis[46]. At high concentrations, bivalent cations inhibit enzyme activity, which suggest the presence of a third inhibitory site[107]. Enolase has been kinetically characterised for *P. falciparum* and binding constants for both substrate and product determined. It was also found that enolase is strongly activated by Mg^{2+}, slightly by K^{+} and inhibited by Na^{+}[107].

2.5.1.13 Pyruvate Kinase

Pyruvate kinase catalyses the substrate level phosphorylation of ADP, using phosphoenolpyruvate and producing pyruvate and ATP. Pyruvate kinase activity was identified in the *P. falciparum* infected human erythrocytes[117] and *P. berghei* infected mice erythrocytes[17]. The enzyme activity appears to increase over 11-fold upon infection[117] and is highly regulated in protozoan parasites, such as *Toxoplasma gondii*, *Trypanosoma brucei* and *Leishmania mexicana*[44,45,90] and *Plasmodium*[27].
Plasmodium possesses two pyruvate kinases (PK1 and PK2), which are both expressed during the asexual phase[28]. PK1 expression is constant and continually high throughout the asexual phase, whereas PK2 expression peaks at approximately 20h post invasion. The expression profile of PK2 appears to follow the apicoplast lipid sythesis genes[28]. Since pyruvate kinase does exist within the apicoplast[109], which is the site of lipid synthesis it may be that PK2 is in fact, localised to this organelle. The isozymes have low amino sequence identity (20%) and it appears that PK2 is unique to the Apicomplexans[28] and the proteins differ in size being 55.6 and 86.6 kDa respectively. It should be possible to determine the localisation of the isozymes using fluorescently tagged antibodies raised against the individual isozymes.

The pyruvate kinase of *P. falciparum* has been cloned, isolated, kinetically characterised and found to be competitively inhibited by ATP with respect to PEP and non-competitively inhibited by citrate[27]. Pyruvate kinase appears

not to be activated by F1,6BP[27], which is a common activator in other species[150]. The insensitivity to F1,6BP may be due to the Lys-Glu 418 substitution. Lys 418 is thought to be involved in the binding the 6-phosphate moiety of F1,6BP, but the malarial enzyme has a glutamate residue in this position[27].

2.5.1.14 Lactate dehydrogenase

LDH is responsible for the recycling of NAD^+ from NADH by reducing the keto group of pyruvate to a hydroxyl group (lactate). Since the energy metabolism is anaerobic glycolysis, the LDH of *P. falciparum* it has been proposed as a potential drug target. Inhibition of LDH has been shown to kill the parasite[120], presumably by preventing the recycling of NAD^+, which in turn prevents ATP production.

P. falciparum LDH is coded by a single gene (1.6 kb mRNA) on chromosome 13[22]. The 316 amino acid protein has a molecular mass of 33 kDa[22]. The parasitic enzyme has been extensively kinetically characterised[15,26,133,160]. Although it was initially thought that LDH was not inhibited by pyruvate as in some organisms[129], it has since been found that *Plasmodium* LDH is weakly inhibited by pyruvate at high concentrations with a K_i of 140mM[133]. The kinetic mechanism has been determined to be an ordered bi-bi mechanism with the coenzyme binding first[133].

A wealth of structural information is available for *Plasmodium* and human LDH. The crystal structure of *P. vivax* LDH in complex with NADH and 3-acetylpyridine adenine dinucleotide (APADH) has been determined[26]. The crystal structure of *P. berghei* LDH has been solved to resolution of 2.3 Å[160]. The crystal structures *P. falciparum*, *P. vivax* and *P. brucei* are highly similar, with no significant alterations observed in the active site or cofactor-binding pocket[15,26]. It is thus likely that inhibitors targeting malarial LDH would be effective across the *Plasmodium* genus[26]. The structures of the heart (H) and muscle (M) forms of human LDH's have also been solved[14].

Comparison between the *P. falciparum* and human LDH crystal structures reveals a shift in the positioning of the NADH cofactor and a larger active site[14,42,95], the latter due to a five amino acid extension of the substrate-binding loop[42].

The problem of selective inhibition of LDH is compounded by the high levels

of LDH present in the infected erythrocyte[95], which requires high potency inhibitors. Gossypol, a polyphenolic binaphthyl disequiterpene found in cottonseed oil, has been shown to inhibit LDH's at submicromolar (0.7 μM) levels[120]. It binds competitively to NADH and displays anti-malarial activity *in vitro*[56], with an IC_{50} of 10 μM[14]. Unfortunately, gossypol is cytotoxic. Derivatives of gossypol have been synthesised in an attempt to decrease toxicity, as well as maintain potency. Napthoic acid based compounds, such as 2,6-dicarboxy naphthalene, have been shown to span across the LDH active site and NADH binding pocket[14]. The malarial and human LDH are very similar and few unique properties exist, which makes selective targeting extremely challenging. There are, however, significant kinetic differences between the human and *P. falciparum* LDH[14], which may be exploited.

2.5.1.15 Kinetic Parameters Present in Literature

The kinetic parameters that were obtained during the literature study are summarised below in Table 2.1. Most of the glycolytic enzymes for *Plasmodium* have been fully or partially characterised, although no kinetic parameters were available for glyceraldehyde 3-phosphate dehydrogenase or phosphoglycerate mutase.

2.5.2 Tricarboxylic Acid Cycle

"The tricarboxylic acid (TCA) cycle is the central wheel of mitochondrial metabolism"[153]. The classical TCA cycle (Fig. 2.2.) occurs in aerobic conditions and utilises acetyl-CoA, produced from glycolytic pyruvate. Acetyl-CoA combines with oxaloacetate, to produce citrate. Citrate is broken down by several steps that produce CO_2, NADH, $FADH_2$, GTP, and ultimately oxaloacetate. NADH and $FADH_2$ are used as electron donors in the electron transport chain (ETC) to generate ATP. Experimentation and analysis of the *Plasmodium* genome has revealed all the classical or equivalent TCA enzymes (reviewed in[153])

The existence or absence of a functional TCA cycle during the asexual stage is still an area of discussion, although it is thought not to contribute much, if at all, towards energy production during the asexual phase. Radioactive

Table 2.1: Binding constants present in literature for *Plasmodium spp.*

Enzyme	Metabolite K_m (mM)				Reference
Hexokinase	Glucose [1]	0.431	ATP	2.0	[104,119]
Phosphoglucoisomerase	F6P [2]	0.258	-		[138]
Phosphofructokinase	F6P	0.032	ATP	0.720	[19,18,17]
Aldolase	FBP	0.020	-		[40]
Triosephosphate Isomerase	GAP	0.350	-		[136]
Glyceraldehyde 3 PDH	-		-		
Phosphoglycerate Kinase	ADP	0.300	BPG	0.0134	[106,118]
Phosphoglycerate Kinase	ATP	0.630	3PGA	0.52	[106,118]
Phosphoglycerate Mutase	-		-		
Enolase	2PGA	0.041	PEP	0.250	[107]
Pyruvate Kinase	PEP	0.337	ADP	0.149	[27]
Lactate Dehydrogenase	Pyr	0.030	NAD	0.086	[56]
Lactate Dehydrogenae	Lac	12	NADH	0.007	[56]
Lactate Dehydrogenase	Pyr	0.055	NAD	0.180	[133]
Lactate Dehydrogenase	Lac	47	NADH	0.011	[133]

[1] *Binding constant determined from lysed Plasmodium-infected erythrocytes and is a function of both Plasmodium and erythrocyte enzyme binding.*

[2] *Average value of three isozymes shown. Standard deviation of the mean is 0.026*

glucose, fed to *P. falciparum* infected erythrocytes, is converted predominantly to lactate with minimal conversion to TCA intermediates[8,21], which suggests that the TCA cycle is not active during the erythrocyte stage of the parasite[153]. Additionally, *Plasmodium* does not have a known accessible source of acetyl-CoA for the TCA cycle. The formation of acetyl-CoA from pyruvate, in most eukaryotes, is catalysed by pyruvate dehydrogenase (PDH) complex, a large muti-enzyme complex localised in the mitochondrion. Plants possess two distinct PDH complexes. One in a plastid, to supply acetyl-CoA for fatty acid biosynthesis, the other in the mitochondrion to supply intermediates for the TCA cycle[50]. *P. falciparum*, however, possesses only one PDH complex located in the apicoplast[50]. The PDH complex in the apicoplast, prevents the supply of acetyl-CoA to the TCA cycle and is thought to play a role in fatty acid biosynthesis[50]. Furthermore, it appears that β-oxidation of fatty acids, which produces acetyl-CoA, does not occur in *Plasmodium*[153]. Percoll density gradient and fluorescence -activated organelle sorting techniques were unable to separate the apicoplast from the mitochondria leading to the suggestion

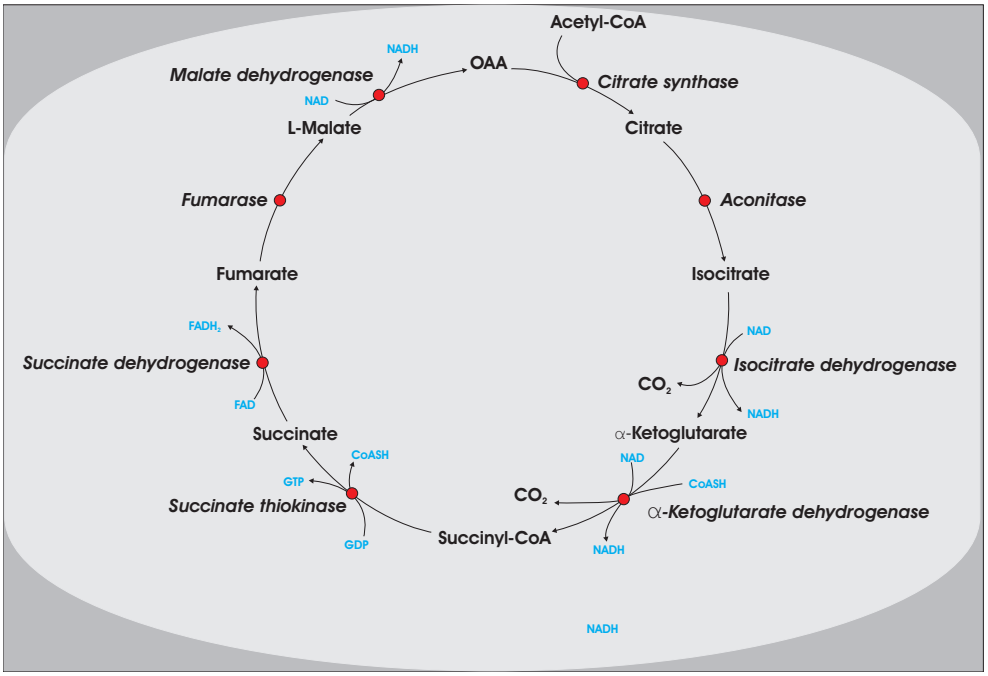

Figure 2.2: Schematic representation of the classical tricarboxylic acid cycle. See text for details.

that these organelles are physically connected[81]. If this is indeed the case, it may be possible that acetyl-coA from the apicoplast is accessible to the mitochondrion. In other organisms, acetyl-CoA may come from the catabolism of amino acids, such as leucine and isoleucine, but not all the enzymes required for this catabolic process are present in the genome of *P. falciparum*[153].

During the asexual stages of the parasite, the TCA cycle is possibly starved of acetyl-CoA, which suggests that it does not play a role in energy metabolism. During the erythrocyte stage this is highly likely, as the electron transport chain has been shown to be essential for maintaining a mitochondrial membrane potential, but not required as a source of ATP[105].
An incomplete TCA cycle could, however, fulfill an anapleurotic function. For example, glutamate can be converted to α-ketoglutarate, which in the TCA cycle will yield NADH, two molecules of $FADH_2$ and GTP. The active degradation of the host cell by the parasite yields a vast supply of amino acids, which could be channeled into the TCA cycle as a source of extra energy or anapleurotic metabolites. The incomplete cycle would result in the

accumulation of oxaloacetate, which would have to be transported out of the mitochondrion, or diverted to biosynthetic processes[153].

2.5.2.1 Mitochondria and Electron Transport Chain

A single mitochondrium is present during the entire *Plasmodium* life cycle with the presence of cristae in avian malarial species, but obvious cristae are lacking in mammalian *Plasmodium* parasites[153]. *Plasmodium* contains the smallest mitochondrial genome ever reported at 6-kb, which encodes three open reading frames[149,47].
The function of the mitochondria during the sexual stages has not been elucidated and the function during the asexual stages remains obscure, but it does not contribute much to the cellular ATP pool[52].
The *Plasmodium* ETC is similar to the classical ETC in many respects, as it possesses homologues of complex III and IV[153]. *Plasmodium* does not possess the usual rotenone-sensitive complex I, but instead has an alternative complex I (type II NADH : dehydrogenase)[54,10]. Evidence for a complete F_1F_0ATP Synthase is lacking, as only the five subunits of the F_1 subunit have conserved homologues in the *P. falciparum* genome[153].
The major role of the electron transport chain appears to be an electron sink, by regenerating ubiquinone, for the dihydroorotate dehydrogenase reaction in the pyrimidine biosynthesis pathway. This was proven in an elegant manner by Painter *et al*[105] who demonstrated that *P. falciparum*, expressing *S. cerevisiae* dihidroorotate dehydrogenase (which does not require ubiquinone as an electron acceptor) is completely resistant to ETC inhibitors.

The small mitochondrial genome would point towards the absence of many classical mitchondrial functions. *Plasmodium* is exquisitely sensitive to compounds removing the membrane potential[105], but since mitochondrial ATP production is not essential the importance of this membrane potential is not known. It has, however, been proposed to be essential for cellular calcium homoeostasis[153].

2.5.3 Pentose Phosphate Pathway

During the erythrocytic stages of the Plasmodium life cycle, the parasite is engaged in intensive nucleotide synthesis and is subjected to endogenously produced oxidative radicals[12]. The rapidly dividing parasitic cells require, in addition to ATP, reducing power in the form of NAPDH[12]. NADPH is used in a variety of important reactions, such as the conversion of ribonucleotides to deoxyribonucleotides, catalysed by ribonucleotide reductase. The pentose phosphate pathway (Fig. 2.1.) is essential for the production of nucleotides and for the detoxification of the oxidative radicals. The detoxification mechanisms, discussed later (Section 2.5.3.3: Link to Oxidative Defense), are largely dependent on NADPH. The PPP serves to convert G6P to ribose-5-phosphate, the latter being used by *Plasmodium* for nucleotide biosynthesis[129,12]. The PPP is important for the production of NADPH, which serves as an electron donor in reductive biosynthesis. The pathway can be divided into an oxidative and non-oxidative branch:

2.5.3.1 Oxidative Branch

The oxidative branch is the first part of the pathway and utilises G6P as a substrate. The oxidative branch produces two molecules of NADPH and ribulose-5-phosphate. Isomerisation of the latter, by ribose phosphate isomerase or ribulose-phosphate-3-epimerase, yields ribose-5-phosphate and xylulose-5-phosphate, respectively. The classical branch consists of three enzymes: glucose-6-phosphate-1-dehydrogenase (G6PD), 6-phosphogluconolactononase (6PGL) and 6-phosphogluconate dehydrogenase[12]. In *P. falciparum* and *P. berghei*, however, an enzyme with both 6-phosphogluconolactononase and 6-phosphogluconate dehydrogenase activity was discovered[29]. This finding indicated the existence of a bifunctional G6PD-6PGL in *Plasmodium*[29].

2.5.3.2 Non-oxidative Branch

The non-oxidative branch of PPP is primarily for the production of 3, 5 and 7-carbon sugars, which may be used for biosynthetic purposes, or channeled into glycolysis for energy production. The first step in the non-oxidative branch, catalysed by transketolase, is the conjunction of ribose-

5-phosphate and a 2-carbon fragment from xylulose-5-phosphate. This reaction yields sedoheptulose-7-phosphate and GAP[12]. The second reaction is catalysed by transaldolase and involves the transfer of three carbons from sedoheptulose-7-phosphate to GAP, yielding erythrose-4-phosphate and fructose-6-phosphate[12]. Transketolase catalyses a further reaction where another molecule of xylulose-5-phosphate donates two carbon atoms to erythrose-4-phosphate, yielding an additional molecule of GAP and F6P. Erythrose-4-phosphate can be fed into the shikimate pathway[12].

The purine salvage pathway, discussed later, can generate five-carbon sugars (e.g. ribose-1-phosphate) and is linked to the PPP, since the sugars can be converted to the glycolytic intermediates F6P and GAP[12].

The flux through the PPP is dependent on enzyme expression and the cellular NADPH/$NADP^+$ ratio[8]. The reduced coenzyme NADPH inhibits G6PD-6PGL, thus inhibiting the oxidative branch of the PPP. The PPP provides a way to adapt to and supply the reductive and intermediate demands of the parasite. During periods where the parasite requires both NADPH and ATP, but not much R5P, the oxidative and non-oxidative branch run to completion, with the resultant GAP and F6P being fed back into the glycolytic pathway. When R5P is required in large quantities, the oxidative pathway is utilised and F6P and GAP from the glycolytic pathway can be used to produce R5P[12].

The non-oxidative pathway can function in reverse, utilising glyceraldhyde 3-phosphate and F6P from the glycolytic pathway to produce ribose-5-phosphate (R5P).

This has been shown to occur in *P. falciparum* by measuring incorporation of [1-14C] glucose into nucleotides in G6PD deficient parasites[5]. It was reported that 80% of the glucose incorporated into the nucleic acids comes from the condensation of F6P and GAP.

A study based on metabolic labeling studies reported that *P. falciparum* infected erythrocyte cells had a 78 fold increase in PPP activity, relative to uninfected cells[5]. The parasites contributed 82% towards the PPP activity and stimulated host activity, presumably in response to oxidative stress and parasite burden.

2.5.3.3 Link to the Oxidative Defense

The importance of the PPP in defence against reactive oxygen species (ROS) is apparent when one has a look at the utilisation of NADPH in the oxidative defence mechanisms. Degradation of haemoglobin provides the parasite with amino acids and creates sufficient space for parasite growth[9]. The degradation of haemoglobin in the acidic food vacuole produces toxic free oxidised haem (ferri/ferroprotoporphyrin IX; FP) and ROS. The acidic environment oxidises the FP in oxyhaemoglobin from the Fe (II) to Fe (III) state, which "consequently results in the formation of superoxide that dismutates spontaneously to H_2O_2 and O_2"[9]. Both FP and H_2O_2 need to be detoxified by the parasite. FP is detoxified by biomineralisation, a process where FP is converted into a crystalline form, known as haemozoin[9]. It is likely that some FP escapes crystallisation and diffuses into the parasite cytoplasm[129]. It has been shown that FP can be present at 100 mM and concentrations lower than this have been shown to inhibit parasite enzymes, lyse erythrocytes and cause substantial redox damage[9]. It is thus essential for the parasite to detoxify free FP.
Glutathione (GSH) and thioredoxin-dependent proteins play an integral role in this detoxification. These proteins are oxidised by peroxides, the latter being converted to H_2O and O_2. The oxidised proteins are reduced again by NADPH, thus producing a continuous detoxification mechanism, provided there is sufficient NADPH. The PPP is responsible for the reduction of $NADP^+$ to NADPH, and is thus essential to the detoxification mechanism.

Despite the importance of the PPP for the survival of the parasite, research aimed at inhibiting enzymes in the pathway is extremely limited. Compared to the vast amount of information existing for the glycolytic pathway, structural and kinetic data for the PPP is sparse, which may explain why researchers have preferred to focusing on the inhibition of glycolytic enzymes.

2.5.3.4 Pentose Phosphate Pathway Enzymes

2.5.3.5 Glucose-6-phosphate dehydrogenase-6-phospho-glucono-lactonase

Early reports suggested that malaria parasites did not possess a G6PD and that they depended on the host cell for NADPH. However, G6PD was found in *P. berghei* and the parasite enzyme was found to account for 5% of the total G6DP present in infected cells[20]. The same enzyme was discovered and purified from *P. falciparum*[85,88]. The G6PD gene has been cloned[101,127]. In its native form the enzyme has an estimated molecular mass of 450 kDa[129], which exists as either a homodimer or homotetramer[8]. The gene of *P. falciparum*, which is located on chromosome 14, suggests an estimated dimer size of 94 kDa, which is striking, as it is almost twice as large as enzymes from other sources[129]. The C-terminus has high homology to enzymes from other sources[8], although a segment of 62 amino acids shows no similarity. The N-terminal has an additional 286[129] to 310[29] amino acid extension, rich in hydrophilic and charged residues, compared to the human enzyme[129]. The N-terminal region showed no homology to other G6PD enzymes, but was homologous to a predicted protein encoded near to the G6PD in *Haemophilus influenzae*, which suggested that it might encode a PPP enzyme[18,126]. The homologous human cDNA was shown to encode for 6-phospho-glucono-lactonase activity[32], which led Clarke et al.[29] to test for 6PGL. It was shown for *P. berhei* that the N-terminal has 6PGL activity, while the C-terminal region has G6PD activity[29]. G6PD-6PGL oxidises the first carbon of G6P to a lactone, which is linked to the reduction of $NADP^+$ to NADPH + H^+. The resulting glucono-1, 5-lactone-6 is converted to 6-phospho-gluconate by the PGL activity of the N-terminal. The 6-phospho-gluconate is decarboxylated and oxidised by G6PD, yielding R5P, a molecule of CO_2 and NADPH + H^+.

Plasmodium have unique insertion sequences at the same genome position, with varying sequence and size[30]. Excision of the insertions removed G6PD, but not 6PGL activity. The function of the insertion is unknown, but is suspected to play a structural role in the enzyme[30]. The insertion sequence may be a potential drug target, since it is highly specific to the parasite.

Inhibition of G6PD-6PGL would prevent the production of NADPH and should result in the parasite suffering from severe oxidative stress. The unique

bifunctional enzyme G6PD-6PGL may allow the enzyme to be selectively inhibited, with potentially excellent inhibitory effects on the parasite. The resolving of a crystal structure of the bifunctional enzyme may reveal several targets that offer specificity and selectivity.

2.5.3.6 6-Phosphogluconate dehydrogenase

This dehydrogenase catalyses the decarboxylation and oxidation of 6-phosphogluconate, yielding R5P, a molecule of CO_2 and NADPH + H^+. The activity of 6-phosphogluconate dehydrogenase has been detected indirectly and presumed to be present in *Plasmodium*[49,143]. The gene coding for the enzyme was identified in *P. falciparum*[12], but further information about the enzyme is limited.

2.5.3.7 Transketolase

Transketolase catalyses a reaction where xyulose-5-phosphate donates 2 carbon atoms to erythrose-4-phosphate, yielding GAP and F6P. The gene coding for transketolase, has been identified in *P. falciparum*[12] and the enzyme has has been expressend, localised and biochemically characterised in *P. falciparum*[72].

2.5.3.8 Transaldolase

The transaldolase reaction involves the transfer of 3 carbons from sedoheptulose-7-phosphate to GAP, yielding erythrose-4-phosphate and F6P. Surprisingly, the gene that codes for transaldolase could not be found in the genome of any *Plasmodium* species, or in any Apicomplexans, although biochemical evidence suggests the presence of a functional non-oxidative branch[12]. It may be possible that a novel enzyme performs the same function.

2.5.3.9 Ribose phosphate isomerase

Ribose phosphate isomerase catalyses the interconversion of ribose 5-phosphate and ribulose 5-phosphate. The genes coding for ribose phosphate isomerase

have been identified in *P. falciparum*[12]. The crystal structure has recently been determined[63], but no research has been directed at kinetically characterising the enzyme.

2.5.3.10 Ribulose-phosphate 3-epimerase

Ribulose-phosphate-3-epimerase catalyses the isomerisation of ribulose-5-phosphate, yielding xylulose-5-phosphate. The gene coding for ribulose-phosphate 3-epimerase has been identified in *P. falciparum*[12]. Recently the crystal structure of *P. falciparum* ribulose-phosphate 3-epimerase was resolved to 2 Å[24]. The structure is a classic TIM-barrel fold, with a coordinated Zn^{2+} ion and a bound sulfate ion in the active site[24].

2.5.4 Ancillary pathways

The malarial parasite has several supplementary pathways, such as purine salvage pathways and carbon dioxide fixation. The latter supplies free amino acids, keto acids and organic acids to the parasite.

2.5.4.1 Carbon dioxide fixation

All the malarial parasites studied are capable of fixing CO_2[129] (Fig. 2.1.) , which is extremely interesting. The exact role of the fixation is not known, but it is indispensable to the parasite[129].
Intra-erythrocyte *P. falciparum* is capable of fixing carbon dioxide, but the contribution of carboxylation towards the utilisation of glucose and ATP yield is unclear[59]. Both phosphoenolpyruvate (PEP) carboxylase and PEP carboxy kinase (PEPCK) are present in *P. berghei*[137]. PEP carboxylase has been isolated and characterised from *P. berghei*[94]. The PEP carboxylase appears to be unique to *P. berghei*, and is not present in other *Plasmodium* species.
PEP carboxylase catalyses the carboxylation of PEP to oxaloacetate. PEPCK is capable of reversible carbon dioxide fixation and is found in mammalian cells, protozoa and plants[59]. PEPCK catalyses the carboxylation of PEP, to yield oxaloacetate and ATP[59]. Carbon dioxide appears essential for parasite growth and survival[59]. The rate at which carbon dioxide is fixed, and the capacity of

carbon dioxide fixation is not known.
It was shown that 14C-labeled bicarbonate was incorporated into certain amino acids and organic acids[130]. Fixation in *P. lophurae* and *P. knowlesi* has been shown to contribute to pyrimidine synthesis, metabolic products, free amino acids, keto acids and organic acids[130,131,145]. The ability to fixate carbon dioxide reduces the dependency on the host cell for intermediates, thus resulting in a more resilient parasite. It would be interesting to quantify the effect of carboxylase inhibition. Cellular carbon dioxide is derived from bicarbonate. Bicarbonate anhydrase catalyses the reversible hydration of carbon dioxide $[CO_2 + H_2O \leftrightarrow HCO_3^- + H^+]$[83,114]. The *de novo* synthesis of pyrimidine requires HCO_3^-, which can be provided by carbonic anhydrase. Bicarbonate anhydrase may also play a role in the transport of bicarbonate into the erythrocyte[53], as well in the regulation of intracellular pH[132]. It would thus appear that the enzyme is essential and linked to carbon dioxide fixation. The human erythrocyte has two isozymes (I & II) of carbonic anhydrase and three isozymes have been identified in *P. falciparum*[83]. Due to high levels of both host and parasite carbonic anhydrase during the erythrocyte phase, inhibition of the parasite enzyme would be expected to inhibit the host enzyme as well. It was shown that the human and parasite enzymes have different inhibition constants (K_i) for acetazolamide (99 nM and 247 nM, respectively) and sulfanilamide (145 μM and 56 μM, respectively)[114]. Derivatives of sulfanilamide may result in a more potent inhibition of the malarial enzyme, whilst leaving the host enzyme relatively unscathed.
The fixation pathway and the enzymes responsible need to be better studied in order to evaluate the possibility of using the pathways in drug development.

2.6 Summary

This review has covered malaria history, treatment and asexual carbohydrate metabolism.
The parasite utilises glucose from the host serum as an energy source. Energy is obtained predominantly by anaerobic glycolysis, with the subsequent production of lactate. Buildup of lactate is prevented by rapidly transporting the acid from the erythrocyte by anion-selective diffusion pathways and a lactate-proton cotransporter.

Since the predominant ATP supply in *Plasmodium* is glycolysis, the pathway has great potential as a drug target. Aldolase, TIM and LDH have been crystallised revealing areas that may be used for drug design. Although these enzymes in isolation have been proposed as drug targets, the pathway as a whole has not been considered. Construction and analysis of a kinetic model of the glycolytic pathway would allow researchers to gain a better understanding of the pathway in its entirety and identify enzymes which control the majority of the flux.

The exact function of the TCA cycle, during the asexual phases, and its importance to the parasite is not known, but it is unlikely to play a major role in ATP production. A plausible hypothesis is presence of an incomplete cycle, which utilises amino acids for anapleurotic functions.

The ETC differs slightly from the classical ETC, as it has an alternative complex I and lacks an complete F_1F_0ATP synthase. The ETC has been proposed to act as an electron sink and may play a role in calcium homeostasis.

The PPP was shown to be extremely important for the oxidative defence mechanism, as it supplies the necessary NADPH for the defence system. The PPP may also function in reverse, converting purines scavenged from the host erythrocyte, to the glycolytic intermediates F6P and GAP. Despite the importance of the PPP to parasite survival, it has not been suggested as a drug target. The novel bifunctional enzyme, G6PD-6PGL, which is essential for the reduction of NADP in the oxidative branch, may prove to be a novel drug target. The enzyme should have several structural differences compared to the separate enzymes, which may provide excellent drug selectivity. Before this avenue could be explored, however, structural features of the bifunctional enzyme would have to be determined.

The peculiar carbon dioxide fixation pathways are essential to the parasite and have been shown to contribute to pyrimidine synthesis, metabolic products, free amino acids, keto acids and organic acids. Further study of the enzymes responsible for the fixation may uncover novel drug targets.

Although membrane structures of the parasites have not been discussed, it has to be mentioned that designing a drug to bind to a specific target in *Plasmodium* is only the beginning of a cure. Delivery of the drug to the target is extremely difficult, as the parasite has its own membrane within the erythrocyte. Drugs, therefore, not only have to selectively inhibit the target enzyme, but must also be able to cross both host and parasite membranes.

The wide range of possible drug targets impedes the rapid development of drugs, as many prove to be inappropriate or ineffective. A systems biology approach to the metabolism may identify the more essential enzymes. Control analysis of the metabolic pathways, can be used to pinpoint the most important regulatory enzymes in a pathway. The enzymes of the glycolytic pathway have nearly all been kinetically characterised, which presents an attractive opportunity to use a systems biology approach and identify the most important regulatory enzymes. Identification of these enzymes may fast track the development of an antidote.

The life cycle of the malarial parasite, its interactions with its host and its metabolism is extremely complex. Unraveling the detail of *Plasmodium* presents a significant challenge, which has to be overcome in order to find new cures for this endemic parasite. The carbohydrate metabolism as a drug target definitely has potential, but much research is required. A global, concerted effort will greatly aid the discovery of effective and selective drugs.

Chapter 3

Methods

3.1 General Overview

The aim of the project was to construct a kinetic model of glycolysis for the the asexual (trophozoite stage) *P. falciparum*. As such, *Plasmodium* had to be cultured, trophozoites isolated from the erythrocyte and the glycolytic enzymes kinetically characterised from parasite lysates. Additionally, validation data in the form of glycolytic fluxes and intermediate metabolites had to be determined in whole trophozoites. All intermediates, enzymes and reagents were obtained from Sigma (Steinheim, Germany), except in the case of Albumax II and RPMI-1640 (Scientific Group in Auckland, New Zealand) and G6P, F6P, 3PGA and 2PGA (Boehringer in Ingelheim, Germany).

3.2 Culturing of *Plasmodium falciparum D10*

Packed human erythrocytes (A^+) were infected with *Plasmodium falciparum* D10 and cultured in RPMI 1640 culture medium supplemented with Albumax II[36,146]. Cultures were incubated with 3% oxygen, 4% carbon dioxide and 93% nitrogen at 37 °C

Incomplete culture medium was prepared as described previously[36] by supplementing RPMI 1640 with Albumax $II^{(R)}$ (0.5% m/v), glucose (22mM), HEPES (25mM), hypoxanthine (3mM) and gentamycin sulphate (50μg/mL).

The medium was sterilised by filtration (0.2μM) and stored at 4°C for up to 2 months. Before use, the medium was completed by adding filter sterilised 5% sodium bicarbonate to a final concentration of 25mM. The complete medium was used within two weeks.

Synchronisation of parasites was achieved by centrifuging infected erythrocytes (750 × g, 3min), suspending the pellet in 5% sorbitol solution and incubating the suspension at 37°C for 5 min[66]. Following further centrifugation (750 × g, 3min) and aspiration of the supernatant, the infected erythrocyte pellet was resuspended in culture media and placed into culture flasks. Sorbitol destroys all but ring stage parasites, thus keeping cultures in a specific phase.

3.3 Trophozoite Isolation

This project used parasites in the mature trophozoite-phase (36-40 hours post erythrocyte invasion). The trophozoites were freed from the erythrocyte using a saponin lysis protocol[123]. Saponin permeabilises the erythrocyte and parasitophorous vacuolar membranes by interacting with cholesterol found in these membranes[3,4], but leaves the parasite plasma membrane intact and able to maintain a transmembrane ion gradient and a substantial membrane potential[123,122] with greater than 95% of parasites isolated in this manner maintain the ability to exclude 0.04% trypan blue[121].

Saponin with a final concentration of 0.05% w/v and 0.005% active component sapogenin was added to infected erythrocytes suspended in culture medium (5% hematocrit). Upon addition of saponin, the suspension was rapidly mixed by inversion and then centrifuged for 6 minutes at 1800 × g. The supernatant was removed and the parasites were resuspended in culture medium and washed twice more in a buffer identical to that used in the applicable assay. Trophozoites isolated in this manner were used within an hour of isolation or stored at -80°C for later use. The supernatant from the final wash was retained as a control and tested for the presence of contaminating erythrocyte enzymes.

3.4 Kinetic Parameter Determination

The literature review yielded kinetic parameters for a large number of glycolytic enzymes (Literature review: Section 2.5.1 Table 2.1). Unfortunately, many of these enzymes were characterised at optimal conditions or in different species or strains of *Plasmodium*, which may yield kinetic parameters that differ significantly from those determined under physiological conditions or *P. falciparum D10*, respectively. Parameters were therefore determined for most of the glycolytic enzymes under physiological conditions. In cases where the parameters were not determined, they were obtained from literature. Characterisation of the asexual *Plasmodium* glycolytic enzymes was performed using trophozoite lysates.

3.4.1 Enzyme Assays

Each glycolytic enzyme was kinetically charaterised in terms of its affinity to each substrate and product, as well as it maximal rate. The assays used for the characterisation of the glycolytic enzymes were adapted from Teusink *et al*[142]. Isolated trophozoites were suspended in an assay buffer containing HEPES (20 mM), MgCl (20 mM), K_2HPO_4 (1 mM), KCl (10 mM) and NaCl (20 mM). The high magnesium concentration was used to ensure that ATP was predominantly in the active MgATP form. The pH was set to 7.17 to match the cytosolic pH of *P. falciparum D10*[163]. It is interesting to note that the cytosolic pH differs substantially between species and strains, especially in those that are chloroquine resistant[163]. Isolated trophozoites were lysed by using three freeze-thaw cycles. Trophozoites were frozen in liquid nitrogen and thawed on ice. The lysis protocol was optimised by the inclusion of a 30 second sonication step between freeze-thaw cycles. The supernatant was retained and used for kinetic determinations after a 10 minute 10 000 $\times$g centrifugation step.

The enzyme rates were determined using enzyme/NADH/NAD/NADP linked reactions, which were be measured at 340nm in 96 well plates (Greiner bio-one Flat Bottom microplate) on a spectrophotometer (VarioSkan microplate reader, Thermo Electron Corporation). For uni-substrate reactions, the substrate concentration was varied. For bi-substrate reactions the rate was determined by varying one substrate concentration whilst maintaining

saturating concentrations of the other substrate. All reagents and enzyme dilutions were made up in the assay buffer described previously.

To ensure that observed enzyme activity was *Plasmodium* enzyme specific the supernatant from the final trophozoite isolate wash was retained and tested for contaminating erythrocyte enzyme activity. This contained negligibly low LDH activity, when compared to the lysate activity. Before substrate was added to commence the assay, activity was measured to ensure no residual substrate or oxidase activity (oxidising NADH/NADPH) was present. The use of excess enzymes in the assay also ensured that only the activity of the enzyme being characterised was limiting the overall reaction.

3.4.1.1 Hexokinase

Forward reaction: The rate of glucose phosphorylation was measured by linking the hexokinase reaction to NADP/G6PDH and measuring the accumulation of NADPH at 340 nm. Glucose was added to wells containing ATP, assay buffer, G6PDH (3U/ml), NADP (0.2mM) and lysate.
Inhibition by G6P: Inhibition of HK by G6P (1 mM) was assayed under saturating concentrations of ATP and glucose by linking the reaction to α-glycerolPDH (4U/ml) and NADH (0.2 mM), via PFK (5U/ml), TPI (5 U/ml) and PGI (20 U/ml)

3.4.1.2 Phosphoglucoisomerase

Forward reaction: The rate of G6P isomerisation was determined by linking the reaction to α-glycerolPDH (4 U/ml) and NADH (0.2 mM) in the presence of excess PFK (12.5 U/ml), TPI (5 U/ml), ALD (4 U/ml) and ATP (1 mM).
Reverse reaction: The conversion rate of F6P to G6P was measured by linking the reaction to G6PDH (3 U/ml) and NADP (0.2 mM).

3.4.1.3 Phosphofructokinase

Forward reaction: The phosphorylation rate of F6P by ATP was measured by linking the reaction to α-glycerolPDH (4U/ml) in the presence of excess ALD

(4U/ml), TPI (5U/ml) and NADH (0.2 mM).
Reverse Reaction: The reverse rate could not be measured reproducibly by linking the reaction to G6PDH (3U/ml) and NADP (0.2 mM), via PGI (20 U/ml).

3.4.1.4 Aldolase

Forward reaction: The rate of aldol cleavage of F 1,6BP was measured by linking the reaction to α-glycerolPDH in the presence of NADH (0.2mM), TPI (5U/ml) and GlycerolPDH (4U/ml).
Reverse reaction The reverse rate in the presence of excess GAP and DHAP could not be measured by linking the reaction to G6PDH (3 U/ml) and NADP (0.2 mM) via ALD (4 U/ml), TPI (5U/ml), PFK (5 U/ml) and PGI (20 U/ml). This is presumed to be due to PFK, which is not very reversible.

3.4.1.5 Triosephosphate Isomerase

Forward reaction: The conversion rate of GAP to DHAP was measured by linking the reaction to α-glycerolPDH (4U/ml) and NADH (0.2 mM).
Reverse reaction: The conversion rate of DHAP to GAP was measured by linking the reaction to G3PDH (10U/ml) and NAD (0.2 mM) in the presence of PGK (50U/ml) and ADP (1 mM) to remove the accumulation of product. The measured rates did not, however, yield a rate that was proportional to substrate concentration.

3.4.1.6 Glyceraldehyde 3 Phosphate Dehydrogenase

Forward reaction: The conversion rate of GAP and NAD to 1,3 BPG and NADH was determined in the presence of PGK (50U/ml) and ADP (1 mM), but did not yield a rate that was proportional to substrate concentration.
Reverse reaction: The G3PDH reaction rate was determined by measuring the decrease in NADH concentration as 1, 3 BPG is converted to GAP with the formation of NAD. Since 1,3 BPG is chemically unstable, 3PGA is used in the presence of excess PGK (50U/ml) and ATP (1mM) to provide the substrate 1, 3 BPG. This method is based on the assumption that all 3PGA is converted

to 1, 3 BPG and a negligible amount is converted to 2PGA by PGM. The rapid rate of PGM, however, would result in an apparent Km that is lower than the actual Km. The V_{max} is not expected to be affected, as it is based on a saturating substrate concentration.

3.4.1.7 Phosphoglycerate Kinase

Forward reaction: The dephosphorylation of 1,3 BPG to 3PGA could not be measured, since 1,3 BPG is chemically unstable.
Reverse reaction: The rate of 3PGA phosphorylation was determined by linking the reaction to G3PDH (10 U/ml) in the presence of NADH (0.2 mM) and measuring the decrease in absorbance at 340 nm.

3.4.1.8 Phosphoglycerate Mutase

Forward reaction: The mutase reaction was linked to LDH (5 U/ml), via PK (10 U/ml) in the presence of ADP (1 mM) and NADH (0.2 mM).
Reverse reaction: The conversion of 2PGA to 3PGA was measured by linking the reaction to G3PDH (10 U/ml) via PGK (5 U/ml) in the presence of ATP (1 mM) and NADH (0.2 mM).

3.4.1.9 Enolase

Forward reaction: The rate of 2PGA conversion to PEP was measured by linking the reaction to LDH (5U/ml) and NADH (0.2 mM) in the presence of excess PK (10 U/ml) and ADP (1 mM)
Reverse reaction: The reverse reaction was linked to G3PDH (10 U/ml) in the presence of NADH (0.2 mM, excess PGM (10 U/ml), PGK (50 U/ml) and ATP (1 mM).

3.4.1.10 Pyruvate Kinase

Forward reaction: The rate of PEP and ADP utilisation was determined by linking the reaction to LDH (5 U/ml) and NADH (0.2mM).

Reverse reaction: The reverse reaction could not be determined reproducibly by linking the reaction to G3PDH.

3.4.1.11 Lactate Dehydrogenase

The rate of substrate or product utilisation was determined by measuring the amount NADH/NAD utilised with time in each reaction, respectively.

3.4.2 Binding Constant Determination

The initial maximum reaction rates were determined over a minimum period of 30 seconds for each different substrate/product concentration by using the linear slope ($R^2 > 0.90$) and the extinction coefficient for NADH (6.22 $mM^{-1}.cm^{-1}$). The pathlength in the Greiner bio-one 96 well plate was determined by using the following equation:

$$pathlength = 465.6(0.01808 + 0.00001384 \cdot volume)^{\frac{1}{3}} - 122.2$$

Where, the pathlength (mm) is given as a function of working volume (μL). The derivation for this equation can be found in Appendix A. The pathlength for the typical 100μL assay working volume was calculated to be 3.0419 mm. By plotting the substrate concentration *versus* the corresponding maximal rates (normalised to protein concentration), a nonlinear curve was typically obtained. Nonlinear regression of these data, using the irreversible Michaelis-Menten equation, yielded binding and V_{max} constants.
It is expected that glycolytic enzyme expression levels vary between *Plasmodium* cultures and isolations, which would alter the V_{max} values as they are a function enzyme concentration and a catalytic rate constant. To counter this problem a homogenate of many trophozoite isolates was prepared and used to determined all the V_{max} values, under saturating conditions. Regression was performed using *Wolfram Mathematica 6.0*, which also provides the statistics of the fits.

3.5 Model Construction

Using the parameter values determined for each enzyme and standard kinetic equations, a kinetic model was constructed in Wolfram Mathematica 6.0. In the model, glucose is entirely converted to lactate with the assumption that flux through the pentose phosphate pathway and carbon dioxide fixation is negligible when compared to the glycolytic flux. This assumption is supported by observations that one mol glucose produces two moles lactate and two moles ATP[129].

In instances, where parameters could not be determined experimentally or obtained from literature, they were fitted or estimated. Estimation was achieved by comparing the kinetic parameters obtained in different organisms and obtaining an average. This approach is based on the assumption that enzymes active sites are conserved and that binding constants would not change by more than an order of magnitude.

The model consists of a set of ordinary differential equations, which describe the change in metabolite concentration over time as a function of enzyme rates. The rate of each each enzyme is described using various rate equations (e.g reversible and irreversible uni-substrate Michaelis-Menten or bi-substrate generic[116], Monod-Wyman-Changreux and Ping-Pong Bi-Bi equations).

3.6 Validation Data: Fluxes and Intermediate Metabolite Concentrations

An important part of kinetic modeling is model validation. The model in this study was constructed using parameters and equations for enzymes that had been characterised in isolation. Steady state analysis of the model provides metabolite concentrations and fluxes, which are predictions of the system working together as a whole. This provides a suitable means of validation since it is possible to experimentally determine steady state fluxes and intermediate concentrations. The validation data is thus also independent of model construction data.

3.6.1 Glucose Uptake and Lactate Production Incubations

In order to determine the glycolytic flux and intermediate metabolite concentrations, isolated trophozoites were washed and incubated in a modified culture medium, which contained RPMI 1640, hypoxanthine (3mM), glucose (10mM), HEPES (25mM) and the pH adjusted to 7.1 to mimic the pH found within the erythrocyte[123]. The trophozoite suspension (approximately 1 - 10 $\times 10^7$ cells/ml) was incubated in a water bath at 37 $^{\circ}C$ for up to 8 hours. At specific time points 200 μL samples of the trophozoite suspension were added to 50 μL PCA ((6% final concentration), immediately placed in liquid nitrogen and stored at -80 $^{\circ}C$ until further use. Following thawing and neutralisation with 1 M sodium hydroxide, the samples were centrifuged at 10 000 $\times$g at 4$^{\circ}C$ for 10 min and the supernatant used for glucose, lactate and internal intermediate metabolite concentrations. Before incubation, the trophozoites were counted and checked for membrane integrity by suspending the cells in 0.04% Trypan blue and visualising them in an improved Nebauer counting chamber. Typically 85 - 95 % of the trophozoites were able to exclude trypan blue.

3.6.2 Glucose and Lactate Assays

Extracellular glucose was assayed using a HK, G6PDH, NADP linked assay. Samples and standards were incubated in a triethanolamine buffer pH 8.6 containing HK (10 U/mL), ATP (0.2 mM), G6PDH (10 U/mL) and NADP (0.5 mM). After a 15 minute incubation period the absorbance at 340 nm was measured. A standard curve in the range of (0-20mM) was constructed and used to determine glucose concentrations present in the samples.
Extracellular L-lactate was assayed using a LDH, NAD^+ linked assay. Samples and standards were read at 340 nm after being incubated for 20 min at room temperature in HEPES buffer (20 mM) containing LDH (10 U/ml), NAD^+ (0.2 mM) and hydrazine (16 μL/ml). Hydrazine is used since it binds to pyruvate and thus thermodynamically drives the unfavourable LDH reaction (reverse) to completion. A calibration curve in the range of 0-20 mM lactate was constructed.

3.6.3 Protein determination

Protein concentrations for the incubations or enzyme assays were performed on lysates. In the case of whole cell incubations, the cells were lysed before protein determination. Protein concentration was determined by using the method of Bradford[13]. The protocol was adapted for use in 96 well plates, where 180 μL of Bradford reagent was added to 5 μL of sample or standard and incubated for 15 minutes followed by reading the absorbance at 595 nm. As a standard, a BSA calibration curve in the range of 0 - 1 mg/mL was utilised.

Chapter 4

Experimental Results and Discussion

This chapter covers the experimental aspects of this work, which includes the kinetic characterisation of the glycolytic enzymes, the determination of glycolytic flux and the establishment of a protocol to measure glycolytic intermediate concentrations. These results are employed for the construction and partial validation of a kinetic model in the upcoming theoretical results chapter (Chapter 5).

4.1 Enzyme Characterisation

Most of the *P. falciparum* glycolytic enzymes were kinetically characterised using trophozoite lysates. In the following section the kinetic parameters (K_m, V_{max}, K_{eq}) as well as the rate equation obtained for each enzymatic reaction are presented.

It should be noted that the K_m values were determined from separate trophozoite isolates and were shown not to differ significantly ($p < 0.1$) between different isolations. The V_{max} values, however, were all determined from a single homogenate, consisting of several isolates, and are thus representative of an average expression level during the trophozoite stage. This approach was utilised, since it has been shown that glycolytic enzyme expression levels (and

thus V_{max}) vary during the asexual stage[23].

Equilibrium constants for each of the enzymatic reactions were obtained by searching the Goldberg database[55], which contains numerous thermodynamic parameters and specifies the conditions under which they were determined. Equilibrium constants which had been determined under conditions similar to those used in this study were chosen.

In instances, where only the reverse V_{max} could be determined, the uni- or bi-substrate Haldane relationship (Eqns. 4.1.1 and 4.1.2 respectively), which describes the relation between maximal rates, binding and equilibrium constants, was used to determine the forward V_{max} or *vice versa*. Additionally, in instances where both the forward and reverse rates were determined, the Haldane relationship was used to determine an apparent K_{eq}. Comparison of this estimated equilibrium constant to values available in literature gives an indication of how accurate the kinetic parameters as a whole are.

$$V_{forward} = \frac{V_{reverse} \cdot K_{substrate} \cdot K_{eq}}{K_{product}} \tag{4.1.1}$$

$$V_{forward} = \frac{V_{reverse} \cdot K_{substrate1} \cdot K_{substrate2} \cdot K_{eq}}{K_{product1} \cdot K_{product2}} \tag{4.1.2}$$

Where, $V_{forward}$ and $V_{reverse}$ are the maximal forward and reverse rates, respectively, $K_{substrate}$ and $K_{product}$ are the affinities of substrate and product for the enzyme and K_{eq} is the equilibrium constant of the reaction.

In the following subsections, the rate equations derived for each glycolytic step are presented with the parameters values that were obtained for the equation.

4.1.1 Glucose Transporter

P. falciparum possesses a single glucose and fructose transporter, PfHT1. A recombinant PfHT1 has been characterised in frog oocytes[71].

Although the transporter was not characterised in this study, it was assumed to follow reversible Michaelis-Menten kinetics (Eq. 4.1.3) and bind internal and external glucose symmetrically. Kinetic parameters that were used for the rate eqaution are displayed in Table 4.1.

Since the expression levels of the transporter in *P. falciparum* during the asexual phase are not known a range of V_{max} values (Table 4.1.) were used for the kinetic model simulations (see Section 5.2.).

$$vGlcTr = \frac{(V_f \cdot glc_{ex}(1 - \frac{glc_{int}}{glc_{ex} \cdot K_{eq}})}{Km_{glc_{ex}}(1 + \frac{glc_{ex}}{Km_{glc_{ex}}} + \frac{glc_{int}}{Km_{glc_{int}}})} \tag{4.1.3}$$

Where $vGlcTr$ is the glucose transporter rate, V_f is the maximal forward reaction rate, glc_{int} is the internal parasite glucose concentration, glc_{ex} is the external parasite glucose concentration, $Km_{glc_{ex}}$ is the affinity of external glucose to the transporter, $Km_{glc_{int}}$ is the affinity of the internal glucose to the transporter and K_{eq} is the equilibrium constant of the reaction.

Table 4.1: Kinetic parameters for the *P. falciparum* hexose transporter.

Metabolite	$K_m(mM)$	Reference
$Glucose_{external}$	0.97 ± 0.34	[71]
$Glucose_{internal}$	0.97 [1]	
Equation Parameters		
$V_{max_{(forward)}}$	0.01-0.12 [2]	μmol.min^{-1}.mg protein^{-1}
K_{eq}	1.0	

[1] *Assumed symmetrical binding.*
[2] *Range of V_{max} values there were used during model simulations.*

4.1.2 Hexokinase

Hexokinase was assumed to be product insensitive and was described by the an irreversible Michaelis-Menten rate equation (Eq 4.1.4.). The enzyme was characterised in terms of its substrates, Glucose and ATP (Fig. 4.1).

$$vHK = \frac{V_f \cdot glc_{int} \cdot atp}{Km_{glc_{int}} \cdot Km_{atp}(1 + \frac{glc_{int}}{Km_{glc_{int}}})(1 + \frac{atp}{Km_{atp}})} \tag{4.1.4}$$

Where vHK is the reaction rate, V_f is the maximal forward rate, glc_{int} is the internal glucose concentration, atp is the ATP concentration, $Km_{glc_{int}}$ is the affinity of internal glucose for hexokinase and Km_{atp} is the affinity of ATP for hexokinase.

The affinities of the enzyme were calculated, using nonlinear regression of the data shown in Fig 4.1 A & B using the above rate equation (Eq. 4.1.4.), to be 0.14 and 0.57 mM for glucose and ATP, respectively (Table 4.2.).
These values are approximately four fold smaller than when previously determined[119]. This discrepancy may be due to the fact that previous determinations (Table 4.2.) were done at a higher pH (7.4) using lysed *P. falciparum* infected erythrocytes (enriched to 60% parasitemia) and thus the apparent K_m estimations are a function of both parasite and erythrocyte enzymes binding. Differences in the V_{max} values under saturating glucose or ATP conditions are a result of different parasite isolations being used for the respective assays.

Table 4.2: Kinetic parameters for *P. falciparum* hexokinase determined previously and in this work.

Metabolite	$K_m(mM)$	Reference	$K_m(mM)$	Reference
$Glucose_{internal}$	0.14 ± 0.017	*This work*	0.431 ± 0.021	[119]
ATP	0.57 ± 0.06	*This work*	3.1 ± 1.4	[119]
Equation Parameters				
$V_{max_{(forward)}}$	0.325 ± 0.0092 μmol.min^{-1}.mg protein^{-1}			*This work*

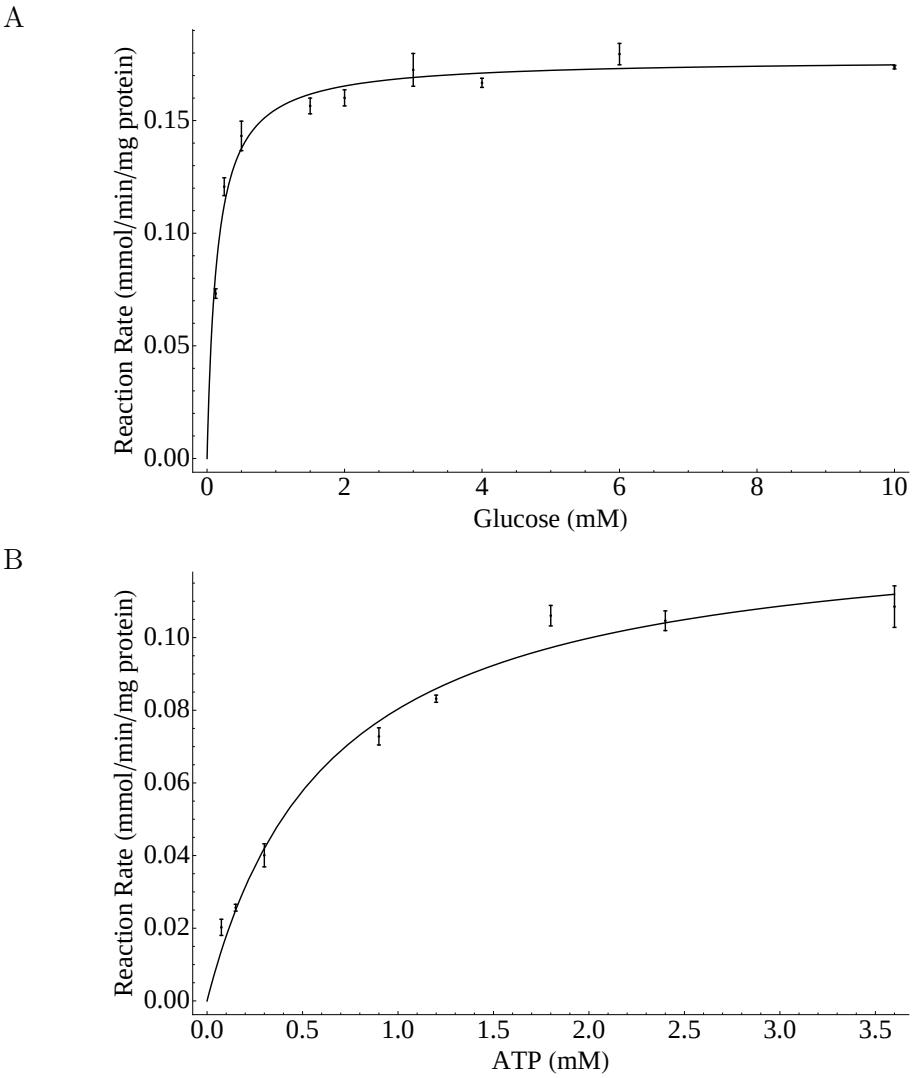

Figure 4.1: Kinetic characterisation of *P. falciparum* hexokinase in terms of its substrates. A) Glucose was varied between 0-25 mM, at saturating ATP concentrations (5 mM) and B) ATP was varied between 0-3.5 mM, at saturating glucose concentrations (10 mM). Fitting with the Michaelis-Menten equation (shown) was used to determine V_{max} and K_m values. Error bars represent standard deviation of the mean (n = 3).

Hexokinase was found to be insensitive to low concentrations (1mM) of G6P (results not shown). Kinetic model predictions of the G6P concentrations as steady state (see Chapter 5.2), however, are higher than 10 mM and it may be that hexokinase is inhibited by higher concentrations of G6P. Assays, which

will measure product sensitivity over a wider range of product concentrations will be performed to determine if the product insensitivity assumption is valid.

4.1.3 Phosphoglucoisomerase

PGI was characterised in term of its substrate and product (Fig. 4.2.) and was described using a reversible Michaelis-Menten equation (Eq. 4.1.5.).

$$vPGI = \frac{V_f \cdot g6p(1 - \frac{f6p}{g6p \cdot K_{eq}})}{(Km_{g6p}(1 + \frac{g6p}{Km_{g6p}} + \frac{f6p}{Km_{f6p}})} \tag{4.1.5}$$

Where $vPGI$ is the reaction rate, V_f is the maximal forward rate, $g6p$ is the internal G6P concentration, $f6p$ is the F6P concentration, Km_{g6p} is the affinity of G6P for PGI and Km_{f6p} is the affinity of F6P for PGI.

Parameters obtained for PGI are presented in Table 4.3. The apparent K_{eq} for the reaction, 0.138 as obtained using the haldane relationship (Eq. 4.1.1.), is the in the same order of magnitude as that present in literature, 0.330. The K_m determined previously by Srivastava *et al*[138] is approximately three times higher than determined in this work (Table 4.3), but the discrepancy may be due to the use of a different *P. falciparum* strain (M25) or different assay conditions (pH 8.0).

Table 4.3: Kinetic parameters obtained for *P. falciparum* phosphoglucoisomerase.

Metabolite	$K_m(mM)$	Reference	$K_m(mM)$	Reference
G6P	0.92 ± 0.098	*This work*		
F6P	0.081 ± 0.0034	*This work*	0.258 ± 0.026[1]	[138]
Equation Parameters				
$V_{max_{(forward)}}$	0.363 ± 0.0326 μmol.min^{-1}.mg protein^{-1}			*This work*
$V_{max_{(reverse)}}$	0.232 ± 0.0354 μmol.min^{-1}.mg protein^{-1}			*This work*
K_{eq}	0.330	[139]	0.138[2]	*This work*

[1] *Average value of three isozymes with standard deviation of the mean shown.*

[2] *Apparent K_{eq} estimated using the Haldane relationship. (See Section 4.1 for details.*

A

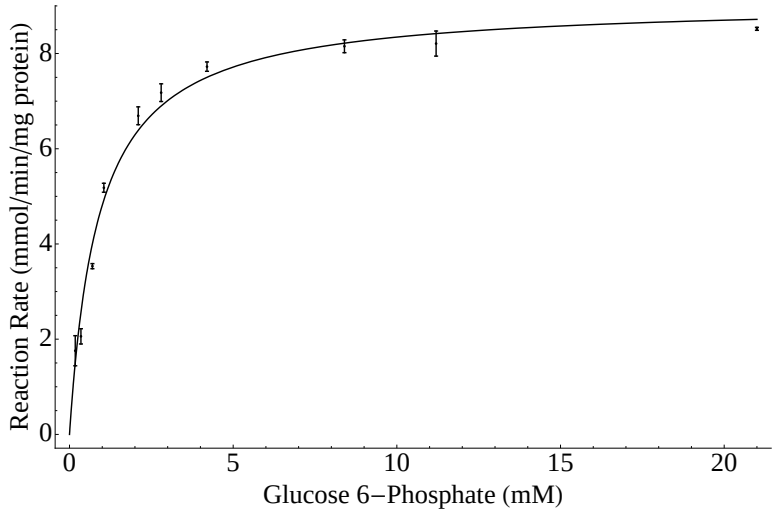

B

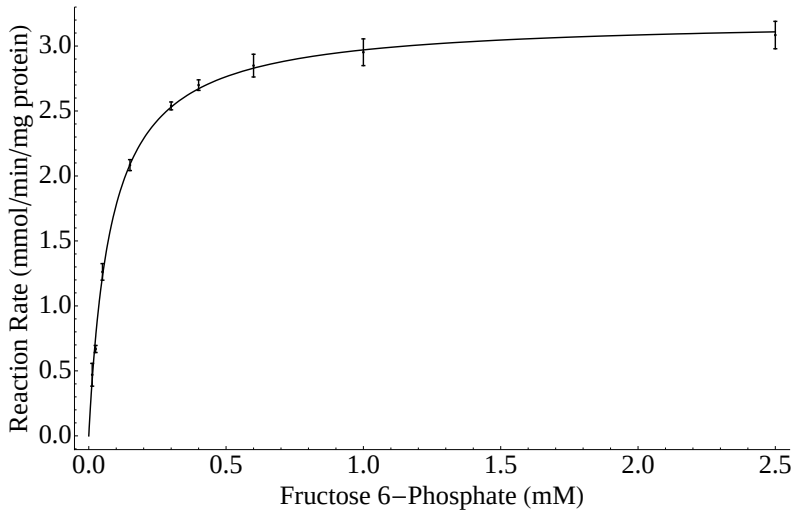

Figure 4.2: *P. falciparum* phosphoglucoisomerase was characterised in terms of A) its substrate, glucose 6-phosphate, and B) its product, fructose 6-phosphate. A) Fitting (shown) of the data to a Michaelis-Menten equation was used to procure V_{max} and K_m values. Error bars represent standard deviation of the mean (n = 3).

4.1.4 Phosphofructokinase

PFK has been extensively characterised previously in terms of allosteric regulation and have not yet been repeated in this study, but will form part of future studies. The reaction was described by a Monod-Wyman-Changeux rate equation (Eq. 4.1.6.) and the corresponding parameter values are presented in Table 4.4.

$$\begin{aligned} vPFK &= \frac{V_f \cdot atp \cdot f6p}{(atp + K_{atp}(1 + \frac{adp}{K_{adp}}))(f6p + K_{f6p})}(\frac{1}{1 + L_o}) \\ L_o &= L(\frac{(1 + \frac{Mg}{K_{mg}})(1 + \frac{atp}{K_{atp}})}{(1 + \frac{f6p}{K_{f6p2}})(1 + \frac{pep}{K_{pep}})})^n \end{aligned} \tag{4.1.6}$$

Where $vPFK$ is the reaction rate, V_f is the maximal forward rate, atp, $f6p$, Mg, adp, pep are the ATP, F6P and Mg^{2+}, ADP and PEP concentrations, K_{adp}, K_{f6p} are Michaelis constants for ADP and F6P, K_{atp}, K_{mg} are inhibition constants for ATP and Mg^{2+}, K_{f6p2}, K_{pep} are activation constants for F6P and PEP, L is the equilibrium constant for the transition between the R and T state and n, is the number of subunits.

Table 4.4: Kinetic parameters obtained predominantly from literature, which were used for the description of phosphofructokinase kinetics.

Metabolite	$K_m(mM)$	Reference
F6P	0.034	[17]
F6P2	0.054	[17]
ADP	0.17	[17]
ATP	0.028	[17]
Mg^{2+}	0.78	[17]
PEP	0.13	[17]
Equation Parameters		
$V_{max_{(forward)}}$	0.142 ± 0.0167 μmol.min^{-1}.mg protein^{-1}	*This work*
Mg^{2+}	0.5 mM	*Assumed*
n	3.92	[17]
L	3.22	[17]

The forward and reverse maximal enzyme rates were determined using substrate and product concentrations ten times greater than the respective K_m values under high magnesium concentrations. Since magnesium is not explicitly modeled in any of the other reactions and that all ATP is assumed to be in the active magnesium bound form, the concentration of free magnesium was fixed at 0.5 mM.

4.1.5 Aldolase

Aldolase was characterised in terms of its substrate, F1,6DP (Fig. 4.3.). The reaction was described using a reversible random order rapid equilibrium rate equation (Eq. 4.1.7.).

$$vALD = \frac{V_f \cdot f16bp(1 - \frac{dhap \cdot gap}{f16dp \cdot K_{eq}})}{Km_{f16dp}(1 + \frac{f16bp}{Km_{f16dp}} + \frac{dhap}{Km_{dhap}} + \frac{gap}{Km_{gap}} + \frac{gap \cdot dhap}{Km_{gap} \cdot Km_{dhap}})} \quad (4.1.7)$$

The substrate (F1,6DP) affinity determined in this work (Table 4.5.) was in the same order of magnitude as determined by Dobeli *et al*[40].

The affinities of the products to the enzyme could not be determined enzymatically and were thus estimated by averaging the values known for *Trypanosmoma brucei*, *Lactococcus lactis* & human erythrocytes (Table 4.5.). The basis for this estimation is the assumption that active sites are conserved, although this may not always be the case. This method, however, is expected to provide a K_m value that is more accurate than choosing an arbitrary value.

Where $vALD$ is the reaction rate, V_f is the maximal forward rate, *dhap*, *gap*, *f16dp* are the DHAP, GAP and F1,6DP concentrations, Km_{gap}, Km_{dhap}, Km_{f16dp} are Michaelis constants for GAP, DHAP and F1,6DP and K_{eq} is the equilibrium constant of the reaction.

Table 4.5: Experimentally determined and estimated kinetic parameters for *P. falciparum* aldolase. See text for details.

Metabolite	$K_m(mM)$	Reference	$K_m(mM)$	Reference
F16BP	0.078 ± 0.01	*This work*	0.025 ± 0.006	[40]
DHAP	0.11 ± 0.089[1]	[61,62,64]		
GAP	0.046 ± 0.019[1]	[61,62,64]		
Equation Parameters				
$V_{max_{(forward)}}$	0.311 ± 0.0354 μmol.min^{-1}.mg protein^{-1}			*This work*
K_{eq}	0.090 mM	[89]		

[1] *Estimated by averaging value of affinities in Trypanosmoma brucei, Lactococcus lactis & human erythrocytes.*

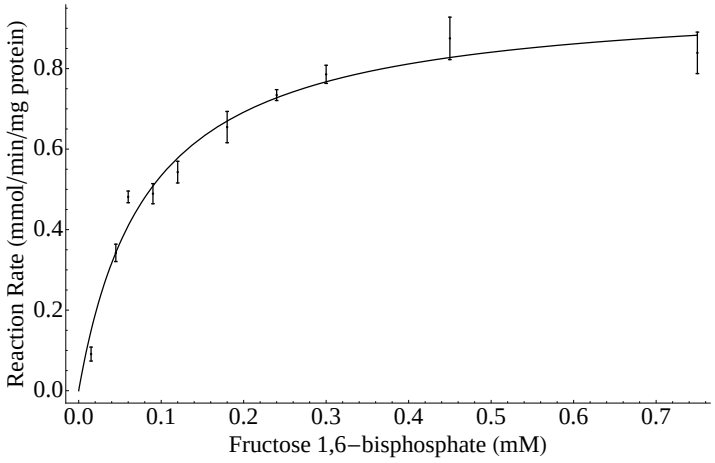

Figure 4.3: Kinetic characterisation of *P. falciparum* aldolase in terms of its substrate, fructose 1,6-bisphosphate. Data is fitted to the Michaelis-Menten equation. Error bars indicate standard deviation of the mean (n = 3).

4.1.6 Triosephosphate Isomerase

Triosephosphate isomerase could not be enzymatically characterised in terms of substrate or product affinities. TPI was modeled using a reversible generic rate equation (Eq. 4.1.8) and the kinetic parameters were obtained from literature or estimated from *T. brucei* and human erythrocytes (Table 4.6).

$$vTPI = \frac{V_f \cdot dhap(1 - \frac{gap}{dhap \cdot K_{eq}})}{Km_{dhap}(1 + \frac{dhap}{Km_{dhap}} + \frac{gap}{Km_{gap}})} \tag{4.1.8}$$

Where $vTPI$ is the reaction rate, V_f is the maximal forward rate, *dhap*, *gap* are the DHAP and GAP, Km_{gap}, Km_{dhap} are Michalis constants GAP and DHAP and K_{eq} is the equilibrium constant of the reaction.

Even though V_{max} values could be measured reproducibly for the forward and reverse reactions, complete saturation curves could not be obtained.
This may be due to the assay approach used (see Methods 4.1) where the conversion of GAP to DHAP (reverse reaction) was linked to the the oxidation of NADH in the presence of α-glycerolPDH. In this assay protocol the oxidation of NADH would allow G3PDH reaction to utilise its substrate GAP in the presence of the produced NAD^+. Ultimately, this would result in the underestimation of the TPI rate.

Table 4.6: Kinetic parameters obtained for *P. falciparum* Triosephosphate isomerase.

Metabolite	$K_m(mM)$	Reference
DHAP	1.0 ± 0.26[1]	61,64
GAP	0.35 ± 0.16	136
	Equation Parameters	
$V_{max_{(forward)}}$	0.285[2]	*This work*
$V_{max_{(reverse)}}$	2.198 ± 0.0426	*This work*
K_{eq}	0.045	155

[1] *Average value of affinities for Trypanosmoma brucei & human erythrocytes.*
[2] *Determined using the Haldane relationship*

At low non-saturating concentrations of GAP, the rate of TPI and G3PDH would approach equality and thus the rate of TPI would approach zero (no net oxidation of NADH). Since the G3PDH reaction requires inorganic phosphate, assays in future will be performed in the absence of phosphate. The forward reaction rate (DHAP converted to GAP) could not be reproducible measured under saturating concentrations of substrate, and was not detected at lower concentrations of substrate.
This may be due to the fact that the rapid TPI reaction converts GAP to DHAP (thermodynamically favourable) and consequently aldolase converts GAP and DHAP to F1,6BP (also thermodynamically favourable). To test if this indeed the case, higher concentrations of G3PDH will be tested, such that this reaction rate is far greater than the TPI and ALD rates.

4.1.7 Glyceraldehyde 3-phosphate Dehydrogenase

Characterisation of *Plasmodium* glyceraldehyde 3-phosphate dehydrogenase has not been published. In this work G3PDH was characterised in the reverse direction (Fig. 4.4) using 3PGA and NADH as substrates.

3PGA was assumed to be entirely converted to the chemically unstable 1, 3BPG. This assumption may not be entirely true and thus the estimated Km (Table 4.7) is expected to be lower than calculated.
Once the model is fully validated parameter sensitivity analysis (see General Discussion, Chapter 5) will be used to determine if an underestimation of this parameter has a significant effect on model outcome. The forward reaction could not be measured reproducibly for reasons mentioned previously (see Section 4.1.6.)

A generic reversible bisubstrate rate equation 4.1.9 was used to describe G3PDH where *vG3PDH* is the reaction rate, V_f is the maximal forward rate, *nad*, *gap*, *nadh*, *bpg* are the NAD^+, GAP, NADH and 1, 3BPG concentrations, Km_{gap}, Km_{nad},Km_{nadh},Km_{bpg} are Michaelis constants for GAP, NAD^+, NADH and DPG and K_{eq} is the equilibrium constant of the reaction.

$$vG3PDH = \frac{V_f \cdot gap \cdot nad \cdot (1 - \frac{bpg \cdot nadh}{(gap \cdot nad \cdot K_{eq}})}{Km_{gap} \cdot Km_{nad}(1 + \frac{gap}{Km_{gap}} + \frac{bpg}{Km_{bpg}})(1 + \frac{nad}{Km_{nad}} + \frac{nadh}{Km_{nadh}})} \tag{4.1.9}$$

Table 4.7: Kinetic parameter values determined and estimated for *P. falciparum* glyercaldehyde 3-phosphate dehrdrogenase.

Metabolite	$K_m(mM)$	Reference
GAP	0.20 ± 0.071[1]	[61,62]
NADH	0.043 ± 0.0051	*This work*
NAD	0.33 ± 0.18[1]	[61,62]
1,3BPG	0.07 ± 0.019	*This work*
Equation Parameters		Reference
$V_{max_{(forward)}}$	0.346[2] μmol.min^{-1}.mg protein^{-1}	*This work*
$V_{max_{(reverse)}}$	0.214 ± 0.0807 μmol.min^{-1}.mg protein^{-1}	*This work*
K_{eq}	0.487	[33]

[1] *Average value of affinities for Trypanosmoma brucei & Lactococcus lactis*
[2] *Determined using the Haldane relationship.*

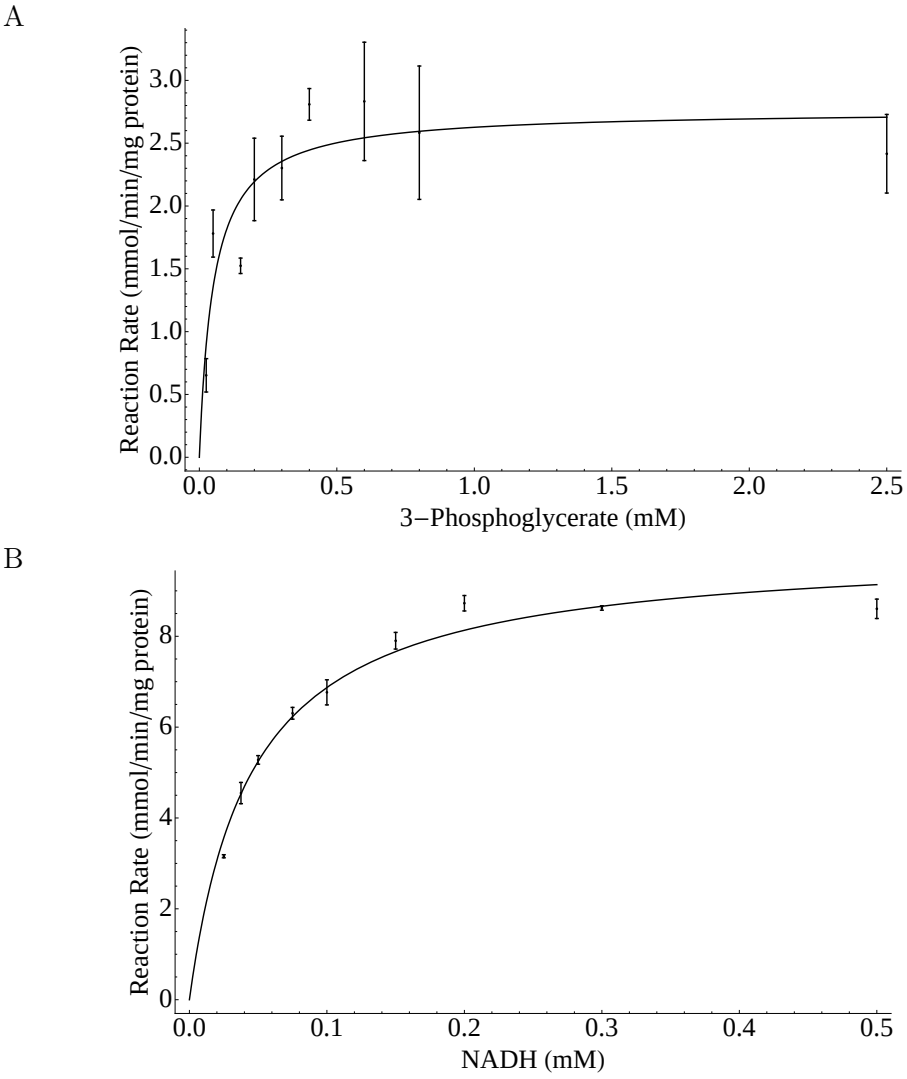

Figure 4.4: Characterisation of *P. falciparum* glyceraldehyde 3-phosphate dehydrogenase in terms of its products. A) Since the substrate 1,3BPG is chemically unstable, 3PGA in the presence of excess PGK and ATP is used to produce 1,3BPG. It is assumed that the majority of 3PGA is converted to 1,3BPG. B) NADH is varied between 0 and 0.5 mM in the presence of saturating 3PGA and excess PGK and ATP. Non-linear regression of the data with the Michaelis-Menten equation is shown. Error bars represented standard deviation of the mean (n = 3).

4.1.8 Phosphoglycerate Kinase

Phosphoglycerate kinase was characterised for the reverse direction using 3-phosphoglycerate and ATP as substrates with the K_m values (n = 3) being determined to be 2.97 ± 1.77 mM and 1.41 ± 1.25 mM, respectively (results not shown). Due to the large error in these parameter values, the kinetic parameters, excepting enzyme activities, were obtained from literature (Table 4.8). Since 1,3BPG is chemically unstable the forward reaction was not characterised.

No regulation is known for *P. falciparum* phosphoglycerate kinase and it was described by a reversible bisubstrate rate equation (Eq. 4.1.10.).

$$vPGK = \frac{V_f \cdot bpg \cdot adp(1 - \frac{3pga \cdot atp}{bpg \cdot adp \cdot K_{eq}})}{Km_{bpg} \cdot Km_{adp}(1 + \frac{dpg}{Km_{bpg}} + \frac{3pga}{Km_{3pga}})(1 + \frac{adp}{Km_{adp}} + \frac{atp}{Km_{atp}})} \tag{4.1.10}$$

Where, $vPGK$ is the reaction rate, V_f is the maximal forward rate, bpg, adp, $3pga$, atp are the 1,3BPG, ADP, 3PGA and ATP concentrations, Km_{bpg}, Km_{adp},Km_{3pga},Km_{atp} are Michaelis constants for 1,3BPG, ADP, 3PGA and ATP and K_{eq} is the equilibrium constant of the reaction.

Table 4.8: Kinetic parameter values obtained for *P. falciparum* 3-phoshoglycerate kinase.

Metabolite	$K_m(mM)$	Reference
1,3BPG	0.0134	[118]
ADP	0.300	[118]
3PGA	0.17	[118]
ATP	0.68	[118]
Equation Parameters		Reference
$V_{max_{(forward)}}$	30.89[1] μmol.min^{-1}.mg protein^{-1}	*This work*
$V_{max_{(reverse)}}$	0.470 ± 0.0075 μmol.min^{-1}.mg protein^{-1}	*This work*
K_{eq}	1890	[33]

[1] *Determined using the Haldane relationship.*

4.1.9 Phosphoglycerate Mutase

Phosphoglycerate mutase, which has not been characterised for *Plasmodium* previously, was characterised in terms of both its substrate and product (Fig 4.5). The determined the kinetic parameters presented in table 4.9. The enzyme rate was described by a reversible Michaelis-Menten equation (Eq. 4.1.11.)

The equilibrium constant determined using the Haldane relationship (Table 4.9.) is approximately 18 times less than expected. No explanation can be offered for this significant difference and in future work each of the parameters will be redetermined in an attempt to resolve the issue.

$$vPGM = \frac{V_f \cdot 3pga(1 - \frac{pga2}{pga3 \cdot K_{eq}})}{Km_{3pga}(1 + \frac{3pga}{Km_{3pga}} + \frac{2pga}{Km_{2pga}})} \tag{4.1.11}$$

Where, $vPGM$ is the reaction rate, V_f is the maximal forward rate, $3pga$, $2pga$ are the 3PGA and 2PGA concentrations, Km_{3pga}, Km_{2pga} are Michaelis constants for 3PGA and 2PGA and K_{eq} is the equilibrium constant of the reaction.

Table 4.9: Kinetic parameters experimentally determined for *P. falciparum* phosphoglycerate mutase.

Metabolite	$K_m(mM)$	Reference
3PGA	2.7 ± 0.39	*This work*
2PGA	0.33 ± 0.029	*This work*

Equation Parameters				Reference
$V_{max_{(forward)}}$	0.601 ± 0.0723	μmol.min^{-1}.mg protein^{-1}		*This work*
$V_{max_{(reverse)}}$	0.133 ± 0.0235	μmol.min^{-1}.mg protein^{-1}		*This work*
K_{eq}	9.8	[89]	0.55[1]	*This work*

[1] *Determined using the Haldane relationship.*

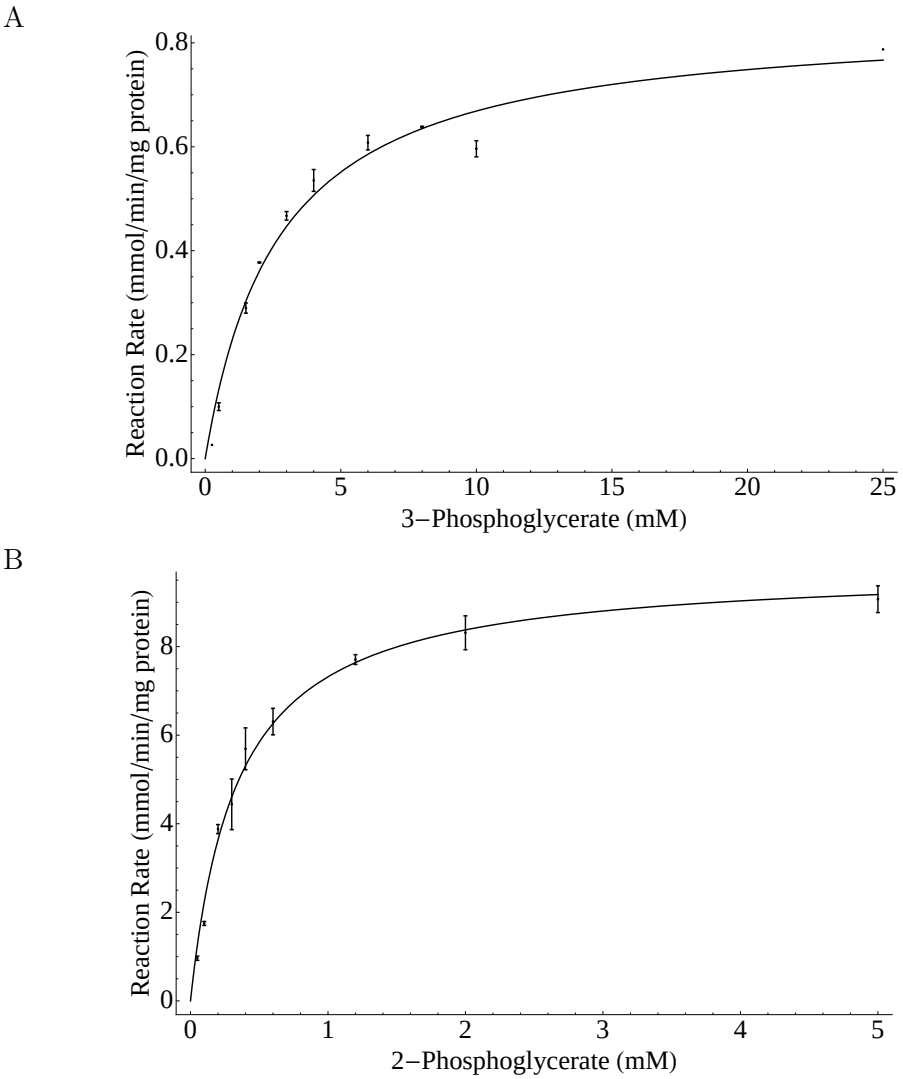

Figure 4.5: Kinetic characterisation of *P. falciparum* PGM in terms of substrate and product. A) Substrate 3-phosphoglycerate was varied between 0-25 mM. B) 2-Phosphoglycerate was varied between 0-5 mM. Fitting with the Michaelis-Menten equation (shown) was used to determine V_{max} and K_m values. Standard deviation of the mean (n = 3) is indicated with error bars.

In the model the $V_{max_{(forward)}}$ parameter value is used as it was considered more accurate than the reverse reaction rate. This assumption was based on the fact that the forward assay is linked via thermodynamically favourable reactions catalysd by ENO, PK and LDH, compared to the less favourable reverse reactions.

4.1.10 Enolase

P. falciparum enolase was characterised for its substrate and product (Figs. 4.6 and 4.7, respectively). Kinetic parameters determined by fitting the experimental data to a reversible Michaelis-Menten equation (Eq. 4.1.12.) are displayed in Table 4.10.

$$vENO = \frac{V_f \cdot 2pga(1 - \frac{pep}{2pga \cdot K_{eq}})}{Km_{2pga}(1 + \frac{pep}{Km_{pep}} + \frac{pga2}{Km_{2pga}})} \tag{4.1.12}$$

Where, *vENO* is the reaction rate, V_f is the maximal forward rate, *2pga*, *pep* are the 2PGA and PEP concentrations, Km_{2pga}, Km_{pep} are Michaelis constants for 2PGA and PEP and K_{eq} is the equilibrium constant of the reaction.

The affinities of substrate and product determined in this work are both approximately a quarter of those determined by Pal *et al*[106]. The discrepancy may be due to the fact that Pal used recombinant *P. falciparum* NF54 enolase and an optimum enzyme activity pH of 7.4.

Table 4.10: Kinetic parameters determined for *P. falciparum* enolase.

Metabolite	$K_m(mM)$	Reference	$K_m(mM)$	Reference
2PG	0.010 ± 0.0026	*This work*	0.041 ± 0.004	[106]
PEP	0.63 ± 0.17	*This work*	0.25 ± 0.03	[106]
Equation Parameters				Reference
$V_{max_{(forward)}}$	0.346 ± 0.019 μmol.min^{-1}.mg protein^{-1}			*This work*
$V_{max_{(reverse)}}$	0.151 ± 0.020 μmol.min^{-1}.mg protein^{-1}			*This work*
K_{eq}	4.6	[89]	44.1[1]	*This work*

[1] *Determined using the Haldane relationship.*

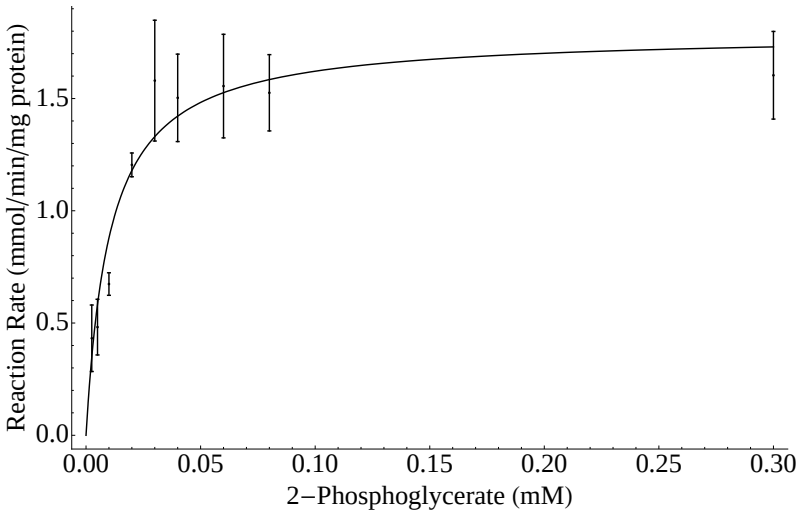

Figure 4.6: *P. falciparum* enolase was kinetically characterised in terms of its substrate 2-phosphoglycerate. Kinetic parameters (V_{max} and K_m) were determined by fitting with the Michaelis-Menten equation (shown). Error bars represent standard deviation of the mean (n = 3).

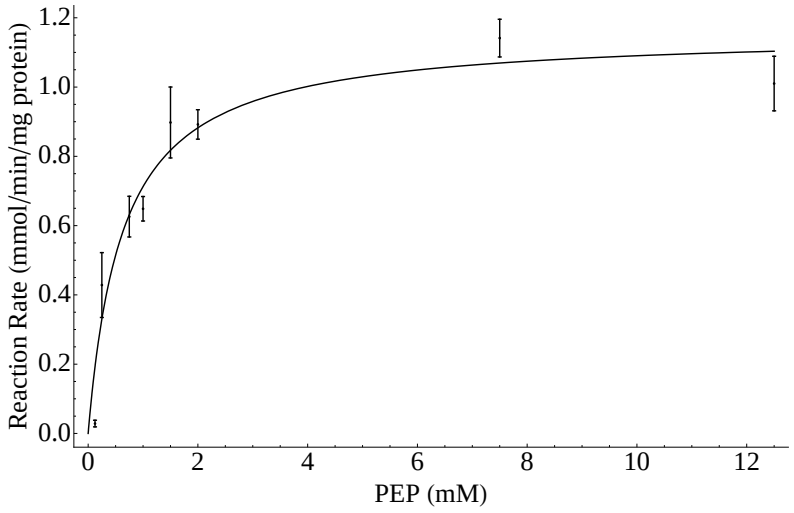

Figure 4.7: *P. falciparum* enolase was kinetically characterised in terms of its product, phosphoenolpyruvate. Kinetic parameters (V_{max} and K_m) were determined by fitting with the Michaelis-Menten equation (shown). Error bars represent standard deviation of the mean (n = 3).

4.1.11 Pyruvate Kinase

Pyruvate kinase was assumed to be irreversible, inhibited by ATP and described by Eq. 4.1.13. PK was characterised in this work, but due to lack of reproducibility and large error the kinetic parameters (except V_{max}) that were used in the kinetic model were obtained from literature (Table 4.11.).

$$vPK = \frac{V_f \cdot pep \cdot adp}{Km_{pep} \cdot adp(1 + \frac{atp}{Ki_{atp}}) + Km_{adp} \cdot pep + adp \cdot pep)} \tag{4.1.13}$$

Where, vPK is the reaction rate, V_f is the maximal forward rate, adp, pep, atp are the ADP, PEP and ATP concentrations, Km_{adp}, Km_{pep} are Michaelis constants for ADP and PEP and Ki_{atp} is the inhibition constant of ATP.

Table 4.11: Kinetic parameters obtained from literature for *P. falciparum* pyruvate kinase.

Metabolite	$K_m(mM)$	Reference
PEP	0.190 ± 0.028	[27]
ADP	0.126 ± 0.043	[27]
Equation Parameters		**Reference**
Ki_{ATP}	1.0 mM[1]	[27]
$V_{max(forward)}$	0.756 ± 0.0147 μmol.min^{-1}.mg protein^{-1}	*This work*

[1] *Estimated from (Fig. 5.) in Chan et al*[27].

4.1.12 Lactate Dehydrogenase

P. falciparum lactate dehydrogenase was characterised in terms of its substrates and products (Figs. 4.8. & 4.9. respectively). A bisubstrate reversible generic rate equation (Eq. 4.1.14.) was used to describe the LDH reaction, with the determined kinetic parameters shown in Table 4.12.

$$vLDH = \frac{V_f \cdot pyr \cdot nadh \cdot (1 - \frac{Lac_{int} \cdot nad}{pyr \cdot nadh \cdot K_{eq}})}{(Km_{pyr} \cdot Km_{nadh})(1 + \frac{pyr}{Km_{pyr}} + \frac{Lac_{int}}{Km_{pyr}})(1 + \frac{nad}{Km_{nad}} + \frac{nadh}{Km_{nadh}})} \tag{4.1.14}$$

Where, *vLDH* is the reaction rate, V_f is the maximal forward rate, *pyr*, *nadh*, *nad*, Lac_{int} are the pyruvate, NADH, NAD^+ and internal lactate concentrations, Km_{pyr}, Km_{nadh}, Km_{nad}, $Km_{Lac_{int}}$ are Michaelis constants for pyruvate, NADH, NAD^+ and internal lactate and K_{eq} is the equilibrium constant of the reaction.

Table 4.12: Kinetic parameters determined for *P. falciparum* lactate dehydrogenase.

Metabolite	$K_m(mM)$	Ref.	$K_m(mM)$	Ref.	$K_m(mM)$	Ref.
Pyr	0.089 ± 0.016	*This work*	0.055	[133]	0.030	[56]
NADH	0.0302 ± 0.0065	*This work*	0.011	[133]	0.007	[56]
Lac	2.39 ± 0.42	*This work*	47	[133]	12	[56]
NAD^+	0.200 ± 0.066	*This work*	0.180	[133]	0.086	[56]
Equation Parameters						Ref.
$V_{max_{(forward)}}$	1.280 ± 0.0871 μmol.min^{-1}.mg protein^{-1}					*This work*
K_{eq}	10684					[159]
$K_{i_{Pyruvate}}$	140 ± 18 mM					[133]

The K_m values determined for pyruvate, NADH and NAD^+ in this and other works (see Table 4.12.) are all within the same order of magnitude, with differences being ascribed to varying assay pH.

Gomez *et al*[56] used a pH of 9.2 for the characterisation of NAD^+, pyruvate and lactate affinity and a pH of 7.5 for NADH, while Shoemark *et al*[133] used a pH of 7.5 for both substrates and products. These different assay conditions may also provide a reason for the large variation in the affinity of lactate for LDH, which varies between 2 and 50 mM.

A.

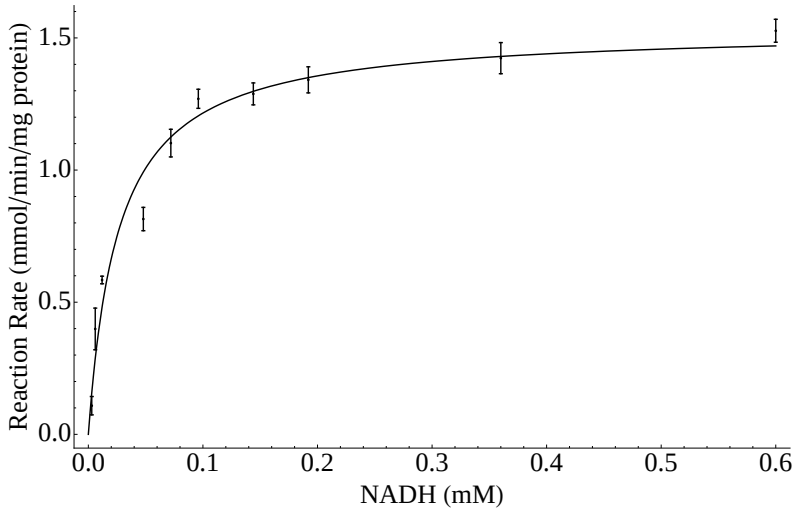

B.

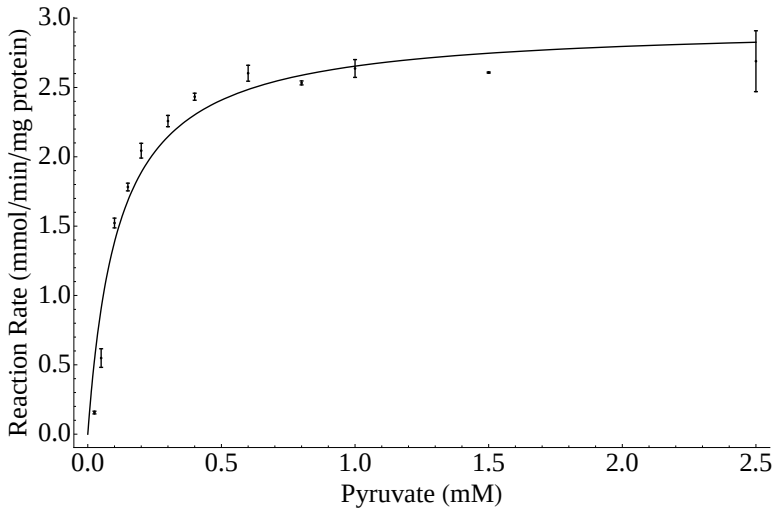

Figure 4.8: *P. falciparum* lactate dehydrogenase characterised in terms of its substrates. A) Characterisation of NADH binding under saturating pyruvate concentrations. B) Pyruvate concentration was varied under saturating NADH concentrations . Fitting with the Michalis-Menten equation (shown) produced V_{max} and K_m values. Standard deviation of the mean (n=3) is indicated by means of error bars.

A.

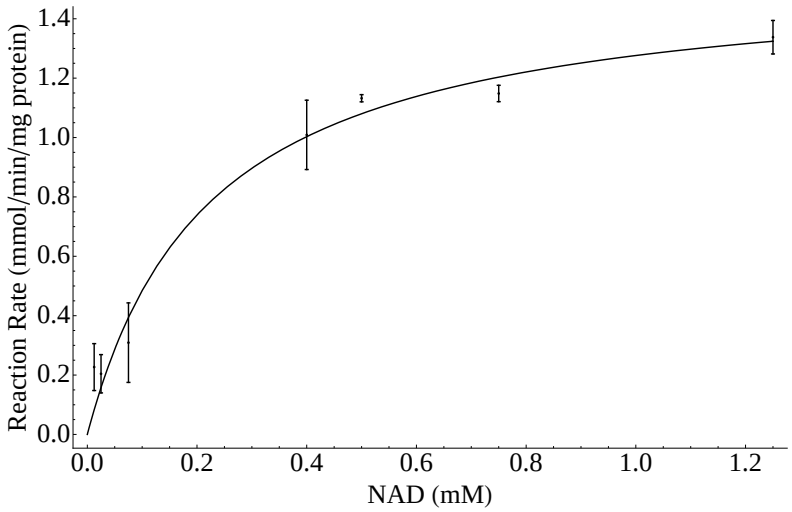

B.

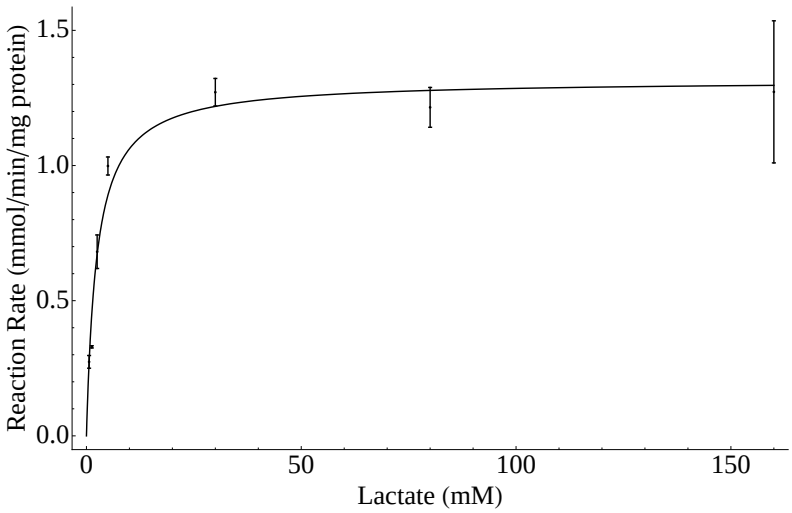

Figure 4.9: Kinetic characterisation of *P. falciparum* lactate dehydrogenase in terms of its products A) NAD^+ and B) lactate. Product concentrations were varied under saturating concentrations of the other product. To determine the kinetic parameters, the data were fitted to the Michaelis-Menten equation. Standard deviation of the mean is indicated by error bars (n = 3).

4.1.13 Lactate Transporter

The transport of lactate in *P. falciparum* has been studied previously[43] and the kinetic parameters, where possible were obtained from literature (Table 4.13.) The transporter was assumed to bind rapidly as well as reversibly and symmetrically (Eq. 4.1.15.)

$$vLac_{Transport} = \frac{V_f \cdot Lac_{ex}(1 - \frac{Lac_{ex}}{K_{eq} \cdot Lac_{int}})}{Km_{Lac_{int}}(1 + \frac{Lac_{ex}}{Km_{Lac_{ex}}} + \frac{Lac_{int}}{Km_{Lac_{int}}})} \tag{4.1.15}$$

Where, $vLac$ is the reaction rate, V_f is the maximal forward rate, Lac_{ex}, Lac_{int} are the external and internal lactate concentrations, $Km_{Lac_{ex}}$, $Km_{Lac_{int}}$ are Michaelis constants for external and internal lactate and K_{eq} is the equilibrium constant of the reaction.

Table 4.13: Kinetic parameter values obtained from literature for the *P. falciparum* lactate transporter.

Metabolite	$K_m(mM)$	Reference
$Lac_{external}$	3.8 ± 0.8	[43]
$Lac_{internal}$	3.8[1]	
Equation Parameters		Reference
$V_{max_{(forward)}}$	1.5[2] μmol.min^{-1}.mg protein^{-1}	*This work*
K_{eq}	1.0	

[1] *Assumed symmetrical binding.*
[2] *Assumed to be rapid.*

4.2 Maximal enzyme rates

The maximal rates of each glycolytic enzyme were all determined (except for the transporters) from a homogenate of trophozoite lysates to counter variation in protein expression levels between batches. Each of the V_{max} parameter values have been displayed in the preceding section, but are summarised here in Table 4.14. for comparison. Since all of the V_{max} values are determined

from a single homogenate on the same day loss of enzyme activity may occur for some enzymes. This may indeed be the case for many of the enzymes where measured maximal enzyme activities are far lower than when determined from saturating curves. Loss of enzyme activity during storage and during enzyme activity assays will be investigated.

Table 4.14: Experimentally determined maximal enzyme rates for the glycolytic enzymes in *Plasmodium falciparum*. Rates are normalised to total protein content and standard deviation of triplicate values determined in a single experiment is indicated.

Enzyme	Maximal Rate ($mmol \cdot min^{-1} \cdot mg\ protein^{-1}$)	
	Forward	*Reverse*
GlucTr	0.01-0.12 [1]	
HK	0.325 ± 0.0092	-
PGI	0.363 ± 0.0326	0.232 ± 0.0354
PFK	0.142 ± 0.0167	-
ALD	0.311 ± 0.0354	-
TPI	0.285[2]	2.198 ± 0.0426
GAPDH	0.346[2]	0.214 ± 0.0807
PGK	30.89[2]	0.470 ± 0.0075
PGM	0.601 ± 0.0723	0.133 ± 0.0235
ENO	0.346 ± 0.0193	0.151 ± 0.0200
PK	0.756 ± 0.0147	-
LDH	1.280 ± 0.0871	-
LacTr	1.5[3]	

[1] *Range of values used.*
[2] *Determined using the Haldane relationship.*
[3] *Assumed to be rapid.*

4.3 Flux Determinations

An important part of any kinetic modeling is validation. In this study we partially validated the kinetic model (see next Chapter) by comparing measured fluxes and the steady state flux predicted by the model (Table 4.15).

The *in vivo* flux was measured by incubating intact trophozoites in a buffer containing glucose and measuring the rate of glucose consumption and lactate production (Fig. 4.10). Not all the glucose is consumed and the consumption rate decreases after approximately 3 hours. This may be due to the decrease in pH of the medium since 15 mM of lactate are produced in a 25 mM HEPES buffer, but this hypothesis has yet to be tested.

It should be noted that the trophozoites were found to be extremely sensitive to the saponin isolation protocol. Trophozoites were removed from saponin contact as soon as possible, in order to maintain membrane integrity and membrane potential. Failure to do so resulted in negligible glycolytic flux (results not shown).

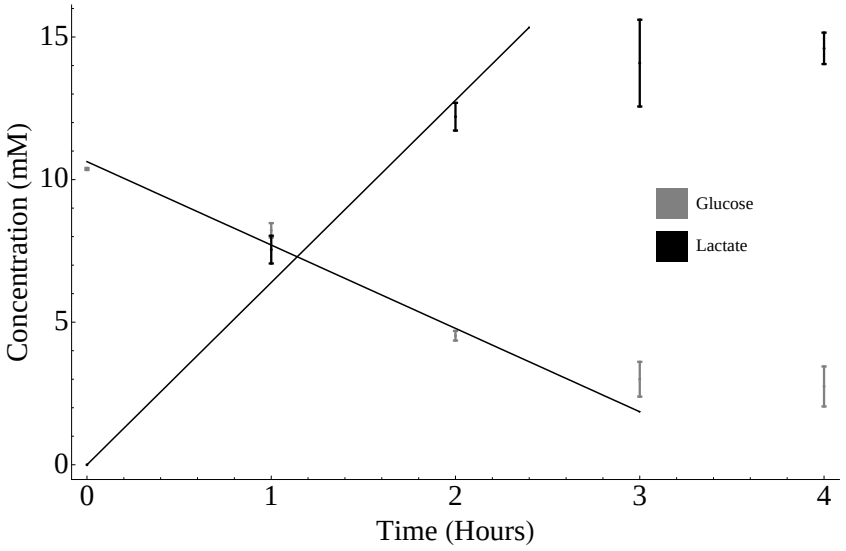

Figure 4.10: Utilisation of glucose and production of lactate in saponin isolated *P. falciparum* trophozoites. Linear regression over the first 3 hours of incubation ($R^2 > 0.97$), yielded flux rates (Table 4.15), where the lactate production rate is approximately double the glucose consumption rate. Lactate data representative of triplicate and glucose in duplicate experiments.

The linear consumption and production rate of glucose and lactate over a period of 3 hours, respectively, were used as the glycolytic fluxes (Table 4.15). The ratio of the production and consumption rates is approximately 2.2, which shows that the assumption that 1 mol glucose is entirely converted to 2 mol lactate, with negligible flux through alternative pathways, is valid.

Table 4.15: Glucose consumption and lactate production rates of intact isolated *P. falciparum* trophozoites incubated in a glucose medium over a period of 3 hours.

Metabolite	Rate ($mmol \cdot min^{-1} \cdot mg\ protein^{-1}$)
Glucose	0.0487
Lactate	0.1065
Lactate : Glucose Ratio	2.186

Whether this flux is in steady state is unknown, since the metabolite concentrations were not measured. A constant flux is not an indicator of steady state, as one could still find slow accumulation of one or more intermediates. At steady state the internal metabolite concentrations would be constant. The method for the determination of the glycolytic intermediates was established (Section 4.4) and future work will include full validation of the model with steady state metabolite concentrations.

4.4 Method Development: Measuring Intermediate Concentrations

Measuring the internal metabolites is of the utmost importance for validating the model. Glycolytic intermediates were determined enzymatically by adapting a protocol described by Maitra *et al*[92]. The advantage of the enzymatic determinations, is their accuracy and simplicity and it was important to determine the sensitivities of the assays, as parasite concentrations in incubations are generally lower than those used for yeast or bacteria.

All the intermediates were determined in four separate stepwise assays where

20 μL sample/standard was added to 80 μL assay buffer (described previously) containing various enzymes and cofactors. G6P was determined by incubating standards or samples in assay buffer containing NADP (2 mM) and G6PDH (20 U/mL) for 10 min, after which the absorbance was measured at 340 nm. Once the absorbance was recorded, F6P was determined by adding PGI (20 U/mL) and incubated for a further 10 min and measuring absorbance at 340 nm.
In a similar step wise manner, DHAP, GAP and FBP were determined by incubating the samples/standards in buffer containing NADH (2 mM) and α-glyceroPDH (20U/mL). Following a 30 minute incubation period, absorbance was measured, followed by the addition of TIM (50U/mL) and a further 30 min incubation period. Lastly FBP was determined by the addition of ALD (20 U/mL) and a 10 min incubation.
3PGA and 2PGA were determined by incubating samples/standards in assay buffer containing NADH (2mM), GAPDH (20 U/mL) and ATP (4 mM). Absorbance was read at 340 nm after a 20 min incubation period, after which 2PGA was determined by the addition of PGM (10 U/mL) and a 20 incubation period.
PEP and pyruvate were determined incubating standards or samples in assay buffer containing LDH (20 U/mL), NADH (2mM) for 20 min and reading the absorbance at 340nm. Pyruvate was determined by the addition of PK (20 U/mL) and ADP (4mM) and incubating for 25 minutes before reading the absorbance at 340 nm.
Incubation times were determined by monitoring the change in absorbance at 340 nm over time until the rate became zero.
Satisfactory calibration curves were obtained for all the glycolytic intermediates (Figures 4.11 and 4.12), except for GAP. The protocol rendered sensitivities (down to 10 μM) for G6P, F6P, PEP and pyruvate and below 100 μM for F 1,6BP and 2PGA. Concentrations of DHAP and 3PGA below 0.3 mM could not be accurately determined.

This protocol was tested on *Plasmodium* incubations, but metabolites were not detectable, due to cell concentration (10^8trophozoites/mL) being too low. Assuming a 30 fL volume for a trophozoite 35 hours post-invasion[2] and the desired ability to measure > 100 μM, and taking into account dilution due to extraction procedures, one would have to incubate at extremely high

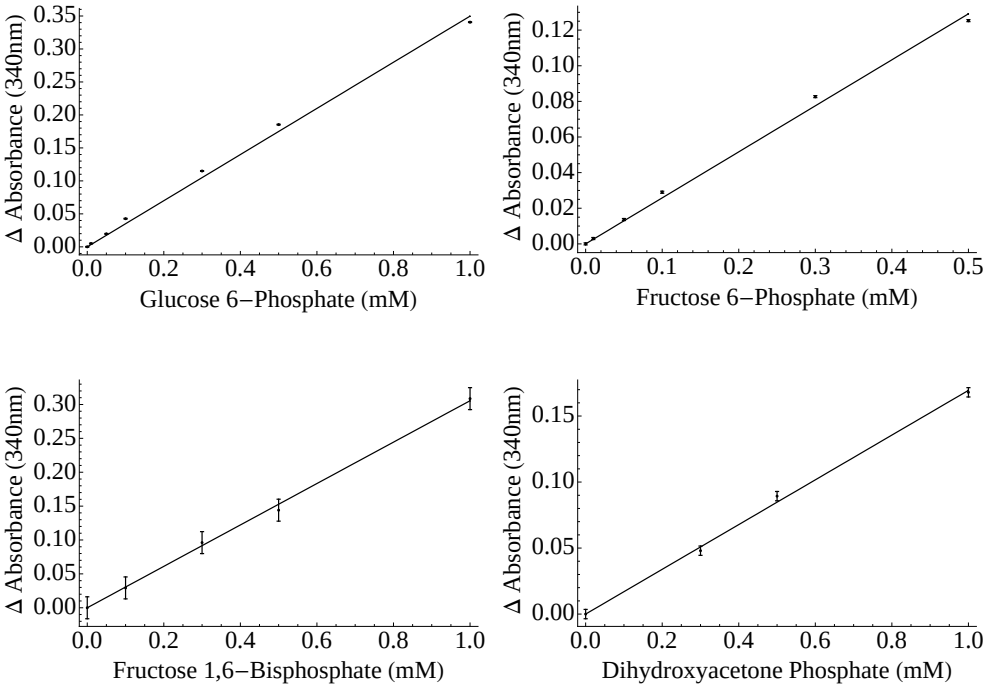

Figure 4.11: Calibration curves obtained from the method established for the enzymatic determination of glucose 6-phosphate, fructose 6-phoshate, fructose 1,6-bisphosphate and dihydroxyacetone phosphate. Data shown with a linear fit ($R^2 > 0.99$) is from a single experiment, but trends are representative of duplicate assays.

concentrations of approximately 10^{10} trophozoites/mL. Culturing such large numbers of parasites is not feasible with 10^9 trophozoites/mL, being more appropriate. Since sample volume and assay sensitivity have been shown to be linear[92], one could increase the assay sensitivity approximately two fold. This method, should thus theoretically be suitable for measuring internal metabolite concentrations in *Plasmodium* above 500μM. Some of the intermediates present at low concentrations, such as the phoshopglycerates may not be detectable. For these metabolites more sensitive detection methods, such as mass spectrometric detection protocols described in[16,151], could be used.

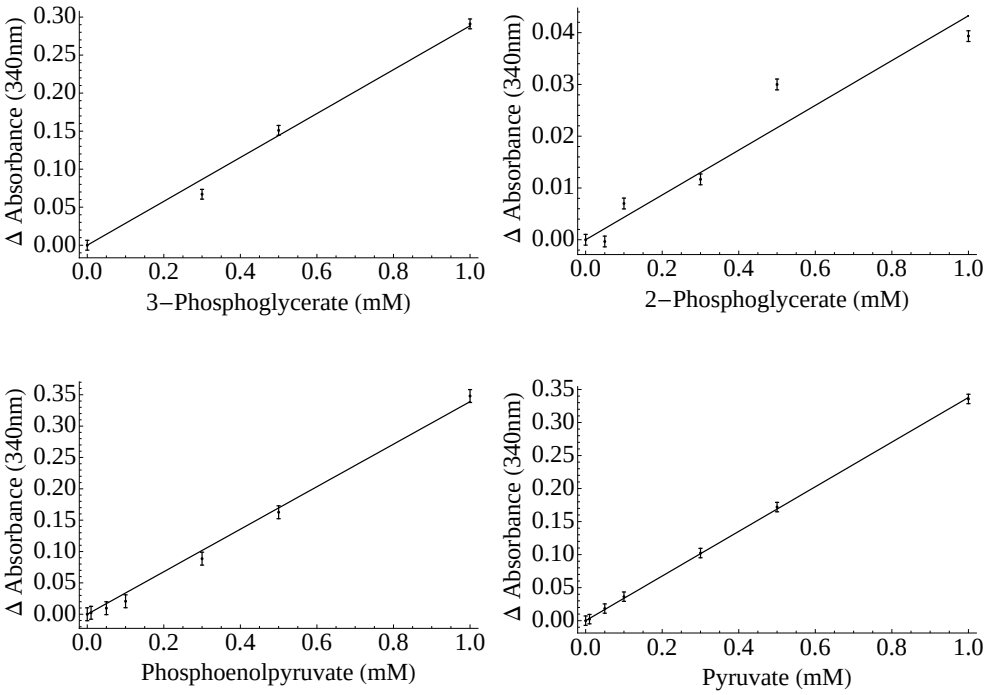

Figure 4.12: Calibration curves obtained from the method established for the enzymatic determination of 3 and 2-phosphoglycerate, phosphoenolpyruvate and pyruvate. Data shown with linear fit ($R^2 > 0.99$, except for phosphoglycerates: $R^2 > 0.9$) is from a single experiment, but trends are representative of duplicate assays.

Chapter 5

Theoretical Results and Discussion

This chapter presents the theoretical aspects of this work, which include the construction and validation of a detailed kinetic model for *P. falciparum* glycolysis. The experimental results used for the construction and validation of the model were presented in the preceding chapter.

5.1 Kinetic Model Construction

The homolactic fermentation of glucose was modelled in thirteen reaction steps (Fig. 5.1). The model consists of a set of ordinary differential equations (Eqns 5.1.1 - 5.1.16), which describe the change in glycolytic metabolite concentrations over time as a function of enzyme rates (Eqns 5.1.17 - 5.1.30).

$$glu'[t] = v0Glutr - v1HK \quad (5.1.1)$$

$$g6p'[t] = v1HK - v2PGI \quad (5.1.2)$$

$$f6p'[t] = v2PGI - v3PFK \quad (5.1.3)$$

$$f16dp'[t] = v3PFK - v4ALD \quad (5.1.4)$$

$$dhap'[t] = v4ALD - v5TIM \quad (5.1.5)$$

$$gap'[t] = v4ALD + v5TIM - v6G3PDH \quad (5.1.6)$$

$$bpg'[t] = v6G3PDH - v7PGK \quad (5.1.7)$$

$$3pga'[t] = v7PGK - v8PGM \quad (5.1.8)$$

$$2pga'[t] = v8PGM - v9ENO \quad (5.1.9)$$

$$pep'[t] = v9ENO - v10PK \quad (5.1.10)$$

$$pyr'[t] = v10PK - v11LDH \quad (5.1.11)$$

$$lac'[t] = v11LDH - v12LACtr \quad (5.1.12)$$

$$atp'[t] = v7PGK + v10PK - v1HK - v3PFK - v13atp \quad (5.1.13)$$

$$adp'[t] = v1HK + v3PFK - v7PGK - v10PK + v13atp \quad (5.1.14)$$

$$nadh'[t] = v6G3PDH - v11LDH \quad (5.1.15)$$

$$nadh'[t] = v11LDH - v6G3PDH \quad (5.1.16)$$

The transporter rates v0Glutr (Eq. 5.1.17.)and v12LACtr (Eq. 5.1.29.) describe the transport of glucose and lactate across the parasite membrane and into or out of the parasite cytosol, respectively. The enzyme rates v1HK (hexokinase, Eq. 5.1.18.), v2PGI (phosphoglucoisomerase, Eq. 5.1.19.), v3PFK (phosphofructokinase, Eq. 5.1.19.), v4ALD (aldolase, Eq. 5.1.21.), v5TIM (triosephosphate isomerase, Eq. 5.1.22.), v6G3PDH (glyceraldehyde phosphate dehydrogenase, Eq. 5.1.24.), v7PGK (phosphoglycerate kinase, Eq. 5.1.24.), v8PGM (phosphoglycerate mutase, Eq. 5.1.25.), v9ENO (enolase, Eq. 5.1.26.), v10PK (pyruvate kinase, Eq. 5.1.27.) and v11LDH (lactate dehydrogenase, Eq. 5.1.28.) describe the modelled enzymatic reactions.
Each enzyme rate (Eqns 5.1.17 - 5.1.30) is described using reversible or irreversible uni-substrate Michaelis-Menten equations or bi-substrate generic rate equations[116], except in the cases of i) v3PFK which uses a Monod-Wyman-Changreux equation obtained from Buckwitz *et al*[17] and ii) v10PK which is a Ping-Pong Bi-Bi kinetic equation.

In *P. falciparum* the activities of PFK and PK are allosterically regulated. The rate equation v3PFK contains allosteric regulation in the forms of PEP activation and ATP inhibition and competitive by ADP.
P. falciparum pyruvate kinase is inhibited by ATP, but this has only been partially characterised by Chan *et al*[27] who showed that ATP is competitive with respect to PEP. The inhibition mechanism of ATP with respect to ADP is unknown, but was assumed to be uncompetitive and thus v10PK follows a ping-pong bi-bi rate mechanism and includes inhibition by ATP.

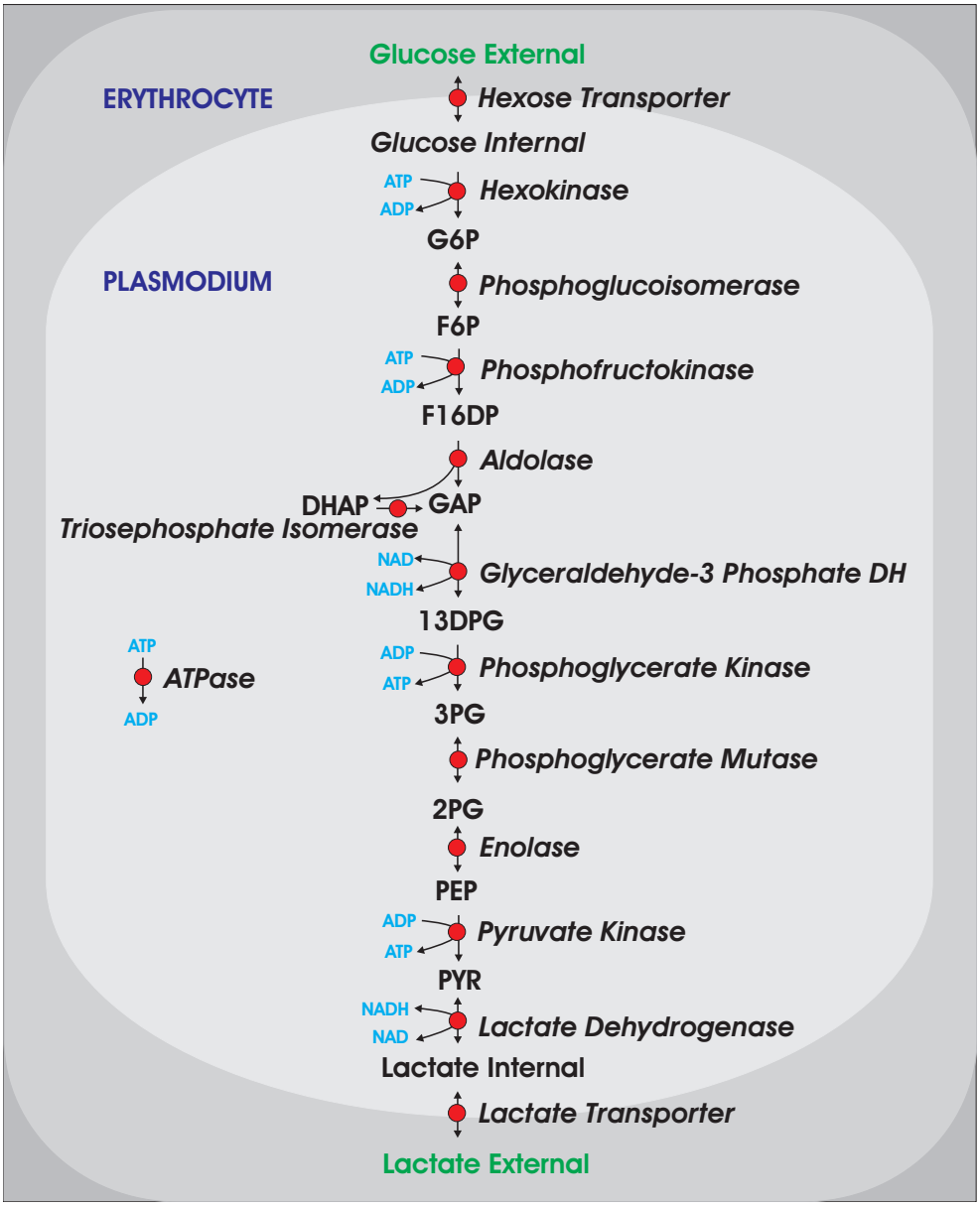

Figure 5.1: Schematic representation of the glycolytic pathway in *P. falciparum*, where glucose is entirely converted to lactate and ATP. Enzymes are indicated by red circles, clamped metabolites in green text, and erythrocyte and parasite compartments in different shades of grey.

The kinetic parameter values that were used in the rate equations are summarised in Table 5.1. See Section 4.1 for specific details of how the constants were determined.
Since the complete conversion of glucose to lactate results in a net production of 2 mol ATP per mol glucose an ATP demand reaction ($v13atp$, Eq. 5.1.30) was included to prevent the accumulation of ATP and thus make a steady state possible. $v13atp$ is a Michaelis-Menten type equation, which acts as an ATPase. The parameter values used for the ATPase reaction (both V_{max} and Michaelis constant, Table 5.1.) were obtained by fitting them to obtain an ATP/ADP ratio of five, which was observed by Fry *et al*[52]. These parameters were fitted as they can not be determined experimentally.

In the model all enzyme rates were expressed in μmol.min^{-1}.mg protein^{-1}, time t in min and the metabolite concentrations in mM. Since the relation between total protein concentration and cytosolic volume could not be determined, there is an inconsistency between the units of the maximal rates and metabolite concentrations. This restricts the current model to steady state evaluations, as were used in the work presented in this thesis. In future, to allow for time integration of the model, the relation between total protein and cytosolic volume will be determined. This relation will allow the maximal rates to be expressed as mM·min^{-1} and thus maintain dimensional consistency.

$$v0Glutr = \frac{(VGLUtr \cdot gluex(1 - \frac{glu[t]}{gluex \cdot Kv0eq})}{Kv0glutr(1 + \frac{gluex}{Kv0glutr} + \frac{glu[t]}{Kv0Gluint})} \tag{5.1.17}$$

$$v1HK = \frac{VHK \cdot glu[t] \cdot atp[t]}{Kv1glu \cdot Kv1atp(1 + \frac{glu[t]}{Kv1glu})(1 + \frac{atp[t]}{Kv1atp})} \tag{5.1.18}$$

$$v2PGI = \frac{VPGI \cdot g6p[t](1 - \frac{f6p[t]}{g6p[t] \cdot Kv2eq})}{(Kv2g6p(1 + \frac{g6p[t]}{Kv2g6p} + \frac{f6p[t]}{Kv2f6p})} \tag{5.1.19}$$

$$
\begin{aligned}
v3PFK &= \frac{VPFK \cdot atp[t] \cdot f6p[t]}{(atp[t] + Kv3atp(1 + \frac{adp[t]}{Kv3adp}))(f6p[t] + Kv3f6p)}(\frac{1}{1 + v3L_o}) \\
v3L_o &= v3L(\frac{(1 + \frac{v3Mg}{Kv3mg})(1 + \frac{atp[t]}{Kv3atp})}{(1 + \frac{f6p[t]}{Kv3f6p2})(1 + \frac{pep[t]}{Kv3pep})})^{v3n} \qquad (5.1.20)
\end{aligned}
$$

$$
v4ALD = \frac{VALD \cdot f16dp[t](1 - \frac{dhap[t] \cdot gap[t]}{f16dp[t] \cdot Kv4eq})}{Kv4f16dp(1 + \frac{f16dp[t]}{Kv4f16dp} + \frac{dhap[t]}{Kv4dhap} + \frac{gap[t]}{Kv4gap} + \frac{gap[t] \cdot dhap[t]}{Kv4gap \cdot Kv4dhap})} \qquad (5.1.21)
$$

$$
v5TIM = \frac{VTIM \cdot dhap[t](1 - \frac{gap[t]}{dhap[t] \cdot Kv5eq})}{Kv5dhap(1 + \frac{dhap[t]}{Kv5dhap} + \frac{gap[t]}{Kv5gap})} \qquad (5.1.22)
$$

(5.1.23)

$$
v6G3PDH = \frac{VG3PDH \cdot gap[t] \cdot nad[t] \cdot (1 - \frac{dpg[t] \cdot nadh[t]}{(gap[t] \cdot nad[t] \cdot Kv6eq})}{(Kv6gap \cdot Kv6nad)(1 + \frac{gap[t]}{Kv6gap} + \frac{dpg[t]}{Kv6dpg}(1 + \frac{nad[t]}{Kv6nad} + \frac{nadh[t]}{Kv6nadh})}
$$

$$
v7PGK = \frac{VPGK \cdot dpg[t] \cdot adp[t](1 - \frac{pga3[t] \cdot atp[t]}{dpg[t] \cdot adp[t] \cdot Kv7eq})}{Kv7dpg \cdot Kv7adp(1 + \frac{dpg[t]}{Kv7dpg} + \frac{pga3[t]}{Kv7pga3})(1 + \frac{adp[t]}{Kv7adp} + \frac{atp[t]}{Kv7atp})} \qquad (5.1.24)
$$

$$
v8PGM = \frac{VPGM \cdot pga3[t](1 - \frac{pga2[t]}{pga3[t] \cdot Kv8eq})}{Kv8pga3(1 + \frac{pga3[t]}{Kv8pga3} + \frac{pga2[t]}{Kv8pga2})} \qquad (5.1.25)
$$

$$
v9ENO = \frac{VENO \cdot pga2[t](1 - \frac{pep[t]}{pga2[t] \cdot Kv9eq})}{Kv9pga2(1 + \frac{pep[t]}{Kv9pep} + \frac{pga2[t]}{Kv9pga2})} \qquad (5.1.26)
$$

$$
v10PK = \frac{VPK \cdot pep[t] \cdot adp[t]}{Kv10pep \cdot adp[t](1 + \frac{atp[t]}{Kiv10}) + Kv10adp \cdot pep[t] + adp[t] \cdot pep[t])} \qquad (5.1.27)
$$

$$
v11LDH = \frac{VLDH \cdot pyr[t] \cdot nadh[t] \cdot (1 - \frac{lac[t] \cdot nad[t]}{pyr[t] \cdot nadh[t]) \cdot Kv11eq})}{(Kv11pyr \cdot Kv11nadh)(1 + \frac{pyr[t]}{Kv11pyr} + \frac{lac[t]}{Kv11pyr})(1 + \frac{nad[t]}{Kv11nad} + \frac{nadh[t]}{Kv11nadh})} \qquad (5.1.28)
$$

$$v12LACtr = \frac{VLACtr \cdot lac[t]}{lac[t] + Kv12lac} \tag{5.1.29}$$

$$v13ATP = \frac{v13katp \cdot atp[t]}{Kv13atp + atp[t]} \tag{5.1.30}$$

5.1.1 Starting Conditions

In the model external metabolite concentrations were clamped and initial internal metabolite concentrations were set as explained below.
External glucose was clamped at 3 mM, which is lower than concentrations found in human plasma (5mM)[1], but glucose concentrations within the erythrocyte and between the parsasite parasitiphorous and plasma membrane are assumed to be lower. The external lactate concentration was fixed at 2 mM, similar to concentrations measured in uninfected red blood cells[147].
Since the external metabolites concentrations (mM) were clamped, the change in concentration due to compartment volume change (erythrocyte to parasite), was ignored. In future, if compartments are explicitly modeled the volume change will be taken into account.

Three moieties are found in the branch of glycolysis, namely (ATP + ADP), (NAD + NADH) and (DPG + 3PGA + 2PGA + PEP + Pyr + NAD). The initial conditions for the metabolites in the latter branch were set, such that the sum is approximately 5 mM. Once internal metabolites have been measured, the sum of the metabolite concentrations in the moiety can be adjusted to the sum of those experimentally determined. The NAD/NADH moiety was set to 4 mM and the sum of ATP and ADP set to 1.2 mM[141].
The initial glycolytic intermediate concentrations for the model (Table 5.2) were obtained by clamping ATP/ADP at a ratio of five and using the steady state metabolite concentrations determined in this clamped state as starting conditions in the unclamped model.

Table 5.1: Kinetic parameters used for the construction of the kinetic model, obtained in this work or from literature (See Chapter 4.1 for details). The parameters have been renamed such that each parameter name contains the reaction number that it applies to as well as an abbreviation of the metabolite name.

Reaction	Kinetic Equation Parameters Values (mM)								Reference
v0GlucTr	Kv0glutr	0.97 ± 0.34	Kv0Gluint[1]	1.0					[71]
v1HK	Kv1glu[2]	0.14 ± 0.017	Kv1atp	0.57 ± 0.06					*This work*
v2PGI	Kv2g6p	0.92 ± 0.098	Kv2f6p[2]	0.081 ± 0.003					*This work*
v3PFK	Kv3f6p	0.034	Kv3atp	0.028	Kv3adp	0.17	Kv3pep	0.13	[17]
v3PFK	Kv3f6p2	0.054	Kv3mg	0.78	v3L	3.22	v3n	3.92	[17]
v4ALD	Kv4f16dp	0.078 ± 0.01	Kv4dhap[3]	1.0	Kv4gap.[3]	1. 0			*This work*
v5TPI	Kv5gap	0.35 ± 0.16	Kv5dhap[3]	1.0					[136]
v6G3PDH	Kv6nadht	0.043 ± 0.005	Kv6dpg[2]	0.07 ± 0.019	Kv6gap[3]	0.10	Kv6nad[3]	0.10	*This work*
v7PGK	Kv7dpg	0.0134	Kv7adp	0.300	Kv7pga3	0.17	Kv7atp	0.68	[118]
v8PGM	Kv8pga3[2]	2.7 ± 0.39	Kv8pga2[2]	0.33 ± 0.029					*This work*
v9ENO	Kv9pep*	0.25 ± 0.03	Kv9pga2[2]	0.013 ± 0.002					*[107], This work*
v10PK	Kv10pep	0.190 ± 0.028	Kv10adp	0.126 ± 0.043	Kiv10[4]	1.0			[27]
v11LDH	Kv11nad	0.200 ± 0.066	Kv11pyrt	0.089 ± 0.016					*This work*
v11LDH	Kv11nadh	0.0302 ± 0.007	Kv11lac[2]	2.39 ± 0.42					*This work*
v12LacTr	Kv12lac[3]	3.8	Kv12lacex	3.8 ± 0.8					[43]
v13ATPase	Kv13atp	0.2[5]	v13katp	0.1405[5]					Fitted

[1] Assumed symmetrical binding.
[2] Determined in triplicate in a single experiment.
[3] Parameters not available and were thus estimated.
[4] Estimated from (Fig. 5.) in[27].
[5] The ATPase reaction parameters were fitted to obtain an ATP/ADP ratio of 5.

Table 5.2: These metabolite concentrations were used as initial starting concentrations in the model.

Metabolite	Concentration (mM)
$\text{Glucose}_{External}$	3
$\text{Glucose}_{Internal}$	0.1
G6P	10.
F6P	4.0
F1,6BP	1.0
DHAP	2.0
GAP	0.1
DPG	0.1
PGA3	0.5
PGA2	0.1
PEP	0.1
Pyr	2.0
Lac	2.0
NADH	0.2
NAD	3.8
ATP	1.0
ADP	0.2
$\text{Lactate}_{internal}$	2

5.2 Model Fitting and Validation

An important part of any kinetic modeling is validation, where data used for validation should be unique and distinct from data used for model construction. Additionally, if model parameters are fitted to the validation data set, further validation with unique data is required to prevent the model merely being able to describe a single set of conditions. Ideally one would want a model that could predict systemic behaviour over a wide range of conditions.

In this study, enzymes were individually characterised and these kinetic data were used to describe the individual reactions of glycolysis. By linking the reactions together, (e.g using a set of ordinary differential equations) in a kinetic model it is possible to predict how the pathway acts as a whole, in terms of steady state flux and metabolite concentrations. Since these system

wide variables can be experimentally measured *in vivo* and are distinct from the enzyme characterisation data, they were chosen as a means of validation for the kinetic model.

The only kinetic parameters that were fitted in the model were those for the ATPase reaction, which were fitted to obtain an ATP/ADP ratio of five. Since the glucose transporter activity was not measured in this work a range of glucose transporter rates (0.01 - 1.2 μmol.min^{-1}.mg protein^{-1}) were tested in the model. This specific range of transporter rates were chosen, as transporter rates higher than 1.2 μmol.min^{-1}.mg protein^{-1} resulted in the massive accumulation of sugar phosphate intermediates ($>$ 50 mM) and rates lower than 0.01μmol.min^{-1}.mg protein^{-1} resulted in an extremely low flux.

For the selected range of glucose transporter rates the model yielded steady state lactate fluxes between 0.015 and 0.171 μmol.min^{-1}.mg protein^{-1} respectively, which was in the same order of magnitude as the measured fluxes.
Setting the glucose transporter rate to 0.07 μmol.min^{-1}.mg protein^{-1} returned steady state glucose and lactate fluxes of 0.0515 and 0.1030 μmol.min^{-1}.mg protein^{-1}, respectively and metabolite concentrations within a physiological feasible range. (Table 5.3.). These predicted fluxes are comparable to those determined experimentally (0.0487 and 0.1065 μmol.min^{-1}.mg protein^{-1}, respectively) in the preceding chapter.

The model can thus predict the measured glycolytic fluxes, and maintain metabolite concentrations within a physiological range. In future the transporter activity will be determined experimentally, which together with steady state intermediate concentrations will provide a more concrete means of validation.

5.3 Brief Model Analysis & Discussion

Although model validation is not entirely complete, some observations were made regarding model behaviour, that may be applicable to the regulation of *P. falciparum* glycolysis.

Table 5.3: Kinetic model predictions of steady state glycolytic fluxes and metabolite concentrations in *P. falciparum* where the glucose transporter rate was set to 0.07 μmol.min^{-1}.mg protein^{-1}. Experimentally determined glucose (J_{GluTr}) and lactate (J_{LacTr}) fluxes were 0.0487 and 0.1065 μmol.min^{-1}.mg protein^{-1}, respectively (See Section 4.3 for experimental details).

Metabolite	Concentration (mM)	Reaction	Flux (μmol.min^{-1}.mg protein^{-1})
Glucose	0.046	J_{GluTr}	0.0515
G6P	11.0	J_{HK}	0.0515
F6P	2.01	J_{PGI}	0.0515
F1,6BP	0.25	J_{PFK}	0.0515
DHAP	0.61	J_{ALD}	0.0515
GAP	0.052	J_{TPI}	0.0515
DPG	3.42×10^{-3}	J_{G3PDH}	0.1030
3PGA	0.78	J_{PGK}	0.1030
2PGA	0.028	J_{PGM}	0.1030
PEP	0.067	J_{ENO}	0.1030
Pyr	1.86	J_{PK}	0.1030
Lac	2.30	J_{LDH}	0.1030
ATP	1.00	J_{LacTr}	0.1030
ADP	0.19	J_{ATP}	0.1030
NADH	0.14		
NAD	3.86		

It was noted during analyses that the low glucose transporter rate plays an essential role in preventing the accumulation of sugar phosphates, such as G6P and F1,6BP. Increasing the transporter rate two fold (by increasing external glucose concentration, or the maximal rate) not only results in a higher steady state flux, but also the accumulation of sugar phosphates ($>$ 100mM), and an increase in the ATP/ADP ratio ($>$ 50). This can be countered to a certain extent by increasing the ATP demand rate, v13ATPase, which lowers the ATP/ADP ratio ($<$1), but does not sufficiently prevent the accumulation of G6P and especially F 1,6BP.

This phenotype has been described for some yeast mutants[144], which lack the ability to inhibit HK that consequently leads to a decrease in ATP and increase in sugar phosphate concentration. At higher transporter rates, ATP/ADP ratio increases due to the fact that v3PFK is not sufficiently inhibited by ATP

and its rate is higher than $v4$ALD, but the flux through the lower branch of glycolysis is still enough to provide a net production of ATP.

P. falciparum may thus have mechanisms to prevent the lethal accumulation of the sugar phosphate intermediates. Several possible ways of avoiding this phenomenon are proposed: 1) Relying on low glucose concentrations within the erythrocyte, 2) Having a low glucose transporter expression level to ensure a low transport rate or 3) Inhibition of HK by G6P, which is known to occur in some organisms[98] and thus provide a measure of sensitivity to G6P accumulation.

Models are often constructed from quantitative data obtained experimentally, which is better than estimating or guessing parameter values, but they may still contain experimental error. The required accuracy of model parameters depends to a large degree on what the model is used for (e.g. qualitative and general or accurate and precise quantitative predictions). Parameter sensitivity analysis can be used to identify which parameters play in key role in model behaviour and prediction. This analysis is useful for pinpointing parameters which should be determined as accurately as possible, as well as identifying parameter values that need not be accurate as they have little effect on model outcome.
The kinetic model presented in this study has numerous experimental parameters, some of which were estimated or determined only in singleton. The possibility that a single key parameter can dramatically alter the model behaviour and prediction exists. To identify, which parameters this model is sensitive to, a sensitivity analysis will be performed by increasing and decreasing each parameter value, in turn as well as combinatorially, by a fixed percentage and examining the percentage change in steady state fluxes and/or metabolite concentrations. In this manner one can obtain a quantitative measure of model sensitivity to specific parameters. Since a change in parameter values may not always lead to a linear reflection on model outcome, gradually increasing or decreasing parameter values in small increments can be used determine stable or unstable ranges of parameters. Using these analyses on the *Plasmodium* model, parameters that 1) lead to a large change or 2) parameters near a boundary, which if crossed would significantly alter model prediction can be identified. These parameters would then be determined as

accurately as possible.
Although the model is not entirely complete in terms of validation, is has be shown that in light of the project aims, the work presented in this chapter demonstrates that the construction and validation of a kinetic model is feasible.

Chapter 6

General Discussion

The object of this study was to establish the feasibility of constructing and validating a detailed kinetic model of glycolysis in asexual *P. falciparum*.

The feasibility of the study was based on the ability to obtain the required kinetic parameters and validation data for the construction and validation of a kinetic model. In this study *Plasmodium* was cultured and the glycolytic enzymes characterised from lysates. Kinetic parameters obtained from the study were used to construct a kinetic model, which was partially validated using experimentally measured glycolytic fluxes. Additional validation of the model by steady state metabolite concentrations is possible in future with the development of an enzyme-based method to measure the majority of glycolytic intermediates. All the criteria set in the aims of the study were met and it can thus be concluded that it is possible to construct and validation a detailed kinetic model of glycolysis in the asexual *P. falciparum*.

Brief analysis of the model revealed the sensitivity of the system to a high glucose transport rate, which results in the accumulation of lethal concentrations of sugar phosphates. These findings highlight the importance of regulation, especially in the first steps of glycolysis, where enzymes are generally insensitive to their products and ATP is first invested before a net production in the later branch of glycolysis[7]. In light of this we will be investigating the possible systems which the organism may use to prevent lethally high sugar phoshphate concentrations. These systems may include

the organism i) relying on low external glucose concentrations within the erythrocyte, ii) maintaining low expression levels of the glucose transporter or iii) having regulatory mechanisms, such as the inhibition of HK by G6P.

The construction and validation of a kinetic model, simple or complex, is just the first step towards answering specific questions. The power of kinetic models is that they can be used to investigate questions and test hypotheses that could otherwise not be examined experimentally. The kinetic model presented in this work has several applications that will be addressed in future: i) Identification of potential drug targets using differential control analysis, where the control structure of the erythrocyte and other human cells are compared to that of *Plasmodium* in the hope that an area of high control in the parasite corresponds to an area of low control in the erythrocyte. ii) Investigation of the effect of parasite infection on the erythrocyte glycolytic metabolism by integrating the *Plasmodium* kinetic model into an existing erythrocyte kinetic model. A specific area of interest in the erythrocyte metabolism, would be the concentrations of 2,3DPG, as this metabolites plays an important role in carbon dioxide homeostasis and alterations in this metabolism, due to parasite infection, may have important pathophysiological implications.

The modelling approach used in this work can be applied to any organism that can be cultivated in sufficient quantities for kinetic parameter determination and steady flux and metabolite measurements. This approach is time consuming, since all the glycolytic enzymes require characterisation. An alternative kinetic modelling approach that may be worth investigating and applicable to metabolic pathways is the construction of a generic glycolytic model(s), where parameter values are based on an average value found over a range of organisms. This generic model could then be adapted to any organism by of interest by including the unique regulatory properties (e.g experimentally characterise regulatory enzymes) of the organism. Such an approach with the addition of parameter sensitivity analysis to identify key parameters for experimental determination, would allow researchers to construct a working kinetic model of an organism within a shorter time span.
A model based on a generic model may not be entirely accurate, but could still provide a tool with sufficient accuracy to analyse systemic properties or answer specific questions. Additionally, such a model could easily be enhanced

by the addition of experimentally determined data.

The kinetic model of *P. falciparum* glycolysis may be applicable to other *Plasmodium* species and could be adapted for each species. Due to high homology between species, it would be expected that the enzyme K_m values and glycolytic regulation would not vary to large degree, although enzyme expression levels (and thus V_{max}) may vary considerably. The *P. falciparum* model could thus be adapted to model alternative species by simply measuring V_{max} values, incorporating them into the current kinetic model and validating it on glycolytic fluxes and intermediate concentrations.

This study has elucidated that the construction of a kinetic model for *P. falciparum* is feasible and that the completed model may lead to the further understanding of *Plasmodium* glycolysis and host-pathogen relationships.

Chapter 7

Conclusion

In this study it was established that constructing a detailed kinetic model of the asexual *Plasmodium falciparum* glycolytic pathway is feasible. Kinetic parameters for the glycolytic enzymes were determined from trophozoites lysates and *in vivo* fluxes were measured in intact, isolated trophozoites. Using the determined kinetic parameters, a detailed kinetic model was constructed and was partially validated using measured fluxes. Further validation using steady state metabolite concentrations is possible as an enzymatic method for the determination of glycolytic intermediates was successfully developed with sensitivities sufficient to quantify all of the intermediate concentrations, except GAP and the phosphoglycerates. A brief analysis of model behaviour revealed the importance of the glucose transporter rate in preventing the lethal accumulation of sugar phosphates and thus prompting the proposal that further regulation may exist in the first steps of glycolysis. The kinetic model, once fully validated, will provide a tool to identify potential drug targets, investigate host-pathogen interaction and gain a better understanding of glycolytic regulation.

Appendix A

Microplate Pathlength Determination

The pathlength of a microplate is dependent on the working volume for each well. Since many assays are dependent on an extinction coefficient, it is essential that the pathlength for a specific working volume is accurately determined. In this appendices I derive (1) a general formula for calculating the pathlength as a function of volume for any tapered well and (2) a formula specific to Greiner bio-one Flat Bottom Microplates, catalogue numbers 655 101, 655 161 & 655 192. The specifications for this microplate can be found at the end of the document and were obtained from:
[http://www.greinerbioone.com/en/row/files/241968/655101.pdf - last checked Dec 2008].

The volume of a tapered well can be determined by using the formula for a truncated cone: [http://wiki.answers.com/Q/Formula_for_calculating_volume_-of_truncated _cone - last checked Dec 2008] as given in equation .

$$Volume = \frac{1}{3}\pi({R_1}^2 + R_1 \cdot R_2 + {R_2}^2)hA \tag{A.0.1}$$

Where R_1 is the base radius, R_2 is the top radius and h is the height of the truncated cone.

As the volume within the well increases, the height increases and so does the top radius. Thus, R_2 is dependent on h and the relationship can be described using the angle (θ) between the base and well wall described in equations A.0.2 and A.0.3.

$$\theta = ArcTan\frac{R_2 - R_1}{maxheight} \tag{A.0.2}$$

$$newR_2 = Tan[\theta] \cdot h + R_1 \tag{A.0.3}$$

We can substitute newR_2 in equation A.0.5 for R_2 in A and describe the well volume, v as a function of filled height, h.

$$v = \frac{1}{3}h\pi({R_1}^2 + R_1(R_1 + h \cdot Tan[\theta]) + (R_1 + h \cdot Tan[\theta])^2) \tag{A.0.4}$$

Equation A.0.4 is not of much use, but it can be be manipulated to obtain a general formula for pathlength height ,h, as a function of volume, v (equation A.0.5):

$$h = \frac{Cot[\theta]^2}{\pi}(\pi^3{R_1}^3Tan[\theta]^3 + 3\pi^2 v \cdot Tan[\theta]^4)^{\frac{1}{3}} - R_1Cot[\theta] \tag{A.0.5}$$

From the Microplate specification sheet we obtain:

$$R_1 = \frac{6.390}{2}mm$$
$$R_2 = \frac{6.960}{2}mm$$
$$maxheight = 10.90mm$$

Using these constant values, θ is calculated to be 0.0261408 rad from equation A.0.2 Consequently equation A.0.5 reduces to a formula specific to the Greiner bio-one flat botton microplates:

$$p = 465.6(0.01808 + 0.00001384 \cdot v)^{\frac{1}{3}} - 122.2 \tag{A.0.6}$$

Where the units of pathlength, p, and volume, v, are mm and μL respectively.

Bibliography

1. Agbenyega, T., Angus, B. J., Bedu-Addo, G., Baffoe-Bonnie, B., Guyton, T., Stacpoole, P. W., & Krishna, S. (2000). Glucose and lactate kinetics in children with severe malaria. *J. Clin. Endocrinol. Metab.*, *85*(4), 1569–1576.

2. Allen, R. J. W., & Kirk, K. (2004). Cell volume control in the *Plasmodium*-infected erythrocyte. *Trends Parasitol.*, *20*(1), 7–10.

3. Ansorge, I., Benting, J., Bhakdi, S., & Lingelbach, K. (1996). Protein sorting in *Plasmodium falciparum*-infected red blood cells permeabilized with the pore-forming protein streptolysin o. *Biochem. J.*, *315*, 307–314.

4. Ansorge, I., Paprotka, K., Bhakdi, S., & Lingelbach, K. (1997). Permeabilization of the erythrocyte membrane with streptolysin o allows access to the vacuolar membrane of plasmodium falciparum and a molecular analysis of membrane topology. *Mol. Biochem. Parasitol.*, *84*(2), 259–261.

5. Atamna, H., Pescarmona, G., & Ginsburg, H. (1994). Hexose-monophosphate shunt activity in intact *Plasmodium falciparum* infected erythrocytes and in free parasites. *Mol. Biochem. Parasitol.*, *67*, 79–89.

6. Aurrecoechea, C., Brestelli, J., Brunk, B. P., Dommer, J., Fischer, S., Gajria, B., Gao, X., Gingle, A., Grant, G., Harb, O. S., Heiges, M., Innamorato, F., Iodice, J., Kissinger, J. C., Kraemer, E., Li, W., Miller, J. A., Nayak, V., Pennington, C., Pinney, D. F., Roos, D. S., Ross, C., Stoeckert, C. J. J., Treatman, C., & Wang, H. (2009). Plasmodb: a functional genomic database for malaria parasites. *Nucleic Acids Res.*, *37*(Database issue), 539–543.

7. Bakker, B. M., Mensonides, F. I., Teusink, B., van Hoek, P., Michels, P. A., & Westerhoff, H. V. (2000). Compartmentation protects trypanosomes from the dangerous design of glycolysis. *Proc. Natl. Acad. Sci. U. S. A.*, *97*(5), 2087–2092.

8. Barrett, M. P. (1997). The pentose phosphate pathway and parasitic protozoa. *Parasitol. Today*, *13*(1), 11–16.

9. Becker, K., Tilley, L., Vennerstrom, J. L., Roberts, D., Rogerson, S., & Ginsburg, H. (2004). Oxidative stress in malaria parasite-infected erythrocytes: host-parasite interactions. *Int. J. Parasitol.*, *34*(2), 163–189.

10. Biagini, G. A., Viriyavejakul, P., O'neill, P. M., Bray, P. G., & Ward, S. A. (2006). Functional characterization and target validation of alternative complex i of *Plasmodium falciparum* mitochondria. *Antimicrob. Agents Chemother.*, *50*(5), 1841–1851.

11. Blackie, W. (1947). *Malaria: With special reference to the African forms*. Cape Town: Peninsula Press.

12. Bozdech, Z., & Ginsburg, H. (2005). Data mining of the transcriptome of *Plasmodium falciparum*: the pentose phosphate pathway and ancillary processes. *Malar. J.*, *4*(1), 17–29.

13. Bradford, M. M. (1976). A rapid and sensitive method for the quantitation of microgram quantities of protein utilizing the principle of protein-dye binding. *Anal. Biochem.*, *72*, 248–254.

14. Brady, R. L., & Cameron, A. (2004). Structure-based approaches to the development of novel anti-malarials. *Curr. Drug Targets*, *5*(2), 137–149.

15. Brown, W. M., Yowell, C. A., Hoard, A., Vander Jagt, T. A., Hunsaker, L. A., Deck, L. M., Royer, R. E., Piper, R. C., Dame, J. B., Makler, M. T., & Vander Jagt, D. L. (2004). Comparative structural analysis and kinetic properties of lactate dehydrogenases from the four species of human malarial parasites. *Biochem.*, *43*(20), 6219–6229.

16. Buchholz, A., Takors, R., & Wandrey, C. (2001 Aug 15). Quantification of intracellular metabolites in escherichia coli k12 using liquid chromatographic-electrospray ionization tandem mass spectrometric techniques. *Anal Biochem*, *295*(2), 129–137.

17. Buckwitz, D., Jacobasch, G., & Gerth, C. (1990). Phosphofructokinase from *Plasmodium berghei*: a kinetic model of allosteric regulation. *Mol. Biochem. Parasitol.*, *40*(2), 225–232.

18. Buckwitz, D., Jacobasch, G., & Gerth, C. (1990). Phosphofructokinase from *Plasmodium berghei*. influence of mg^{2+}, atp and mg^{2+}-complexed atp. *Biochem. J.*, *267*(2), 353–357.

19. Buckwitz, D., Jacobasch, G., Gerth, C., Holzhutter, H. G., & Thamm, R. (1988). A kinetic model of phosphofructokinase from *Plasmodium berghei*. influence of atp and fructose-6-phosphate. *Mol. Biochem. Parasitol.*, *27*(2-3), 225–232.

20. Buckwitz, D., Jacobasch, G., Kuckelkorn, U., Plonka, A., & Gerth, C. (1990). Glucose-6-phosphate dehydrogenase from *Plasmodium berghei*: kinetic and electrophoretic characterization. *Exp. Parasitol.*, *70*(3), 264–275.

21. Byrant, C., Voller, A., & Smith, M. (1964). The incorporation of radioactivity from (14c) glucose into soluble metabolic intermediates of malarial parasites. *Am. J. Trop. Med. Hyg.*, *13*, 515–519.

22. Bzik, D. J., Fox, B. A., & Gonyer, K. (1993). Expression of *Plasmodium falciparum* lactate dehydrogenase in *Escherichia coli*. *Mol. Biochem. Parasitol.*, *59*(1), 155–166.

23. Calvo, E., Rubiano, C., Vargas, A., & Wasserman, M. (2002). Expression of housekeeping genes during the asexual cell cycle of *Plasmodium falciparum*. *Parasitol. Res.*, *88*(3), 267–271.

24. Caruthers, J., Bosch, J., Buckner, F., Van Voorhis, W., Myler, P., Worthey, E., Mehlin, C., Boni, E., DeTitta, G., Luft, J., Lauricella, A., Kalyuzhniy, O., Anderson, L., Zucker, F., Soltis, M., & Hol, W. G. (2006). Structure of a ribulose 5-phosphate 3-epimerase from *Plasmodium falciparum*. *Proteins*, *62*(2), 338–342.

25. Casimiro, S., Coleman, M., Mohlai, P., Hemingway, J., & Sharp, B. (2006). Insecticide resistance in *Anopheles funestus* (diptera: Culidcidae) from mozambique. *J. Med. Entomol.*, *43*, 267–275.

26. Chaikuad, A., Fairweather, V., Conners, R., Joseph-Horne, T., Turgut-Balik, D., & Brady, R. L. (2005). Structure of lactate dehydrogenase from *Plasmodium vivax*: complexes with nadh and apadh. *Biochem.*, *44*(49), 16221–16228.

27. Chan, M., & Sim, T. (2005). Functional analysis, overexpression and kinetic characterisation of pyruvate kinase from *Plasmodium falciparum*. *Biochem. Biophys. Res. Comm.*, *326*, 188–196.

28. Chan, M., Tan, D. H., & Sim, T. S. (2007). *Plasmodium falciparum* pyruvate kinase as a novel target for antimalarial drug-screening. *Travel Med. Infect. Dis.*, *5*(2), 125–131.

29. Clarke, J. L., Scopes, D. A., Sodeinde, O., & Mason, P. J. (2001). Glucose-6-phosphate dehydrogenase-6-phosphogluconolactonase. a novel bifunctional enzyme in malaria parasites. *Eur. J. Biochem.*, *268*(7), 2013–2019.

30. Clarke, J. L., & Sodeinde, P. J., O. Mason (2003). A unique insertion in *Plasmodium berghei* glucose-6-phosphate dehydrogenase-6-phosphogluconolactonase: evolutionary and functional studies. *Mol. Biochem. Parasitol.*, *127*, 1–8.

31. Cloonan, N., Fischer, K., Cheng, Q., & Saul, A. (2001). Aldolase genes of *Plasmodium* species. *Mol. Biochem. Parasitol.*, *113*(2), 327–330.

32. Collard, F., Collet, J. F., Gerin, I., Veiga-da Cunha, M., & Van Schaftingen, E. (1999). Identification of the cdna encoding human 6-phosphogluconolactonase, the enzyme catalyzing the second step of the pentose phosphate pathway. *FEBS Lett.*, *459*(2), 223–226.

33. Cornell, N. W., Leadbetter, M., & Veech, R. L. (1979). Effects of free magnesium concentration and ionic strength on equilibrium constants for the glyceraldehyde phosphate dehydrogenase and phosphoglycerate kinase reactions. *J. Biol. Chem.*, *254*(14), 6522–6527.

34. Cox-Singh, J., Davis, T. M. E., Lee, K.-S., Shamsul, S. S. G., Matusop, A., Ratnam, S., Rahman, H. A., Conway, D. J., & Singh, B. (2008). *Plasmodium knowlesi* malaria in humans is widely distributed and potentially life threatening. *Clin. Infect. Dis.*, *46*(2), 165–171.

35. Cranmer, S. L., Conant, A. R., Gutteridge, W. E., & Halestrap, A. P. (1995). Characterization of the enhanced transport of l- and d-lactate into human red blood cells infected with *Plasmodium falciparum* suggests the presence of a novel saturable lactate proton cotransporter. *J. Biol. Chem.*, *270*(25), 15045–15052.

36. Cranmer, S. L., Magowan, C., Liang, J., Coppel, R. L., & Cooke, B. M. (1997). An alternative to serum for cultivation of *Plasmodium falciparum in vitro*. *Trans. R. Soc. Trop. Med. Hyg.*, *91*(3), 363–365.

37. Daubenberger, C. A., Poltl-Frank, F., Jiang, G., Lipp, J., Certa, U., & Pluschke, G. (2000). Identification and recombinant expression of glyceraldehyde-3-phosphate dehydrogenase of *Plasmodium falciparum*. *Gene*, *246*(1-2), 255–264.

38. Davidov, E., Holland, J., Marple, E., & Naylor, S. (2003). Advancing drug discovery through systems biology. *Drug Discov. Today*, *8*(4), 175–183.

39. Dinglasan, R., & et al (2007). Disruption of plasmodium falciparum development by antibodies against a conserved mosquito midgut antigen. *Proc. Natl. Acad. Sci. U. S. A.*, *104*, 13461–13466.

40. Dobeli, H., Trzeciak, A., Gillessen, D., Matile, H., Srivastava, I. K., Perrin, L. H., Jakob, P. E., & Certa, U. (1990). Expression, purification, biochemical characterization and inhibition of recombinant *Plasmodium falciparum* aldolase. *Mol. Biochem. Parasitol.*, *41*(2), 259–268.

41. Dunaway, G. A., Kasten, T. P., Sebo, T., & Trapp, R. (1988). Analysis of the phosphofructokinase subunits and isoenzymes in human tissues. *Biochem. J.*, *251*(3), 677–683.

42. Dunn, C. R., Banfield, M. J., Barker, J. J., Higham, C. W., Moreton, K. M., Turgut-Balik, D., Brady, R. L., & Holbrook, J. J. (1996). The structure of lactate dehydrogenase from *Plasmodium falciparum* reveals a new target for anti-malarial design. *Nat. Struct. Biol.*, *3*, 912–915.

43. Elliott, J. L., Saliba, K. J., & Kirk, K. (2001). Transport of lactate and pyruvate in the intraerythrocytic malaria parasite, *Plasmodium falciparum*. *Biochem. J.*, *355*, 733–739.

44. Ernest, I., Callens, M., Opperdoes, F., & Michels, P. (1994). Pyruvate kinase of *Leishmania mexicana*. cloning and analysis of the gene, overexpression in *Escherichia coli* and characterization of the enzyme. *Mol. Biochem. Parasitol.*, (pp. 43–54).

45. Ernest, I., Callens, M., Uttaro, A., Chevalier, N., Opperdoes, F., Muirhead, H., & Michels, P. (1998). Pyruvate kinase of *Trypanosoma brucei*: overexpression, purification, and functional characterization of wild-type and mutated enzyme. *Protein Expr. Purif.*, *13*, 373–382.

46. Faller, L., Baroudy, B., Jonson, A., & Ewall, R. (1977). Magnesium ion requirements for yeast enolase activity. *Biochem.*, *16*, 3864–3869.

47. Feagin, J. (1992). The 6-kb element of *Plasmodium falciparum* encodes mitochondrial cytochrome genes. *Mol. Biochem. Parasitol.*, *52*, 145–148.

48. Fegan, G., Noor, A., Akhwale, W., Cousens, S., & Snow, R. (2007). Effect of expanded insecticide-treated bednet coverage on child survival in rural kenya: a longitudinal study. *Lancet*, *370*, 1035–1039.

49. Fletcher, K., Canning, M., & Theakston, R. (1977). Electrophoresis of glucose-6-phosphate and 6-phosphogluconate dehydrogenases in erythrocytes from malaria-infected animals. *Ann. Trop. Med. Parasitol.*, *71*, 125–130.

50. Foth, B. J., Stimmler, L. M., Handman, E., Crabb, B. S., Hodder, A. N., & McFadden, G. I. (2005). The malaria parasite *Plasmodium falciparum* has only one pyruvate dehydrogenase complex, which is located in the apicoplast. *Mol. Microbiol.*, *55*(1), 39–53.

51. Frevert, U., & Cristanti, A. (1998). Invasion of vertabrate cells: hepatocytes. In I. Sherman (Ed.) *Malaria: parasite biology, pathogenesis and protection*, (pp. 73–91). Washington D.C.: ASM Press.

52. Fry, M., Webb, E., & Pudney, M. (1990). Effect of mitochondrial inhibitors on adenosinetriphosphate levels in *Plasmodium falciparum*. *Comp. Biochem. Physiol. B*, *96*(4), 775–782.

53. Fujikawa, A., Nishimori, I., Taguchi, T., & Onishi, S. (1999). Human carbonic anhydrase xiv (ca14): cdna cloning, mrna expression, and mapping to chromosome 1. *Genomics*, *61*, 74–81.

54. Gardner, M. J., Hall, N., Fung, E., White, O., Berriman, M., Hyman, R. W., Carlton, J. M., Pain, A., Nelson, K. E., Bowman, S., Paulsen, I. T., James, K., Eisen, J. A., Rutherford, K., Salzberg, S. L., Craig, A., Kyes, S., Chan, M. S., Nene, V., Shallom, S. J., Suh, B., Peterson, J., Angiuoli, S., Pertea, M., Allen, J., Selengut, J., Haft, D., Mather, M. W., Vaidya, A. B., Martin, D. M., Fairlamb, A. H., Fraunholz, M. J., Roos, D. S., Ralph, S. A., McFadden, G. I., Cummings, L. M., Subramanian, G. M., Mungall, C., Venter, J. C., Carucci, D. J., Hoffman, S. L., Newbold, C., Davis, R. W., Fraser, C. M., & Barrell, B. (2002). Genome sequence of the human malaria parasite *Plasmodium falciparum*. *Nature*, *419*(6906), 498–511.

55. Goldberg, R., Tewari, Y., & Bhat, T. (2004). Thermodynamics of enzyme-catalyzed reactions - a database for quantitative biochemistry. *Bioinformatics*, *20*(16), 2874–2877.

56. Gomez, M. S., Piper, R. C., Hunsaker, L. A., Royer, R. E., Deck, L. M., Makler, M. T., & Vander Jagt, D. L. (1997). Substrate and cofactor specificity and selective inhibition of lactate dehydrogenase from the malarial parasite *P. falciparum*. *Mol. Biochem. Parasitol.*, *90*(1), 235–246.

57. Greenwood, B. M., Fidock, D. A., Kyle, D. E., Kappe, S. H. I., Alonso, P. L., Collins, F. H., & Duffy, P. E. (2008). Malaria: progress, perils, and prospects for eradication. *J. Clin. Invest.*, *118*(4), 1266–1276.

58. Hays, J. (2005). *Epidemics and pandemics: Their impacts on human history*. USA: ABC-CLIO.

59. Hayward, R. E. (2000). *Plasmodium falciparum* phosphoenolpyruvate carboxykinase is developmentally regulated in gametocytes. *Mol. Biochem. Parasitol.*, *107*(2), 227–240.

60. Heinrich, R., & Rapoport, T. A. (1974). A linear steady-state treatment of enzymatic chains. general properties, control and effector strength. *Eur. J. Biochem.*, *42*(1), 89–95.

61. Helfert, S., Estevez, A. M., Bakker, B., Michels, P., & Clayton, C. (2001). Roles of triosephosphate isomerase and aerobic metabolism in trypanosoma brucei. *Biochem J*, *357*(Pt 1), 117–125.

62. Hoefnagel, M. H. N., Starrenburg, M. J. C., Martens, D. E., Hugenholtz, J., Kleerebezem, M., Van Swam, I. I., Bongers, R., Westerhoff, H. V., & Snoep, J. L.

(2002). Metabolic engineering of lactic acid bacteria, the combined approach: kinetic modelling, metabolic control and experimental analysis. *Microbiology*, *148*(Pt 4), 1003–1013.

63. Holmes, M. A., Buckner, F. S., Van Voorhis, W. C., Verlinde, C. L., Mehlin, C., Boni, E., DeTitta, G., Luft, J., Lauricella, A., Anderson, L., Kalyuzhniy, O., Zucker, F., Schoenfeld, L. W., Earnest, T. N., Hol, W. G., & Merritt, E. A. (2006). Structure of ribose 5-phosphate isomerase from *Plasmodium falciparum*. *Acta Crystallograph. Sect. F Struct. Biol. Cryst. Commun.*, *62*(5), 427–431.

64. Holzhutter, H.-G. (2004). The principle of flux minimization and its application to estimate stationary fluxes in metabolic networks. *Eur J Biochem*, *271*(14), 2905–2922.

65. Honigsbaum, M. (2002). *The fever trail: In search of the cure for malaria*. Great Britain: Pan Books.

66. Hoppe, H. C., Verschoor, J. A., & Louw, A. I. (1991). Plasmodium falciparum: a comparison of synchronisation methods for in vitro cultures. *Exp Parasitol*, *72*(4), 464–467.

67. Hornberg, J. J., Bruggeman, F. J., Bakker, B. M., & Westerhoff, H. V. (2007). Metabolic control analysis to identify optimal drug targets. *Prog Drug Res*, *64*, 171, 173–89.

68. Itin, C., Burki, Y., Certa, U., & Dobeli, H. (1993). Selective inhibition of *Plasmodium falciparum* aldolase by a tubulin derived peptide and identification of the binding site. *Mol. Biochem. Parasitol.*, *58*(1), 135–143.

69. Joet, T., Chotivanich, K., Silamut, K., Patel, A. P., Morin, C., & Krishna, S. (2004). Analysis of *Plasmodium vivax* hexose transporters and effects of a parasitocidal inhibitor. *Biochem. J.*, *381*(3), 905–909.

70. Joet, T., Eckstein-Ludwig, U., Morin, C., & Krishna, S. (2003). Validation of the hexose transporter of *Plasmodium falciparum* as a novel drug target. *Proc. Natl. Acad. Sci. U. S. A.*, *100*(13), 7476–7479.

71. Joet, T., Holterman, L., Stedman, T. T., Kocken, C. H., Van Der Wel, A., Thomas, A. W., & Krishna, S. (2002). Comparative characterization of hexose transporters of *Plasmodium knowlesi, Plasmodium yoelii* and *Toxoplasma gondii* highlights functional differences within the apicomplexan family. *Biochem. J.*, *368*, 923–929.

72. Joshi, S., Singh, A. R., Kumar, A., Misra, P. C., Siddiqi, M. I., & Saxena, J. K. (2008). Molecular cloning and characterization of *Plasmodium falciparum* transketolase. *Mol. Biochem. Parasitol.*, *160*(1), 32–41.

73. Joubert, F., Neitz, A. W., & Louw, A. I. (2001). Structure-based inhibitor screening: a family of sulfonated dye inhibitors for malaria parasite triosephosphate isomerase. *Proteins*, *45*(2), 136–143.

74. Kacser, H., & Burns, J. A. (1973). The control of flux. *Symp. Soc. Exp. Biol.*, *27*, 65–104.

75. Kanaani, J., & Ginsburg, H. (1991). Transport of lactate in *Plasmodium falciparum*-infected human erythrocytes. *J. Cell. Physiol.*, *149*(3), 469–476.

76. Kaslow, D., & Hill, S. (1990). Cloning metabolic pathways by complementation in *Escherichia coli*. *J. Biol. Chem.*, *265*, 12337–12341.

77. Kell, D. B. (2006). Systems biology, metabolic modelling and metabolomics in drug discovery and development. *Drug Discov. Today*, *11*(23-24), 1085–1092.

78. Khan, S., & Waters, A. (2004). Malaria parasite transmission stages: an update. *Trends Parasitol.*, *20*(12), 575–580.

79. Kim, H., Certa, U., Dobeli, H., Jakob, P., & Hol, W. G. (1998). Crystal structure of fructose-1,6-bisphosphate aldolase from the human malaria parasite *Plasmodium falciparum*. *Biochem.*, *37*(13), 4388–9436.

80. Kirk, K. (2001). Membrane transport in the malaria-infected erythrocyte. *Physiol. Rev.*, *81*(2), 495–537.

81. Kobayashi, T., Sato, S., Takamiya, S., Komaki-Yasuda, K., Yano, K., Hirata, A., Onitsuka, I., Hata, M., Mi-ichi, F., Tanaka, T., Hase, T., Miyajima, A., Kawazu, S.-i., Watanabe, Y.-i., & Kita, K. (2007). Mitochondria and apicoplast of *Plasmodium falciparum*: behaviour on subcellular fractionation and the implication. *Mitochondrion*, *7*(1-2), 125–132.

82. Krishna, S., Woodrow, C. J., Burchmore, R. J. S., Saliba, K. J., & Kirk, K. (2000). Hexose transport in asexual stages of *Plasmodium falciparum* and *Kinetoplastidae*. *Parasitol. Today*, *16*(12), 516–521.

83. Krungkrai, S. R., Suraveratum, N., Rochanakij, S., & Krungkrai, J. (2001). Characterisation of carbonic anhydrase in *Plasmodium falciparum*. *Int. J. Parasitol.*, *31*(7), 661–668.

84. Kumar, S., & Banyal, H. S. (1997). Purification and characterisation of the hexokinase of *Plasmodium berghei*, a murine malaria parasite. *Acta Vet. Hung.*, *45*(2), 119–126.

85. Kurdi-Heidar, B., & Luzzato, L. (1990). Expression and characterization of glucose-6-phosphate dehydrogenase of *Plasmodium falciparum*. *Mol. Biochem. Parasitol.*, *41*, 83–92.

86. Kwon, H., Lu, T., Rutzler, M., & Zwiebel, L. (2006). Olfactory responses in a gustatory organ of the malaria vector mosquito *Anopheles gambiae*. *Proc. Natl. Acad. Sci. U. S. A.*, *103*, 13526–13531.

87. Lang-Unnasch, N., & Murphy, A. D. (1998). Metabolic changes of the malaria parasite during the transition from the human to the mosquito host. *Annu. Rev. Microbiol.*, *52*, 561–590.

88. Ling, I., & Wilson, R. (1988). Glucose-6-phosphate dehydrogenase activity of the malaria parasite *Plasmodium falciparum*. *Mol. Biochem. Parasitol.*, *31*, 47–56.

89. Lowry, O., & Passonneau, J. (1964). The relationship between substrates and enzymes of glycolysis in brain. *J. Biol. Chem.*, *239*, 31–42.

90. Maeda, T., Saito, T., Oguchi, Y., Nakazawa, M., Takeuchi, T., & Asai, T. (2003). Expression and characterization of recombinant pyruvate kinase from *Toxoplasma gondii* tachyzoites. *Parasitol. Res.*, *89*(4), 259–265.

91. Maithal, K., Ravindra, G., Nagaraj, G., Singh, S. K., Balaram, H., & Balaram, P. (2002). Subunit interface mutation disrupting an aromatic cluster in *Plasmodium falciparum* triosephosphate isomerase: effect on dimer stability. *Protein Eng.*, *15*(7), 575–584.

92. Maitra, P., & Estabrook, R. (1964). A fluorometric method for the enzymatic determination of glycolytic intermediates. *Anal. Biochem.*, *7*, 472–474.

93. Marrelli, M., Li, C., Rasgon, J., & Jacobs-Lorena, M. (2007). Transgenic malaria-resistance mosquitoes have a fitness advantage when feeding on *Plasmodium*-infected blood. *Proc. Natl. Acad. Sci. U. S. A.*, *104*, 5580–5583.

94. McDaniel, H., & Siu, P. (1972). Purification and characterization of phosphoenolpyruvate carboxylase from *Plasmodium berghei*. *J. Bacteriol.*, *109*, 385–390.

95. Mehlin, C. (2005). Structure-based drug discovery for *Plasmodium falciparum*. *Comb. Chem. High Throughput Screen.*, *8*(1), 5–14.

96. Meier, B., Dobeli, H., & Certa, U. (1992). Stage specific expression of aldolase isozymes in the rodent malaria parasite *P. berghei*. *Mol. Biochem. Parasitol.*, *52*, 15–28.

97. Mota, M. M., & Rodriguez, A. (2004). Migration through host cells: the first steps of *Plasmodium* sporozoites in the mammalian host. *Cell. Microbiol.*, *6*(12), 1113–1118.

98. Newsholme, E. A., Rolleston, F. S., & Taylor, K. (1968). Factors affecting the glucose 6-phosphate inhibition of hexokinase from cerebral cortex tissue of the guinea pig. *Biochem. J.*, *106*(1), 193–201.

99. Noedl, H. (2005). Artemisinin resistance: how can we find it? *Trends Parasitol.*, *21*, 404–405.

100. Nyunt, M. M., & Plowe, C. V. (2007). Pharmacologic advances in the global control and treatment of malaria: combination therapy and resistance. *Clin. Pharmacol. Ther.*, *82*(5), 601–605.

101. O' Brian, E., Kurdi-Haidar, B., Wanachiwanawin, W., Carvajal, J., Vulliamy, T., Cappadoro, V., Mason, P., & Luzzatto, L. (1994). Cloning of the glucose-6-phosphate dehydrogenase from *Plasmodium falciparum*. *Mol. Biochem. Parasitol.*, *64*, 313–326.

102. O'Donnell, R., & Blackman, M. (2005). The role of malaria merozoite proteases in red blood cell invasion. *Curr.Opin. Microbiol.*, *8*(4), 422–427.

103. Olafsson, P., & Certa, U. (1994). Expression and cellular localisation of hexokinase during the bloodstage development of *Plasmodium falciparum*. *Mol. Biochem. Parasitol.*, *63*(1), 171–174.

104. Olafsson, P., Matile, H., & Certa, U. (1992). Molecular analysis of *Plasmodium falciparum* hexokinase. *Mol. Biochem. Parasitol.*, *56*(1), 89–101.

105. Painter, H. J., Morrisey, J. M., Mather, M. W., & Vaidya, A. B. (2007). Specific role of mitochondrial electron transport in blood-stage *Plasmodium falciparum*. *Nature*, *446*(7131), 88–91.

106. Pal, B., Pybus, B., Muccio, D. D., & Chattopadhyay, D. (2004). Biochemical characterization and crystallization of recombinant 3-phosphoglycerate kinase of *Plasmodium falciparum*. *Biochim. Biophys. Acta*, *1699*(1-2), 277–280.

107. Pal-Bhowmick, I., Sadagopan, K., Vora, H., Sehgal, A., Sharma, S., & Jarori, G. (2004). Cloning, over-expression, purification and characterization of *Plasmodium falciparum* enolase. *Eur. J. Biochem.*, *271*, 4845–4854.

108. Parthasarathy, S., Eaazhisai, K., Balaram, H., Balaram, P., & Murthy, M. (2003). Structure of *Plasmodium falciparum* triose-phosphate isomerase-2-phosphoglycerate complex at 1.1-a resolution. *J. Biol. Chem.*, *278*(52), 52461–70.

109. Patel, A. P., Staines, H. M., & Krishna, S. (2008). New antimalarial targets: the example of glucose transport. *Travel Med. Infect. Dis.*, *6*(1-2), 58–66.

110. Pattanaik, P., Raman, J., & Balaram, H. (2002). Perspectives in drug design against malaria. *Curr. Top. Med. Chem.*, *2*(5), 483–505.

111. Ranie, J., Kumar, V. P., & Balaram, H. (1993). Cloning of the triosephosphate isomerase gene of *Plasmodium falciparum* and expression in *Escherichia coli*. *Mol. Biochem. Parasitol.*, *61*(2), 159–169.

112. Ravindra, G., & Balaram, P. (2005). *Plasmodium falciparum* triosephosphate isomerase: New insights into an old enzyme. *Pure Appl. Chem.*, *77*(1), 281–289.

113. Read, M., Hicks, K. E., Sims, P. F., & Hyde, J. E. (1994). Molecular characterisation of the enolase gene from the human malaria parasite *Plasmodium falciparum*. evidence for ancestry within a photosynthetic lineage. *Eur. J. Biochem.*, *220*(2), 513–520.

114. Reungprapavut, S., Krungkrai, S. R., & Krungkrai, J. (2004). *Plasmodium falciparum* carbonic anhydrase is a possible target for malaria chemotherapy. *J. Enzyme Inhib. Med. Chem.*, *19*(3), 249–256.

115. Rocco, F. (2003). *The miraculous fever tree*. London: HarperCollins Publishers.

116. Rohwer, J. M., Hanekom, A. J., Crous, C., Snoep, J. L., & Hofmeyr, J. H. S. (2006). Evaluation of a simplified generic bi-substrate rate equation for computational systems biology. *Syst. Biol. (Stevenage)*, *153*(5), 338–341.

117. Roth, E., Calvin, M., Max-Audit, J., Rosa, J., & Rosa, R. (1988). The enzymes of the glycolytic pathway in erythrocytes infected with *Plasmodium falciparum* malaria parasites. *Blood*, *72*, 1922–1925.

118. Roth, E., Joulin, V., Miwa, S., Yoshida, A., Akatsuka, J., Cohen-Solal, M., & Rosa, R. (1988). The use of enzymopathic human red cells in the study of malarial parasite glucose metabolism. *Blood*, *71*(5), 1408–1413.

119. Roth, E. F., & Jr. (1987). Malarial parasite hexokinase and hexokinase-dependent glutathione reduction in the *Plasmodium falciparum*-infected human erythrocyte. *J. Biol. Chem.*, *262*(32), 15678–15682.

120. Royer, R., Deck, L., Campos, N. M., Hunsaker, L. A., & Vander Jagt, D. L. (1986). Biologically active derivatives of gossypol: synthesis and antimalarial activities of periacylated gossylic nitriles. *J. Med. Chem.*, *29*, 1799–1801.

121. Saliba, K. J., Horner, H. A., & Kirk, K. (1998). Transport and metabolism of the essential vitamin pantothenic acid in human erythrocytes infected with the malaria parasite *Plasmodium falciparum*. *J. Biol. Chem.*, *273*(17), 10190–10195.

122. Saliba, K. J., Horner, H. A., & Kirk, K. (1998 Apr 24). Transport and metabolism of the essential vitamin pantothenic acid in human erythrocytes infected with the malaria parasite *Plasmodium falciparum*. *J. Biol. Chem.*, *273*(17), 10190–10195.

123. Saliba, K. J., & Kirk, K. (1999). ph regulation in the intracellular malaria parasite, *Plasmodium falciparum*. h^+ extrusion via a v-type h^+-atpase. *J. Biol. Chem.*, *274*(47), 33213–33219.

124. Saliba, K. J., Krishna, S., & Kirk, K. (2004). Inhibition of hexose transport and abrogation of ph homeostasis in the intraerythrocytic malaria parasite by an o-3-hexose derivative. *FEBS Lett.*, *570*(1-3), 93–96.

125. Sanchez, C. P., Stein, W. D., & Lanzer, M. (2008). Dissecting the components of quinine accumulation in plasmodium falciparum. *Mol Microbiol*, *67*(5), 1081–1093.

126. Scopes, D., Bautista, J., Vulliamy, T., & Mason, P. (1997). *Plasmodium falciparum* glc6pd ± the n-terminal portion is homologous to a predicted protein encoded near to glc6pd in *Haemophilus Influenzae*. *Mol. Microbiol.*, *23*, 847–848.

127. Shahabuddin, M., Rawlings, D., & Kaslow, D. (1994). A novel glucose-6-phosphate dehydrogenase in *Plasmodium falciparum*: cdna and primary protein structure. *Biochim. Biophys. Acta.*, *1219*, 191–194.

128. Sharma, S., & Pathak, S. (2008). Malaria vaccine: a current perspective. *J. Vector Borne Dis.*, *45*(1), 1–20.

129. Sherman, I. (1998). Carbohydrate metabolism of asexual stages. In I. Sherman (Ed.) *Malaria: Parasite biology, pathogenesis and protection*, (pp. 135–143). Washington, D.C.: ASM Press.

130. Sherman, I., & I.P., T. (1966). Carbon dioxide fixation in malaria (*Plasmodium lopurae*). *Nature*, *24*, 639–642.

131. Sherman, I., & I.P., T. (1968). Carbon dioxide fixation in malaria - ii. *Plasmodium knowlesi* (monkey malaria). *Comp. Biochem. Physiol.*, *24*, 639–642.

132. Sherman, I. W. (1979). Biochemistry of *Plasmodium* (malarial parasites). *Microbiol. Rev.*, *43*(4), 453–495.

133. Shoemark, D. K., Cliff, M. J., Sessions, R. B., & Clarke, A. R. (2007). Enzymatic properties of the lactate dehydrogenase enzyme from *Plasmodium falciparum*. *FEBS J.*, *274*(11), 2738–2748.

134. Sidjanski, S., & Vanderberg, J. P. (1997). Delayed migration of *Plasmodium* sporozoites from the mosquito bite site to the blood. *Am. J. Trop. Med. Hyg.*, *57*(4), 426–429.

135. Singh, A. R., Joshi, S., Arya, R., Kayastha, A. M., Srivastava, K. K., Tripathi, L. M., & Saxena, J. K. (2008). Molecular cloning and characterization of *Brugia malayi* hexokinase. *Parasitol. Int.*, *57*(3), 354–361.

136. Singh, S. K., Maithal, K., Balaram, H., & Balaram, P. (2001). Synthetic peptides as inactivators of multimeric enzymes: inhibition of *Plasmodium falciparum* triosephosphate isomerase by interface peptides. *FEBS Lett.*, *501*(1), 19–23.

137. Siu, P. (1967). Carbon dioxide fixation in plasmodia and the effect of some antimalarials on the enzyme. *Comp. Biochem. Physiol.*, *23*, 785–795.

138. Srivastava, I. K., Schmidt, M., Grall, M., Certa, U., Garcia, A. M., & Perrin, L. H. (1992). Identification and purification of glucose phosphate isomerase of *Plasmodium falciparum*. *Mol. Biochem. Parasitol.*, *54*(2), 153–64.

139. Staples, J., & Suarez, R. (1997). Honeybee flight muscle phosphoglucose isomerase: matching enzyme capacities to flux requirements at a near-equilibrium reaction. *J Exp Biol*, *200*(Pt 8), 1247–1254.

140. Teklehaimanot, A., Singer, B., Spielman, A., Tozan, Y., & Schapira, A. (2005). *Coming to grips with malaria in the new millennium*. London: Earthscan.

141. Teng, R., Junankar, P., Bubb, W., Rae, C., Mercier, P., & Kirk, K. (2008). Metabolite profiling of the intraerythrocytic malaria parasite *Plasmodium falciparum* by (1)h nmr spectroscopy. *NMR Biomed.*.

142. Teusink, B., Passarge, J., Reijenga, C. A., Esgalhado, E., van der Weijden, C. C., Schepper, M., Walsh, M. C., Bakker, B. M., van Dam, K., Westerhoff, H. V., & Snoep, J. L. (2000). Can yeast glycolysis be understood in terms of in vitro kinetics of the constituent enzymes? testing biochemistry. *Eur J Biochem*, *267*(17), 5313–5329.

143. Theakston, R., & Fletcher, K. (1973). An electron cytochemical study of 6-phosphogluconate dehydrogenase activity in infected erythrocytes during malaria. *Life Sci*, (pp. 405–410).

144. Thevelein, J. M., & Hohmann, S. (1995). Trehalose synthase: guard to the gate of glycolysis in yeast? *Trends Biochem. Sci.*, *20*(1), 3–10.

145. Ting, I., & Sherman, I. (1966). Carbon dioxide fixation in malaria - i. kinetic studies in *Plasmodium lophurae*. *Comp. Biochem. Physiol.*, *19*, 855–869.

146. Trager, W., & Jensen, J. (1976). Human malaria parasits in continuous culture. *Science*, *193*, 673–675.

147. Travis, S. F., Morrison, A. D., Clements, R. S. J., Winegrad, A. I., & Oski, F. A. (1971). Metabolic alterations in the human erythrocyte produced by increases in glucose concentration. the role of the polyol pathway. *J. Clin. Invest.*, *50*(10), 2104–2112.

148. Uyeda, K. (1979). Phosphofructokinases. *Adv. Enzymol.*, *48*, 193–244.

149. Vaidya, A. B., Akella, R., & Supliek, K. (1989). Sequences similar to genes for two mitochondrial proteins and portions of ribosomal rna in tandemly arrayed 6-kilobase-pair dna of a malarial parasite. *Mol. Biochem. Parasitol.*, *35*(97-108).

150. Valentini, G., Chiarelli, L., Fortin, R., Speranza, M. L., Galizzi, A., & Mattevi, A. (2000). The allosteric regulation of pyruvate kinase. *J. Biol. Chem.*, *275*(24), 18145–18152.

151. van Dam, J., Eman, M., J.Frank, Lange, H., van Dedem, G., & Heijnen, S. (2002). Analysis of glycolytic intermediates in *Saccharomyces cerevisiae* using anion exchange chromatography and electrospray ionization with tandem mass spectrometric detection. *Anal. Chim. Acta*, *460*, 209–218.

152. van Dooren, G. G., Marti, M., Tonkin, C. J., Stimmler, L. M., Cowman, A. F., & McFadden, G. I. (2005). Development of the endoplasmic reticulum, mitochondrion and apicoplast during the asexual life cycle of *Plasmodium falciparum*. *Mol. Microbiol.*, *57*(2), 405–419.

153. van Dooren, G. G., Stimmler, L. M., & McFadden, G. I. (2006). Metabolic maps and functions of the *Plasmodium* mitochondrion. *FEMS Microbiol. Rev.*, *30*(4), 596–630.

154. Vanderberg, J. P. (1977). *Plasmodium berghei*: quantification of sporozoites injected by mosquitoes feeding on a rodent host. *Exp. Parasitol.*, *42*, 169–181.

155. Veech, R. L., Raijman, L., Dalziel, K., & Krebs, H. A. (1969). Disequilibrium in the triose phosphate isomerase system in rat liver. *Biochem. J.*, *115*(4), 837–842.

156. Velanker, S. S., Ray, S. S., Gokhale, R. S., Suma, S., Balaram, H., Balaram, P., & Murthy, M. R. (1997). Triosephosphate isomerase from *Plasmodium falciparum*: the crystal structure provides insights into antimalarial drug design. *Structure*, *5*(6), 751–761.

157. Wanidworanun, C., Nagel, R. L., & Shear, H. L. (1999). Antisense oligonucleotides targeting malarial aldolase inhibit the asexual erythrocytic stages of *Plasmodium falciparum*. *Mol. Biochem. Parasitol.*, *102*(1), 91–101.

158. White, N. J. (2008). Qinghaosu (artemisinin): the price of success. *Science*, *320*(5874), 330–334.

159. Williamson, D. H., Lund, P., & Krebs, H. A. (1967). The redox state of free nicotinamide-adenine dinucleotide in the cytoplasm and mitochondria of rat liver. *Biochem. J.*, *103*(2), 514–527.

160. Winter, V. J., Cameron, A., Tranter, R., Sessions, R. B., & Brady, R. L. (2003). Crystal structure of *Plasmodium berghei* lactate dehydrogenase indicates the unique structural differences of these enzymes are shared across the *Plasmodium* genus. *Mol. Biochem. Parasitol.*, *131*(1), 1–10.

161. Woodrow, C. J., Burchmore, R. J., & Krishna, S. (2000). Hexose permeation pathways in *Plasmodium falciparum*-infected erythrocytes. *Proc. Natl. Acad. Sci. U. S. A.*, *97*(18), 9931–9936.

162. Woodrow, C. J., Penny, J. I., & Krishna, S. (1999). Intraerythrocytic *Plasmodium falciparum* expresses a high affinity facilitative hexose transporter. *J. Biol. Chem.*, *274*(11), 7272–7277.

163. Wunsch, S., Sanchez, C. P., Gekle, M., Grosse-Wortmann, L., Wiesner, J., & Lanzer, M. (1998). Differential stimulation of the na^+/h^+ exchanger determines chloroquine uptake in *Plasmodium falciparum*. *J. Cell. Biol.*, *140*(2), 335–345.